1. Report No.	2. Government Accession No.	3. Recipient's Catalog No.
NASA CR 135306		N78-17216

4. Title and Subtitle	5. Report Date
DEVELOPMENT OF Si_3N_4 AND SiC OF IMPROVED TOUGHNESS	October 25, 1977
	6. Performing Organization Code

7. Author(s)	8. Performing Organization Report No.
John J. Brennan and Charles O. Hulse	R77-912252-23
	10. Work Unit No.

9. Performing Organization Name and Address	11. Contract or Grant No.
United Technologies Research Center East Hartford, CT 06108	NAS3-19731
	13. Type of Report and Period Covered
12. Sponsoring Agency Name and Address National Aeronautics and Space Administration Washington, DC 20546 and U.S. Army Research and Technology Laboratories (AVRADCOM) Moffet Field, CA 94035	Contractor Report - Final
	14. Sponsoring Agency Code

15. Supplementary Notes

Final Report - Project Manager, William A. Sanders, NASA-Lewis Research Center and Propulsion Laboratory, U.S. Army Research & Technology Laboratories Cleveland, OH 44135

16. Abstract

The application of energy absorbing surface layers to Si_3N_4 and SiC was investigated. Among the layers studied were microcracked materials such as iron titanate and a silica-zircon mixture and porous materials such as reaction sintered Si_3N_4. Energy absorption due to microcrack extension upon impact was found not to be an important mechanism. Instead, the fivefold improvement in Charpy and ballistic impact at elevated temperatures (1250°C and 1370°C) found for Fe_2TiO_5 was due to plastic deformation while similar improvement found for silica-zircon mixtures at RT was due to crushing of the porous material. Due to thermal expansion mismatch, these two materials could not withstand thermal cycling when used as energy absorbing surface layers on Si_3N_4.

Reaction sintered Si_3N_4 layers on dense Si_3N_4 were found to give up to a sevenfold increase in ballistic impact resistance due to crushing of the layer upon impact. High porosity (45%), large particle size R.S. Si_3N_4 layers fabricated from -100, +200 mesh Si powder gave better impact improvement than less porous (30%), small particle size layers fabricated from -325 mesh Si powder. Thermal cycling from 200°C to 1370°C for 50 cycles in air did not degrade the impact properties of the nitrided -100, +200 Si layers on NC-132 Si_3N_4 but did cause the impact resistance to drop along with interfacial debonding to occur for nitrided -325 Si layers on NC-132 Si_3N_4, due to excessive internal oxidation.

In addition, a brief study was conducted dealing with the severe loss in impact and bend strength of commercial NC-132 Si_3N_4 upon exposure to temperatures >1200°C in air atmospheres.

17. Key Words (Suggested by Author(s))	18. Distribution Statement
Ceramics for Gas Turbines Silicon Nitride Impact Resistance Improvement Energy Absorbing Surface Layers High Temperature Oxidation of Si_3N_4	Unclassified - Unlimited

19. Security Classif. (of this report)	20. Security Classif. (of this page)	21. No. of Pages	22. Price*
Unclassified	Unclassified	130	

* For sale by the National Technical Information Service, Springfield, Virginia 22151

Development of Si_3N_4 and SiC of Improved Toughness

TABLE OF CONTENTS

I. INTRODUCTION 1

II. SUMMARY 3

III. TECHNICAL PROGRESS SUMMARY 7

3.1 Fabrication and Characterization of Specimens 7
3.2 Charpy Impact Testing of Si_3N_4 and SiC Controls 7
3.3 Task I - Development of Toughening Treatments for Si_3N_4 and SiC 8
3.3.1 The Carburization of Si_3N_4 8
3.3.2 The Oxidation of Si_3N_4 9
3.3.3 The Heat Treatment of SiC 11
3.3.4 Energy Absorbing Surface Layers 12
3.3.4.1 Plasma Sprayed Mullite on SiC 12
3.3.4.2 Partially Stabilized ZrO_2 on Si_3N_4 and/or SiC 13
3.3.4.3 Titanate Layers on Si_3N_4 and/or SiC 14
3.3.4.4 Silica-Zircon Layers on Si_3N_4 and/or SiC 15
3.3.5 MOR Testing 17
3.3.6 Ballistic Impact Testing 18
3.4 Task II - Effect of Thermal Exposure on Toughness Improvement Retention 21
3.5 Iron Titanate and Silica-Zircon Microstructural Characterization 23
3.6 Task III - Evaluation of Porous Si_3N_4 Layers on Dense Si_3N_4 . . . 24
3.6.1 Fabrication of Specimens 24
3.6.2 Charpy Impact Testing 25
3.6.3 Ballistic Impact Testing 26
3.6.4 Artificially Introduced Porosity 27
3.6.5 Mixed Particle Size R.S. Si_3N_4 Layers 30
3.6.6 R.S. Si_3N_4 - NC-132 Si_3N_4 Interfacial Strength Degradation 30

TABLE OF CONTENTS (Cont'd)

3.6.7 Thermal Cycling of R.S. Si_3N_4 Layers on NC-132 Si_3N_4 32

IV. CONCLUSIONS 36

V. REFERENCES 39

TABLES I - XXXII 41

FIGURES 1 - 58 73

APPENDIX A

APPENDIX B

I. INTRODUCTION

The application of refractory ceramic materials for use in gas turbine engines has, for the past few years, been an extremely active area of interest. The use of refractory ceramic materials in aircraft, automotive, and power generating gas turbines can produce distinct advantages over superalloys in the areas of:

(1) Cost Reduction - Substitution of a solid ceramic part for a complex cooled and coated metal part, possibly with an increase in life.

(2) Better Performance - Reduction in cooling air which is necessary to achieve a reasonable life in a metal part, or an increase in operating temperature without additional cooling penalty.

(3) Reduced Weight - On a fixed shape, a lower density ceramic offers a weight benefit per se, and a related reduction in supporting structure weight.

In addition, improved resistance to oxidation and corrosion (especially for industrial turbines operating on low quality fuels) has been demonstrated for ceramics over superalloys. The two candidate materials receiving the most attention are hot pressed Si_3N_4 and SiC, due to their high strength, good thermal shock properties, low density, and good oxidation resistance. Unfortunately, the use of these materials in critical gas turbine applications may be severely limited due to their very low fracture toughness (i.e., impact strength). Thus, it is imperative that research be done to improve the toughness of Si_3N_4 and SiC and, at the same time, retain the good mechanical and thermal properties of the two materials.

Various research programs having the objective of improving the impact resistance of Si_3N_4 and SiC have been completed during the last few years. These programs were based on three general approaches:

(1) Improving the impact resistance by fiber reinforcement (Refs. 1-3).

(2) Improving the strength and impact resistance by compressive surface layers (Refs. 4-6).

(3) Improving the impact resistance by energy absorbing surface layers (Refs. 1,7-9).

The first of these approaches has been studied extensively at United Technologies Research Center over the past five years, with excellent results for improving the impact resistance of hot-pressed Si_3N_4 through the use of tantalum wire reinforcement. The emphasis of the current NASA program, however, is to investigate the second and, in particular, the third of these approaches in greater detail.

The original objective of this program was to develop toughness treatment methods that would consistently result in Si_3N_4 and SiC specimens having Charpy impact strengths greater than 1.35 joules (1 foot-pound) at temperatures up to 1370°C. The program was divided into two tasks plus a later program extension designated as Task III:

Task I - Development of Toughness Treatments for Si_3N_4 and SiC. The treatments included:

A. The Carburization of Si_3N_4
B. Heat Treatment of SiC
C. Energy Absorbing Surface Layers

Task II - Effect of Thermal Exposure on Toughness Improvement Retention

Task III - Evaluation of Porous Si_3N_4 Layers on Dense Si_3N_4.

II. SUMMARY

The development of Si_3N_4 and SiC of improved toughness was carried out through three different approaches: (1) the carburization of Si_3N_4, (2) the oxidation of SiC and (3) the application of energy absorbing surface layers. The first two approaches had a common goal, that of forming a fused silica coating on the surface of the Si_3N_4 and SiC materials which would lead to the formation of compressive surface layers. The third approach, which proved to be the only successful one, attempted to apply crushable surface layers of 1 mm thickness to the two materials. These surface layers were designed to be primarily microcracked (such as zirconia, iron and magnesium titanate, and silica-zircon) or porous (such as plasma sprayed mullite or reaction sintered Si_3N_4). The toughness increase of the Si_3N_4 and SiC materials was measured through the use of Charpy and ballistic impact from RT to 1370°C.

During the course of carburizing runs, it was found that NC-132 Si_3N_4, oxidized for as little as 24 hrs at 1370°C, suffers a marked decrease in RT impact strength and maximum load to failure. The cause of this decrease is apparently due to the formation of Ca and Mg containing silicates on the specimen surface that cause fracture initiating pits to form. Si_3N_4 densified with Y_2O_3 additive was found to suffer a much less severe loss in mechanical properties on oxidation compared to NC-132 Si_3N_4.

The Charpy impact strength of NC-132 Si_3N_4 control samples remains essentially constant from RT to 1370°C whereas the Charpy impact strength of NC-203 SiC at 1370°C drops to half that at RT. At all temperatures, the Charpy impact strength of SiC is significantly lower than that of Si_3N_4. This statement is also true for the ballistic impact strength of the two materials, using a 4.4 mm chrome-steel sphere as the impacting projectile. It was also found that the ballistic impact strength of NC-132 Si_3N_4 is greater at 1250°C and 1370°C than at RT, whereas the ballistic impact strength of NC-203 SiC remains the same at 1250°C and RT.

The carburization of Si_3N_4, the heat treatment of SiC, and plasma sprayed mullite layers on SiC resulted in little or no improvement in Charpy impact strength at RT, 1250°C, and 1370°C over control specimens. Partially stabilized ZrO_2 and $MgTi_2O_5$ layers on Si_3N_4 gave moderate (~50%) improvement in Charpy impact strength at RT, 1250°C, and 1370°C. Iron titanate (Fe_2TiO_5) layers on Si_3N_4 resulted in impact strengths on the order of 2.5 joules (25 in-lbs) at 1250°C and 1370°C compared to control values of 0.4 joules (3.5 in-lbs). In contrast, silica-zircon layers on Si_3N_4, which gave RT Charpy impact values of approximately 1.5 joules (15 in-lbs), resulted in only moderate (~50%) improvement at 1250°C and 1370°C.

From the results of the Charpy impact tests, it was decided to concentrate ballistic impact testing on the two energy absorbing surface layers that exhibited over 1.5 joules (15 in-lbs) in Charpy impact: iron titanate and silica-zircon. Bonding these two materials to Si_3N_4 and/or SiC plates, it was found that a moderate improvement in ballistic impact can be achieved with Fe_2TiO_5 layers on NC-132 Si_3N_4 at RT with a dramatic four to fivefold increase at 1250°C and 1370°C. Silica-zircon layers on NC-132 Si_3N_4 showed a fivefold improvement in ballistic impact strength at RT and up to a sevenfold improvement at 1370°C over the corresponding Si_3N_4 control values. Four to fivefold improvement for these two layers on NC-203 SiC at 1250°C over SiC controls was also shown, although the absolute values of the impact energies were still half or less of those recorded for the same layers on NC-132 Si_3N_4.

From microstructural characterizations of the Fe_2TiO_5 and silica-zircon energy absorbing surface layers, it was concluded that microcracking in these materials does not appear to be a prerequisite for energy absorption on impact. It is believed that for Fe_2TiO_5, the large amount of energy absorption occurring at elevated temperatures is due to plastic flow; and in the case of silica-zircon the energy absorption noted at all temperatures is caused by the porous nature of this material.

It has also been found that these two energy absorbing surface layers on NC-132 Si_3N_4 cannot withstand thermal cycling between 200°C and 1370°C or thermal aging at 1370°C without debonding due to the large difference in thermal expansion coefficient between the surface layers and the NC-132 Si_3N_4 substrate. It was thus decided to concentrate further efforts on porous R.S. Si_3N_4 layers on dense Si_3N_4 that would possess similar thermal expansion coefficients and could be expected to absorb energy upon impact due to crushing and crack diversion as well as be able to withstand a thermal cycling environment such as would be encountered in a gas turbine engine.

Charpy and ballistic impact specimens of R.S. Si_3N_4 layers on NC-132 Si_3N_4 were fabricated in situ by nitriding a layer of silicon metal powder that had been applied using a water or toluene based slurry. The types of R.S. Si_3N_4 surface layers investigated varied from relatively dense (70%), fine-grained R.S. Si_3N_4 made from -325 mesh Si powder to quite porous (55% dense), large particle-sized layers made from -100, +200 mesh Si powder. Combinations of these two powders, as well as -200 mesh Si and -325 mesh Si plus polystyrene spheres to form large voids, were also investigated. All layers were approximately 1 mm thick.

The results of Charpy impact tests at RT and 1370°C showed that the nitrided -200 Si and -325 Si layers on NC-132 Si_3N_4 did not increase the Charpy impact resistance significantly over Si_3N_4 control values. In contrast to the nitrided -325 Si and -200 Si layers, however, the higher porosity large grain size nitrided -100, +200 Si layers on NC-132 Si_3N_4 exhibited Charpy impact energies 2 1/2 times NC-132 Si_3N_4 controls at RT and slightly over twice that recorded for Si_3N_4 controls at 1370°C. From the instrumented Charpy impact load vs time curve it was evident that crushing of the R.S. Si_3N_4 layer occurred during impact.

Ballistic impact tests at RT and 1370°C of R.S. Si_3N_4 layers on NC-132 Si_3N_4 resulted in a fivefold to sixfold improvement in impact energy before substrate failure for nitrided -100, +200 Si and -200 Si layers but only a two to threefold improvement for nitrided -325 Si layers over NC-132 Si_3N_4 control values. To realize optimum energy absorption during a ballistic impact event, a combination of porosity and fairly large particle size appear to be necessary to allow crushing of the R.S. Si_3N_4 layer but at the same time, be somewhat resistant to penetration by the projectile.

Combinations of large grain size -100, +200 Si and small particle size -325 Si were investigated as well as mixtures of -325 Si plus polystyrene microspheres to artificially introduce large pores into a fine grain size material. The polystyrene microspheres were decomposed to voids during the formation of the R.S. Si_3N_4 from Si. The results of these investigations showed that artificially introduced large voids or pores in a fine grained R.S. Si_3N_4 matrix increased the Charpy impact strength significantly over NC-132 Si_3N_4 controls but not the ballistic impact strength. It appears that the large spherical pores in this material lead to crushing and energy absorption during the low velocity Charpy impact event but the material is just too porous to build up sufficient resistance to the high velocity steel ball as it penetrates the R.S. Si_3N_4 layer during the ballistic test. Even though the porosity simulates that of a -100, +200 mesh Si layer, the particle size is much smaller. It is possible that the large particle size of the -100, +200 mesh nitrided Si layer is necessary for optimum energy absorption during a high velocity impact.

From the results of Charpy and ballistic impact tests on mixtures of -325 Si and -100, +200 Si, which resulted in R.S. Si_3N_4 layers with large grains plus small grains filling the large voids, it was found that the impact resistance of these layers was as high, or higher, than that obtained previously for the -100, +200 Si nitrided surface layers. Thus, filling the large voids does not adversely affect the ability of the layer to absorb energy upon impact and that the large grain size of the nitrided -100, +200 Si layers, or possibly the fairly large amount of unreacted silicon present, is the controlling factor for energy absorption.

In order to evaluate the effect of the R.S. Si_3N_4 energy absorbing surface layers on the strength of the NC-132 Si_3N_4 when the interface between the R.S. Si_3N_4 and NC-132 Si_3N_4 is subjected to tensile (bending) stresses, a series of Charpy impact tests were performed with the samples impacted on the side opposite the R.S. Si_3N_4 layer. The results of these tests showed that well bonded R.S. Si_3N_4 layers degraded the Charpy impact strength and bend strength of the NC-132 Si_3N_4 by up to 50%. In general, the large particle and pore size nitrided -100, +200 Si layers degraded the strength more than the smaller particle and pore size nitrided -325 Si layers. The possibility that the degradation is due to the large pores in the R.S. Si_3N_4 layer near the interface acting as stress concentrating flaws suggests that minimizing pore size at the R.S. Si_3N_4/H.P. Si_3N_4 interface by using a graded density R.S. Si_3N_4 layer could help alleviate this problem.

Thermal cycling of R.S. Si_3N_4 surface layers on NC-132 Si_3N_4 between 200°C and 1370°C in air for up to 50 cycles resulted in a large amount of silica formation in the high surface area -325 Si layers that caused debonding at the R.S. Si_3N_4/H.P. Si_3N_4 interface due to thermal expansion mismatch between the silica and the NC-132 Si_3N_4. The larger particle size nitrided -100, +200 Si layers did not form sufficient silica to cause debonding during thermal cycling with the result that the ballistic impact resistance of these cycled layers was the same as noncycled layers at RT and much higher at 1370°C. The increase at elevated temperature is possibly due to plastic deformation of the silica during the high temperature ballistic impact event. For a practical R.S. Si_3N_4 energy absorbing surface layer that must operate in a gas turbine environment, it may be necessary to have an outer layer of dense, impermeable CVD Si_3N_4 covering the R.S. Si_3N_4 surface to add oxidation and possibly erosion resistance.

In addition, as detailed in the Appendix, no significant effect was observed in the Charpy impact energy of control Plexiglas samples through the use of counterweights on the Charpy impact hammer, which are necessary for elevated temperature impact testing. Although the center of percussion of the instrument is changed significantly when counterweights are used, the effect on relatively low impact energy samples is minimal.

III. TECHNICAL PROGRESS SUMMARY

3.1 Fabrication and Characterization of Specimens

The silicon nitride and silicon carbide samples used in this program were obtained from the Norton Co., Worcester, MA and consist of fully dense hot-pressed NC-132 Si_3N_4 and NC-203 SiC. Six inch by six inch by one inch billets (five of each material) were obtained from Norton Co. and subsequently machined into 6.4 x 6.4 x 51 mm (0.25 x 0.25 x 2.00 in.) Charpy impact specimens, 25.4 x 38.1 x 6.4 mm (1.0 x 1.5 x 0.25 in.) ballistic impact specimens and 2.54 x 5.08 x 44.5 mm (0.1 x 0.2 x 1.75 in.) modulus of rupture specimens. All specimens were subjected to Zyglo dye penetrant inspection and those exhibiting cracks or pits were rejected. The rejection rate was found to be very low; about three out of every one hundred samples.

Randomly selected specimens from each billet were subjected to spectrochemical analysis in order to determine the amounts of impurity elements present. The results of this analysis are given in Table I. From Table I it can be seen that Al, Fe, Mg, and W are the major impurities present in NC-132 Si_3N_4, the Mg being added as a densification aid and the W resulting from ball milling the powder with WC balls. Al and Fe are undoubtedly present in the starting powder. It is gratifying to note that the Ca content is very low, since this element is responsible for poor elevated temperature properties in Si_3N_4. It is apparent that NC-203 SiC contains fewer impurities than NC-132 Si_3N_4, but those present are there in greater amounts. In particular, the tungsten content is quite high (5 wt %), and must result from excessive wear of the WC balls during ball milling of the SiC powder. The Al content is also very high and could be due to the particular densification aid used in the hot-pressing procedure. Samples of each material were also subjected to electron microscope examination with determinations made as to average grain size, distribution, and morphology. These results are given in Table II. From Table II and Figs. 1 and 2, it can be seen that the NC-203 SiC grain size is much larger than the NC-132 Si_3N_4 with the SiC grains equiaxed whereas the Si_3N_4 grains are a mixture of equiaxed and elongated. No direct evidence of any impurity phases present in either material can be observed.

3.2 Charpy Impact Testing of Si_3N_4 and SiC Controls

Control samples of NC-132 Si_3N_4 and NC-203 SiC were tested at RT, 1250°C and 1370°C in instrumented Charpy impact. Ten samples of each material were tested at each temperature, with the averages being given in Table III. From Table III it can be seen that the impact strength of Si_3N_4, which averaged 0.40 joules (3.5 in.-lbs) at RT, has increased to 0.45 joules (4.0 in.-lbs) at 1250°C

and then decreased somewhat at 1370°C down to the RT value of 0.40 joules (3.5 in-lbs). As expected, the maximum load to failure decreases gradually with increasing temperature. A typical instrumented Charpy impact trace for Si_3N_4 at RT is shown in Fig. 3. The area under the load curve represents the amount of energy absorbed during the impact event. The slope of the load curve at RT is somewhat greater than at elevated temperatures. The slope of the load curves at 1250°C and 1370°C are very similar with the energy difference being due to the lower load to failure at 1370°C.

The impact strength of NC-203 SiC, as shown in Table III, remains constant at 1250°C with the average of 0.20 joules (1.8 in.-lbs) being the same as that recorded at RT. The maximum load to failure, however, drops drastically from 2.9 kN at RT to 1.7 kN at 1250°C. At 1370°C, the Charpy impact strength of SiC drops significantly to 0.11 joules (1.0 in.-lbs) accompanied by a further drop in maximum load to 1.5 kN. The drop in impact strength of NC-203 SiC at elevated temperatures had been observed previously at UTRC. Avco has also noted a drop in the impact strength of their hot-pressed SiC (Ref. 1). Ceramic Finishing Co., however, noted an increase in the Charpy impact strength of NC-203 SiC at elevated temperatures (Refs. 6,7). A detailed description of the elevated temperature Charpy impact apparatus is given in Appendix A.

The fracture origins at all temperatures for both materials were approximately evenly divided between the sample edges and the sample faces. A typical fracture origin for Si_3N_4, tested at RT, at a face is shown in Fig. 4 and that at a sample edge in Fig. 5. Very few fracture origins were at identifiable flaws or inclusions, either external or internal. It was noticed that the samples with high impact energies fractured into four or more pieces, while the low impact energy samples fractured essentially into two pieces. Also, the weaker samples had a much smoother fracture surface than the stronger samples.

3.3 Task I - Development of Toughening Treatments for Si_3N_4 and SiC

3.3.1 The Carburization of Si_3N_4

The carburization of Si_3N_4 in the presence of small amounts of oxygen to form a fused silica coating was studied. The formation of fused SiO_2, stabilized in the glassy state by the presence of carbon, could result in the formation of compressive surface prestresses at all temperatures lower than the carburization temperature. At elevated temperatures the SiO_2 coating could lead to energy absorption during impact by viscous flow processes. Accordingly, Si_3N_4 Charpy impact samples were packed in NUCARB ND 3000 carburizing media from which the gross white activator particles had been removed. Three samples were run in a partially sealed tube and seven in a completely sealed tube which

contained air when it was sealed. Heat treating was done at 1350°C for 24 and 48 hrs. The samples run partially sealed lost about .02 mm (1 mil) from their surface and exhibited weak characteristic X-ray peaks for α-cristobalite, WC, (grinding media contamination) and possibly trace SiC. Those completely sealed also lost approximately .02-.05 mm from their surface and exhibited only characteristic X-ray peaks for WC and trace amounts of carbon.

The results of the Charpy impact tests on carburized Si_3N_4 are given in Table IV. The average RT impact strength of 0.38 joules (3.3 in.-lbs) is slightly less than control samples of NC-132 Si_3N_4 (0.40 joules), and the maximum load before failure of 3.0 kN (670 lbs) is significantly less than the controls (3.7 kN). A carburization run was done at 1400°C for 48 hrs as compared to 1350°C for prior runs in order to determine the effect of the increased carburization temperature on the impact properties. Carburization was done in a completely closed tube with the samples packed in NUCARB ND 3000 from which the gross white activator particles had been removed. All samples lost approximately .08 mm from their surface during this treatment compared to .02-.05 mm loss at 1350°C, and exhibited a decreased average impact strength of Si_3N_4 compared to the results from the 1350°C carburization, which had already resulted in a slight decrease in impact strength over Si_3N_4 controls.

Carburized samples of NC-132 Si_3N_4 were also tested at 1250°C and 1370°C in instrumented Charpy impact. No indication of impact strength improvements for carburized samples tested at 1250°C and 1370°C over control samples was observed. In fact, the impact strength of carburized samples at all temperatures was decreased somewhat over control values with the maximum load to failure being decreased substantially. This is in contrast to the results of Kirchner (Ref. 2) at Ceramic Finishing Co. where a small increase in the impact strength of similarly carburized NC-132 Si_3N_4 was observed. In any case, the carburizing treatment falls far short of the program goal of a 1.35 joule (12 in-lb) impact strength. Therefore, from the results of Si_3N_4 carburizing treatments on the Charpy impact strength at RT, 1250°C and 1370°C it was recommended that this toughening treatment be dropped from further consideration. This recommendation was accepted by the NASA program manager.

3.3.2 The Oxidation of Si_3N_4

During the course of the carburizing runs, a set of NC-132 samples was also run at 1350°C but with the tube completely open and no ND 3000 present to get base line data for simply oxidized Si_3N_4. The results of the RT instrumented impact tests on these samples are given in Table V. The effect of the oxide surface layer formed on these samples was disastrous. The impact strength dropped from 0.40 joules (3.5 in.-lbs) for the controls to 0.14 joules (1.2 in.-lbs) for the oxidized specimens. The maximum load sustained also dropped

from 3.7 kN (840 lbs) to 2.0 kN (440 lbs). In order to verify this drastic drop in maximum load to failure, a slow 3-point bend test was run on similarly oxidized samples with the resultant strength being 410 MPa (59.3 ksi) compared to 910 MPa (132 ksi) for control samples.

Two oxidized Si_3N_4 samples were diamond ground on one side until all evidence of an oxidized surface was removed (~.13 mm). They were then tested in Charpy impact with the ground side opposite the impact point, i.e. tension side. These samples had an average impact strength of 0.28 joules (2.5 in.-lbs), about twice that of the normal oxidized samples, but still 30% less than Si_3N_4 controls. The fracture origin of these samples was not on the ground tension surface but on the edge of one side (Fig. 6). Thus, the removal of .13 mm indeed strengthened the tensile surface but the oxidized side surfaces were still weak enough to originate fracture. This drastic reduction in strength has also been reported by the Westinghouse Corporation in an ARPA Interim Report on Brittle Materials Design, High Temperature Gas Turbine (Ref. 10). It appears to be due to the formation of silicates on the oxidized surface which form voids or pits on the surface that act as crack initiators. X-ray analysis of oxidized surfaces revealed that, in addition to α-cristobalite approximately an equal amount of enstatite ($MgSiO_3$) was present. Kiehle, et al (Ref. 11) also found cristobalite and enstatite on oxidized (1350°) surfaces of Norton HS-130 Si_3N_4 in addition to lesser amounts of akermanite ($Ca_2MgSi_2O_7$), forsterite (Mg_2SiO_4) and diopside ($CaMg(SiO_3)_2$). Kiehle also noted the surface pitting present after oxidation.

In contrast to the results obtained for NC-132 Si_3N_4, Si_3N_4 fabricated at UTRC with 15 wt % Y_2O_3 additive after a 60 hr oxidation at 1350°C exhibited a drop in impact strength of 22% and a drop in maximum load of 13% compared to 68% and 48%, respectively, for NC-132. These results are also shown in Table V. Figures 3 and 7-9 show the difference in the instrumented impact traces for NC-132 and Si_3N_4 + 15% Y_2O_3, both oxidized and unoxidized. From scanning electron microscopy studies the oxidized surface of NC-132 Si_3N_4 was found to consist of rough particles of $MgSiO_3$ (Fig. 10) with minor amounts of Mn, Ca, Fe, and Al present, the latter three primarily located between the $MgSiO_3$ grains. On occasion, large pits on the oxidized surface are noticed and form the fracture origin during impact. The fracture origin of an oxidized sample of NC-132 is an exceptionally large surface pit (Fig. 11). In contrast to the oxidized surface appearance of NC-132 Si_3N_4, UTRC Si_3N_4 + 15% Y_2O_3 when oxidized 60 hrs at 1350°C has the surface shown in Fig. 12. The large tabular crystals consist of yttrium silicate ($Y_2Si_2O_7$) with the underlying matrix being SiO_2 with a minor amount of Al present. No Ca, Mn, or Fe was detected. Thus, while the surface of oxidized Si_3N_4 + 15% Y_2O_3 is rougher in terms of silicate grain size then NC-132 Si_3N_4, the lack of large surface pits leads to a much less severe drop in impact strength and maximum load to failure.

The drop in strength and impact resistance of oxidized Si_3N_4 is very disturbing and could be a very important factor in the use of this material in gas turbine engines. Further investigation of this problem is imperative with emphasis on additives other than MgO or additives to MgO that will eliminate the surface pitting phenomenon.

3.3.3 The Heat Treatment of SiC

This approach, like the carburization of Si_3N_4, was thought to promote the formation of a fused silica coating on the SiC substrate, thus resulting in compressive surface prestresses at temperatures below the heat treatment temperature and viscous surface layers above this temperature.

Five SiC impact samples that were oxidized in air at 1300°C for 48 hrs and appeared to have a glassy fused silica coating approximately .01 mm thick were tested at RT, 1250°C and 1370°C in instrumented impact. The results of these tests are given in Table VI. The data show that the impact strength and maximum load to failure at RT appear to be slightly increased over the SiC controls (Table III). Additional SiC samples were oxidized at a higher temperature (1400°C) in order to assess the effect of a slightly thicker fused silica coating on the impact strength. However, the coating thickness turned out to be still about .01 mm with the resultant impact strength similar to the previously tested oxidized SiC samples.

The results of 1250°C and 1370°C instrumented Charpy impact tests on heat-treated NC-203 SiC samples show that the impact strength of oxidized samples at 1250°C is lower than comparable control values and at 1370°C is identical to SiC controls tested at that temperature. Again, these results contradict those observed by Kirchner (Ref. 6) at elevated temperatures for similarly treated samples where a substantial increase in impact strength was noted. In fact, the elevated temperature impact values obtained by Kirchner for a variety of systems, including both Si_3N_4 and SiC, are invariably higher than those obtained under the present program. These discrepancies can possibly be explained by the expected greater compliance of Kirchner's graphite-alumina specimen support compared to the stainless steel-alumina support used at UTRC.

From the results obtained on oxidized SiC specimens, it appears that no significant advantage exists for this toughening treatment. In use, SiC will naturally form an oxidized surface with little or no benefit realized from preoxidizing the material. Thus, it was recommended that this toughening treatment be dropped from further consideration. This recommendation was accepted by the NASA program manager.

3.3.4 Energy Absorbing Surface Layers

Three different basic approaches were initially studied under this general topic, (a) plasma sprayed mullite layers on SiC, (b) partially stabilized ZrO_2 layers on Si_3N_4 and/or SiC, and (c) microcracked layers of magnesium or iron titanate on Si_3N_4 and/or SiC. Later on in the contract the system of silica-zircon layers on Si_3N_4 and/or SiC was added to the investigation. And, during the final nine months of the contract, the system of porous reaction sintered Si_3N_4 energy absorbing surface layers on dense Si_3N_4 was studied under an extension to Task II. Each of these approaches will be discussed in turn.

3.3.4.1 Plasma Sprayed Mullite on SiC

This approach is based on depositing a refractory oxide material on SiC that has a good thermal expansion match with SiC and can be applied by the plasma spray process with controlled porosity and morphology. With a large enough porosity, crushing of the material upon impact could occur with concurrent damping of the impact stress wave and energy absorption.

Forty samples of NC-203 SiC were plasma sprayed with mullite by Metallizing Service Co., Elmwood, CT. Thirty of the samples had a 1 mm thick layer while ten had a 1.75 mm thick mullite surface layer. It was found to be impossible to spray a very porous mullite layer 1 mm thick as the impacting particles would erode away the porous mullite layer and no buildup would occur. Therefore, as porous a layer as possible was applied to the samples. The results of instrumented Charpy impact tests on this system are presented in Table VII.

A 1 mm thick mullite layer on SiC results in a small increase in RT Charpy impact energy from 0.20 joules (1.8 in.-lbs) to 0.22 joules (2.0 in.-lbs) but a decrease in the maximum load to failure from 2.9 kN (650 lbs) to 2.3 kN (500 lbs). Thicker mullite layers (1.75 mm) apparently result in a decrease in impact resistance and maximum load to failure. The results of 1250°C and 1370°C instrumented Charpy impact tests on 1.0 mm and 1.75 mm thick layers of plasma sprayed mullite (77% dense) on SiC show that the 1 mm thick layer results in a slight decrease in impact strength at 1250°C over SiC controls (0.19 joules compared to 0.20 joules) but an increase at 1370°C over controls (0.17 joules compared to 0.11 joules). The limited tests on 1.75 mm thick layers result in an apparent increase in impact strength at 1250°C over SiC controls and also a slight increase at 1370°C.

That the RT Charpy impact strength for 1 mm thick mullite layers on SiC increased slightly while the maximum load decreased indicates that some energy absorption due to the layer was occurring, as can be seen in Fig. 13. The irregular shape of the load curve is indicative of some crushing of the layer

occurring. It is unfortunate that a more porous layer was not able to be applied as it would undoubtedly offer a greater opportunity for crushing to occur. The observation by Palm (Ref. 8) that plasma sprayed layers decrease the strength of SiC is supported in this program by Charpy impact tests with the plasma sprayed mullite layer on the tensile side. Both the impact strength and maximum load to failure were decreased dramatically from that recorded for SiC controls.

From the instrumented impact traces of most samples there is evidence of some crushing of the mullite layer upon impact which cannot, however, be seen by microscopic examination of the impacted sample. The amount of energy absorbed is not large and the program goal of 1.35 joules appears to be unattainable for this toughening treatment. The advisability of continuing this treatment into the next phase of ballistic and modulus of rupture testing was open to question especially since it had been demonstrated that the maximum load is decreased drastically when the sample is impacted with the plasma sprayed mullite layer on the tensile side. MOR tests would surely have reflected this result. It was thus decided to drop this approach from further consideration.

3.3.4.2 Partially Stabilized ZrO_2 on Si_3N_4 and/or SiC

Samples of partially stabilized ZrO_2 containing many microcracked grains due to large internal stresses developing on crystallographic transformation from tetragonal to monoclinic during cooling, as described by Green, Nicholson, and Embury (Ref. 12) were furnished by Prof. Nicholson. Fifteen plates of this material 6.4 mm wide x 19.2 mm long x 1.0 mm thick were bonded to NC-132 Si_3N_4 Charpy impact samples using Carbofrax 3445 phosphate bonded SiC cement. Five samples were tested at each of the three test temperatures, RT, 1250°C, and 1370°C, the results of which are given in Table VIII.

From these results it is apparent that the use of a ZrO_2 layer on Si_3N_4 leads to a 90% increase in impact strength at RT and a 25% increase at 1250°C and 1370°C. The maximum load to failure is increased slightly at all three temperatures. From the instrumented Charpy impact traces, Fig. 14, it is evident that some energy absorption on impact due to the ZrO_2 layer is occurring (compare the slope of Fig. 14a with that of Fig. 14b).

While this toughening treatment does indeed result in an increase in impact strength, the increase is still well short of the program goal of 1.35 joules. Other energy absorbing surface layers were found to have reached this goal and it was thus recommended that the ZrO_2 layer approach be dropped from further consideration. This recommendation was accepted by the NASA program manager.

3.3.4.3 Titanate Layers on Si_3N_4 and/or SiC

The basis for this approach is to create a ceramic layer that contains microcracks formed by thermal expansion anisotropy which, upon impact, will cause extensive fracturing and crushing of the layer with energy being absorbed by the creation of extensive areas of surface. $MgTi_2O_5$ and Fe_2TiO_5 were selected because of the good results obtained in previous NASA contracts (Refs. 6,7).

Samples of both magnesium and iron titanate were obtained from Prof. Richard Bradt at Penn State University and bonded to NC-132 Si_3N_4 Charpy impact samples using Norton Co. RA 1055 and 1139 alundum cements. Difficulty in bonding the titanate layers to the Si_3N_4 was encountered with both cements, although the higher fired (1300°C) 1139 cement appeared to work best. Upon impact in all cases the cement bond was broken with no titanate material remaining bonded to the Si_3N_4. Later titanate samples were bonded with Carbofrax 3445 which consists of finely divided SiC mixed with monoaluminum phosphate and water which results in a paste that, on drying at 500°F, bonds quite well to both the energy absorbing layers and the two substrates.

The results of the instrumented Charpy impact tests of titanate layers on NC-132 Si_3N_4 are presented in Table IX. In general, the Fe_2TiO_5 layers appear to absorb about the same amount of energy at RT as the $MgTi_2O_5$ but significantly more at elevated temperatures. While both titanate layers on Si_3N_4 resulted in a respectable 0.66 to 0.69 joule (5.8 to 6.1 in.-lbs) impact strength at RT, the Fe_2TiO_5 layers at 1250°C exhibited 2.56 joules (22.7 in.-lbs) of energy and at 1370°C averaged 2.14 joules (18.9 in.-lbs). These values represent an increase over Si_3N_4 controls of 470% and 440%, respectively, well over the program goal of 1.35 joules. The reproducibility of results was impressive also, with no sample being under the 1.35 joule program goal.

From the instrumented impact load vs time traces (see Fig. 15) it is evident that a large amount of energy absorption is occurring with well over half of the total impact energy being due to the crushing of the iron titanate layer, represented by the area under the first load peak in Fig. 15. The second load peak records the fracturing of the Si_3N_4 substrate. One-half of the crushed titanate layer is shown in Fig. 16. Cracks are evident extending out from the point of impact along the indent made by the Charpy hammer. A few tests were done at 1370°C using iron titanate layers on NC-203 SiC with some of the resulting impact energies close to the 1.35 joule objective, (Fig. 17). A number of the SiC samples did not exhibit the double load peak, characteristic of crushing of the titanate layer, however. This is due to the quite high load put on the piece during crushing of the titanate and is usually about 2.3 kN (500 lbs). Si_3N_4 can withstand this amount of load without breaking; however,

SiC normally cannot. The SiC sample in Fig. 17 was able to withstand the load that occurred during crushing of the titanate and thus failed at a higher load, indicated by the second load peak. However, the SiC sample shown in Fig. 18 failed during crushing of the titanate coating at a maximum load of slightly over 1.8 kN (400 lbs). The resulting impact energy was higher than SiC controls at 1370°C (0.35 joules compared to 0.11 joules) but not anywhere close to what it would have been if the SiC had not fractured. The sample shown in Fig. 17 had a high impact energy due to the titanate layer being crushed at a load somewhat less than 1.7 kN (400 lbs) and the SiC substrate being slightly stronger than normal, failing at 2.2 kN (480 lbs). Therefore, in the Charpy impact test, iron titanate layers on SiC do not offer the great improvement as seen using Si_3N_4 substrate material.

Even though the iron titanate layers on Si_3N_4 did not offer spectacular improvement in RT Charpy impact strength, the large amount of improvement at elevated temperatures argued for the continuation of this approach to the next phases of ballistic impact and modulus of rupture testing, using both Si_3N_4 and SiC substrates.

3.3.4.4 Silica-Zircon Layers on Si_3N_4 and/or SiC

A series of runs were done using a bonded layer of silica-zircon on NC-132 Si_3N_4. The silica-zircon material is 70% SiO_2 - 30% zircon by volume and is used as a core material for the casting of nickel base superalloys. The material used was made by Sherwood-TRW, Cleveland, Ohio and is approximately 60% dense. Previous experience with silica-zircon as a ceramic mold material has shown that it is very refractory but rather weak and porous and has a tendency to crush when impacted. All tests were performed using an impacting energy of 10 ft-lbs to insure that the hammer velocity was not significantly affected upon impact.

The results of the instrumented Charpy impact tests are given in Table X. Although the Charpy impact energy appeared to decrease with increasing temperature, the average at RT and 1250°C was over the program goal of 1.35 joules with one RT value being 2.56 joules. All high energy impact samples tended to fracture into a large number of fragments near the impact point. Figure 19 shows the very unusual instrumented impact trace for the 2.56 joule sample where the first energy absorbed must be due to the silica-zircon layer fracturing and the second due to the Si_3N_4 fracturing. Approximately half of the RT samples exhibited this type of curve while the other samples exhibited the type of impact trace shown in Fig. 20 for a sample exhibiting a 1.0 joule impact energy. Although the fracturing of the silica-zircon layer is not as noticeable in this instance, the fact that the energy absorbed is triple that of a Si_3N_4 control indicates that energy absorption by the cemented layer is indeed occurring.

At elevated temperatures, only one sample tested (at 1250°C) gave the characteristic double load peak curve in the instrumented impact test with a resulting energy of 2.82 joules. It appears that this energy absorbing layer is not as crushable at elevated temperatures as it is at RT. It is also possible that the load necessary to crush the layer is higher, in most cases, than the load necessary to fracture the Si_3N_4. From these results, it was found that the maximum load to crush the silica-zircon layer (first peak) was almost identical to the load to fracture the Si_3N_4 (second peak); approximately 3.1 kN (700 lbs). It is possible that the other samples tested at 1250°C and 1370°C had layers that required an even higher load to crush them.

The silica-zircon material being used consists of 65-70 w/o SiO_2 - 30-35 w/o $ZrSiO_4$ with 85% of the particle sizes being less than 44μ (-325 mesh). Upon firing the material, which is injection molded, some (or all) of the SiO_2 can transform from fused silica to cristobalite depending on the firing temperature. The cristobalite then undergoes a displacive phase transformation to low cristobalite on cooling at temperatures of 200-275°C. This transformation involves a volume change and can result in microcracking of the cristobalite grains. This microcracking could be the controlling factor in the energy absorption upon impact of the cemented silica-zircon layers. Accordingly, three silica-zircon samples that had been either initially fired or subsequently heat-treated to different temperatures were subjected to thermal expansion analysis in order to determine the relative amount of cristobalite present. The results of these tests are shown in Fig. 21. It is apparent that the UTRC sample contains no cristobalite (having been fired at 1090°C) since a smooth thermal expansion is recorded through the critical 200-275°C range (1.6×10^{-6}/°C). After heating to temperatures above 1200°C this same material was found to exhibit a pronounced volume expansion on heating through the temperature range of 200-225°C, indicative of a large amount of cristobalite formation. From Fig. 21, which also shows the heating and cooling curves for commercial Sherwood silica-zircon material, it is evident that this material contains some cristobalite in the as-received condition. After heating to slightly above 1300°C and then cooling through the cristobalite inversion temperature a large volume decrease is noted. Thus, the cristobalite content of this material has been increased greatly by heating to 1300°C.

Samples of UTRC material, fired to 1090°C, as received Sherwood material, evidently fired somewhat above 1100°C, and Sherwood material heat treated to 1200°C were then cemented to Si_3N_4 Charpy impact specimens and tested at RT, to evaluate the effect of microcracking (i.e. cristobalite formation) on energy absorption during impact. The results of these tests are given in Table XI. From these results it appears that microcracking, or amount of cristobalite present, is not a determining factor in energy absorption during impact. If

two samples with as-received Sherwood layers, whose layers did not have a chance to crush before the substrate fractured, are eliminated from the data, very little difference in either impact resistance or maximum load to fracture is noted for the three types of silica-zircon coatings. Incidentally, the porosity of all sample layers is nearly identical at about 24%. Thus, at least at RT, the mechanism responsible for the very high impact energies of Si_3N_4 with silica-zircon coatings is not obvious.

It is also not apparent at this time why these materials do not appear to be as crushable at elevated temperatures as they are at RT. Above 1200°C the silica-zircon material does tend to densify somewhat, so that material heated to the test temperatures of 1250°C and 1370°C not only would transform to a cristobalite-zircon mixture but would be somewhat less porous. In order to identify the controlling mechanism in this system, an extensive study of all the variables present such as porosity, pore size, grain size, extent of microcracking, material-cement interaction, etc. would have to be done. A study of this nature was not within the scope of the present contract; however, a microstructural characterization of the Fe_2TiO_5 and silica-zircon systems was undertaken and will be reported in a following section.

3.3.5 MOR Testing

In order to assess the degradation in strength due to the application of energy absorbing surface layers (if it exists), a series of 4-point bend tests at RT, 1250°C, and 1370°C was done with the layer side of the sample in tension. The sample dimensions were 5.08 mm (0.200 in.) by 2.54 mm (0.100 in.) by 44.4 mm (1.75 in.) long. The outer span was 38.1 mm (1.50 in.) with an inner span of 19.0 mm (0.75 in.). All layer thicknesses were approximately 1 mm.

The results of the MOR testing for NC-132 Si_3N_4 controls and with Fe_2TiO_5 and silica-zircon layers cemented with Carbofrax 3445 cement are shown in Table XII. From Table XII it can be seen that the RT 4-point bend strength of NC-132 Si_3N_4 is approximately 690 MPa (100 ksi) and is not affected by the presence of the cemented layers. The 1250°C and 1370°C 4-point MOR of NC-132 Si_3N_4 is approximately 414 MPa (60 ksi) and 228 MPa (33 ksi), respectively, and does not decrease with the cemented layers present. Thus, it can be concluded that the cementing of energy absorbing surface layers to NC-132 Si_3N_4 using Carbofrax 3445 cement does not degrade the inherent strength of the substrate material.

3.3.6 Ballistic Impact Testing

The two energy absorbing surface layers that gave Charpy impact energies over 1.35 joules when bonded to Si_3N_4 and/or SiC substrates were tested in ballistic impact at RT, 1250°C, and 1370°C, along with control samples of NC-132 Si_3N_4 and NC-203 SiC. Two types of ballistic pellets were used for the RT tests; a 4.5 mm soft steel pellet weighing 0.37 gms and a 4.4 mm hardened chrome-steel pellet weighing 0.34 gms. The procedure for testing the control samples of NC-203 SiC and NC-132 Si_3N_4 at RT was as follows. The plates of SiC or Si_3N_4 were held at one end in a vise arrangement so that a 2.54 x 2.54 x 0.64 cm (1.0 in. x 1.0 in. x 0.25 in.) thick square was available for impact. Steel pellets were fired from a modified Crossman air pistol or rifle (for higher velocities) at the center of the 2,54 cm x 2.54 cm square. Helium pressure was set at an appropriate pressure corresponding to 150 m/sec pellet velocity and the sample impacted. If the sample did not fracture, the helium pressure was raised in 50 psi increments until failure occurred. Failure always initiated on the reverse (tensile) side of the sample using the soft steel pellets. No Hertzian damage was evident (by dye penetrant inspection) on the impact surface prior to sample failure. After the sample fractured, usually into three or four large pieces, a star burst pattern of cracks emanating from the fracture origin was evident on the reverse side, especially for SiC samples as shown in Fig. 22. A few cracks were sometimes noted on the impact side also.

The results of RT ballistic impact tests on Si_3N_4 and SiC controls using soft steel pellets are given in Table XIII. As was observed from Charpy impact tests, the average ballistic impact strength of NC-132 Si_3N_4 is higher than that of NC-203 SiC, being 4.2 to 8.9 joules for Si_3N_4 and 4.2 to 5.8 joules for SiC. A typical failure is shown in Fig. 23 for NC-132 Si_3N_4. Some samples were impacted up to six times at increasingly higher energies until failure occurred. Figure 24 shows the flattened face of a steel pellet after impact, in this case the last of six pellets fired at an NC-203 SiC sample. The deformation of the pellet undoubtedly absorbs a substantial amount of the impacting energy.

Room temperature ballistic impact tests were also done with silica-zircon cemented layers on Si_3N_4 and SiC using the soft steel pellets. Thirty plates approximately 12.7 x 19.0 x 1 mm (0.50 in. x 0.75 in. x 0.040 in.) were cemented with Carbofrax 3445 onto SiC and Si_3N_4 ballistic samples. Fourteen silica-zircon on SiC and twelve silica-zircon on Si_3N_4 samples were subjected to RT ballistic impact with the initial impact velocity set at 163 m/sec for the SiC samples and 191 m/sec for the Si_3N_4 samples, which was the average failure velocity (or somewhat higher) for the controls. At impacting velocities from 163 m/sec to 259 m/sec for the silica-zircon layers on SiC, the layer shattered with the SiC sample suffering no damage, which was confirmed using Zyglo

inspection. When the silica-zircon layer shattered, a visible flash of sparks could be seen. At 178 m/sec, the pellet was not flattened but was slightly roughened with some silica-zircon material imbedded at the point of impact. At 259 m/sec, the pellet was slightly flattened with imbedded silica-zircon material in the center of the flat area, indicating that the pellet came in contact with the SiC surface. At 272 m/sec, which fractured the SiC plate, the pellet was quite roughened and flattened at the impact point. The increase in ballistic impact energy from 4.6 to 13.6 joules (a factor of 3) for SiC with the silica-zircon layer is impressive, especially considering the fact that very little increase was noted for this system in Charpy impact.

The results of the silica-zircon layers on Si_3N_4 in RT ballistic impact using soft steel pellets show that this system is similar to the silica-zircon on SiC except that the impacting energy to cause failure of the Si_3N_4 plate is somewhat higher, 16.8 joules compared to 13.6 joules, which is consistent with the higher ballistic impact energy of Si_3N_4 controls over SiC controls.

Due to the observation that substantial deformation of the soft steel pellet occurs during impact, all further ballistic testing was done using the hardened 4.4 mm chrome-steel projectiles. Thus, the ballistic testing of NC-132 Si_3N_4 and NC-203 SiC controls was redone at RT using the harder projectiles. These data, along with 1250°C and 1370°C ballistic tests on the two substrates, are presented in Table XIV. The average energy to fail the Si_3N_4 and SiC samples at RT is much less than found for the softer steel projectiles, with Si_3N_4 again giving higher values than SiC. The fracture origin at RT using the hardened pellets is almost always at the point of impact and is due to Hertzian cracking. The projectiles are flattened slightly upon impact, but not nearly as much as the softer Crossman pellets.

The elevated temperature (1250°C and 1370°C) ballistic impact testing of NC-203 SiC and NC-132 Si_3N_4, both with and without energy absorbing surface layers, was done the same as that described for ballistic testing at RT except that the samples were heated to the test temperature on the reverse side with an oxyacetelene torch arrangement. Temperatures were read on the front or impact face of the sample with an optical pyrometer. All elevated temperature ballistic testing was done using 0.34 gm, 4.4 mm, hardened chrome-steel ball bearings. It was initially found that NC-203 SiC could not withstand the stresses developed due to the thermal gradient obtained in the sample on heating. Even when the torch was moved toward the SiC samples very slowly, fracture resulted when the temperature at the impact zone reached approximately 1200°C. At this temperature, the part of the sample in the vise is just starting to glow red, so the ΔT is approximately 400-500°C. However, with a refinement in the torch arrangement to reduce this ΔT, it became possible to reach 1250°C without fracturing the SiC but attempts to reach 1370°C were unsuccessful.

The results of the 1250°C and 1370°C ballistic impact tests on NC-132 Si_3N_4 controls given in Table XIV show that the ballistic impact strength of Si_3N_4 is greater at 1250°C than RT (3.3 joules to 1.9 joules) falling off slightly at 1370°C to 2.8 joules. Whereas the predominant mode of failure at RT for Si_3N_4 impacted with the hardened steel balls was Hertzian failure, at elevated temperatures the mode of failure is about equally divided between Hertzian failure and tensile failure on the reverse side of the sample.

The results of ballistic impact tests at RT, 1250°C, and 1370°C of Fe_2TiO_5 layers on Si_3N_4 are given in Table XV. It can be seen that the 1250°C impact energy of 12.5 joules and the 1370°C impact energy of 15.4 joules represent a four to fivefold improvement in fracture energy over the Si_3N_4 controls at these temperatures (3.3 and 2.8 joules, respectively). That the 1370°C ballistic impact energy of Fe_2TiO_5 layers on Si_3N_4 is higher than that at 1250°C is not surprising, since at the higher temperature the Fe_2TiO_5 is becoming quite plastic and ductile and it is energy absorption due to plastic flow, and not microcracking, that is now believed to be the mechanism responsible for energy absorption in this system at elevated temperatures. This was demonstrated by impacting a nonheat-treated Fe_2TiO_5 layer on Si_3N_4 at 1370°C at 260 m/sec (11.4 joules) with no damage to the Si_3N_4 substrate. The Fe_2TiO_5 in this case should not have been microcracked in the as-fabricated condition.

It is interesting to contrast the impact characteristics of the Fe_2TiO_5-Si_3N_4 system at different impacting velocities. Figure 25 shows a sample after a 202 m/sec impact at 1250°C. It can be seen that the Fe_2TiO_5 layer is completely shattered; however, some of the Carbofrax cement is still adhering to the surface of the Si_3N_4 and, at the point of impact, a cone shaped mass of crushed Fe_2TiO_5 is evident. At higher velocities, as shown in Fig. 26 for sample 132-BI-51 at 260 m/sec, the cement has been blown away and the Fe_2TiO_5 at the point of impact is now only slightly evident. Also, at higher velocities the steel ball shows evidence of contact with the Si_3N_4, being somewhat flattened with Fe_2TiO_5 imbedded in the ball at the point of impact. At very high velocities where the Si_3N_4 fractures, as shown in Fig. 27 for sample 132-BI-52 impacted at 282 m/sec at 1250°C, it is found that Hertzian stresses are sufficient to initiate fracture at the point of impact.

Table XVI gives the results of ballistic impact tests of silica-zircon layers on Si_3N_4 at RT, 1250°C, and 1370°C. It can be seen that an impact velocity of over 300 m/sec was necessary to fail Si_3N_4 at both elevated temperatures. The impact energies for failure of the Si_3N_4 of 17.2 joules at 1250°C and 19.0 joules at 1370°C represent a fivefold and sevenfold improvement over the respective Si_3N_4 control values and approximately double the RT impact energy noted for silica-zircon layers on Si_3N_4 (9.1 joules). In this case, it is thought that the controlling mechanism for energy absorption is crushing

of the silicon-zircon due to porosity and not microcracking. The increase in ballistic impact energy of the silica-zircon layers on Si_3N_4 at elevated temperatures over that at RT is most likely due to the increased resistance of the Si_3N_4 substrate to ballistic impact at elevated temperatures. Si_3N_4 control values are 1.9 joules, 3.3 joules, and 2.8 joules at RT, 1250°C, and 1370°C, respectively.

Figures 28 and 29 contrast the ballistic impact results for silica-zircon layers on Si_3N_4 at RT and 1370°C and 230 m/sec and 315 m/sec impacting velocities, respectively. At RT and 230 m/sec (Fig. 28) the sample fractured with obvious Hertzian failure of the Si_3N_4 while at 1370°C and 315 m/sec (Fig. 29) the sample is undamaged except for the loss of the silica-zircon layer. The difference in size of the imprint made by the steel ball can be clearly seen on the surface of the two samples, reflecting the difference in impact velocity. The higher the impact velocity, the greater the amount of flattening of the soft ball, thus the larger the contact area on the sample surface.

Table XVII gives the 1250°C ballistic impact results for NC-203 SiC with Fe_2TiO_5 and silica-zircon layers. As with these layers on Si_3N_4, a four to fivefold improvement in impact energy over the SiC control values at 1250°C is observed. Reflecting the much lower impact resistance of NC-203 SiC compared to NC-132 Si_3N_4, the samples with surface layers still fracture at about half or less of the fracture energy it takes to fail either Fe_2TiO_5 or silica-zircon layers on Si_3N_4 at this temperature. Thus, from the results of both Charpy and ballistic impact tests at RT and elevated temperatures it is apparent that SiC, at least Norton NC-203, is much inferior to Si_3N_4 in impact resistance and thus is not a good candidate to explore the application of energy absorbing surface layers to achieve optimum impact properties.

3.4 Task II - Effect of Thermal Exposure on Toughness Improvement Retention

Charpy impact samples of silica-zircon and Fe_2TiO_5 layers on both Si_3N_4 and SiC were subjected to thermal cycling between RT and 1370°C. A thermal cycle consisted of heating from RT to 1370°C in approximately 10 min in a resistance heated air furnace, holding at 1370°C for 1 hr, and then cooling to RT in approximately 15 min. The results of these tests were very discouraging. All layer-substrate combinations began to fail after one cycle and completely failed after three cycles. Failure consisted, in most cases, of the separation of the bonding cement and the Si_3N_4 or SiC substrate. Some of the Fe_2TiO_5 layers also exhibited debonding between the Fe_2TiO_5 and the Carbofrax 3445 cement. Figure 30 shows a sample of silica-zircon on Si_3N_4 after undergoing one cycle with debonding between the Carbofrax 3445 cement and the Si_3N_4 quite evident. Figure 31 shows a similarly exposed sample of Fe_2TiO_5 on Si_3N_4 with debonding beginning to occur at both cement interfaces. Charpy impact testing of the samples was not performed since none of the energy absorbing surface layers remained adhered to the substrates.

Provisions of the contract called for isothermal exposure of treated specimens if thermal cycling was not feasible. Accordingly, samples of silica-zircon and Fe_2TiO_5 on Si_3N_4 and SiC substrates were heat treated in air at 1370°C for 50 hrs. After this treatment the furnace was allowed to cool slowly by shutting the power off. It was observed that the iron titanate layers debonded from the samples at temperature while the silica-zircon layers remained bonded until the samples were removed from the furnace at approximately 300°C. When the samples were set on a laboratory bench to cool from 300°C to RT it was observed that very suddenly all the silica-zircon layers, with the cement attached, began to lift up from the substrates (Fig. 32). Apparently, the thermal contraction of the silica as it passes through the high to low cristobalite transformation at 200-275°C was great enough to break the quite weak bond between the substrate and the cement.

An additional heat treatment in air was done for the shorter time of 24 hrs at 1370°C with similar results for the Fe_2TiO_5 layers but a few of the silica-zircon layers remained bonded after heat treatment. One of these, a sample of silica-zircon on Si_3N_4, was subjected to a RT instrumented Charpy impact test. The resultant impact energy was 0.24 joules (2.2 in.-lbs) with a maximum load to failure of 1.9 kN (430 lbs). After impact, the layer remained cemented to the Si_3N_4. From this test it would be very difficult to determine whether or not the silica-zircon layer was still capable of absorbing energy on impact since after 24 hrs at 1370°C the Si_3N_4 itself is so weak, as shown previously, that the maximum load is not high enough to allow crushing of the layer to occur. Some energy absorption due to the layer may have occurred, however, since the average impact energy and maximum load of an oxidized (24 hrs at 1370°C) NC-132 Si_3N_4 control is 0.14 joules and 2.0 kN, respectively. The fracture origin of the sample with the silica-zircon layer was a surface pit formed during oxidation of the NC-132 Si_3N_4.

It appeared obvious, therefore, that the titanate and silica-zircon materials possessed too large a difference in thermal expansion coefficient between themselves and the Si_3N_4 and/or SiC substrate materials to be useful in any applicating requiring thermal cycling. It also became apparent that the degradation in strength of commercial hot-pressed Si_3N_4 after high temperature thermal exposure would limit its usefulness as a substrate for energy absorbing surface layers when exposed to temperatures over 1200°C for longer than a few hours. In addition, whether or not microcracking plays a significant role in the energy absorption noted for the titanate and silica-zircon materials was unresolved. It was thus decided to microstructurally characterize the two materials in order to decide whether or not the emphasis of the program should be shifted to other materials possessing thermal expansion coefficients more closely matching the Si_3N_4 substrate.

3.5 Iron Titanate and Silica-Zircon Microstructural Characterization

In order to evaluate the question of whether or not microcracking is playing a significant role in the energy absorption noted for the Fe_2TiO_5 and silica-zircon layers, a transmission electron microscope examination of both materials was done. An iron titanate sample, heat treated for 24 hrs at 1200°C to cause grain growth and microcracking due to thermal expansion anisotropy, is shown in Fig. 33. This sample consists largely of equiaxed grains, 2-20μ in size, with a powdery appearing second phase which often resided at triple-point areas. No attempt was made to identify the second phase.

According to R. C. Bradt (Ref. 13) Fe_2TiO_5 material of this grain size with thermal expansion coefficients of $0.6 \times 10^{-6}/°C$ in the a direction, $10.1 \times 10^{-6}/°C$ in the b direction, and $16.3 \times 10^{-6}/°C$ in the c direction, should exhibit extensive intergranular microcracking on cooling from the heat-treating temperature. It is difficult to substantiate this for the Fe_2TiO_5 material used in this program, as shown in Fig. 33; however, the existence or nonexistence of microcracks appears to be a moot point since energy absorption occurs in this material whether it is heat-treated or not as previously mentioned. It is believed that the major amount of energy absorption at elevated temperature in this material is due to plastic flow.

A typical TEM of a replica from the silica-zircon material used in this program is shown in Fig. 34. The large grains are mainly fused silica while the smaller ones are mainly zircon. Very little cristobalite was observed and thus very few grains were microcracked. If this material is heat-treated at 1200°C for 1 hr, however, the fused silica recrystallizes to cristobalite, as shown in Fig. 35. Recrystallization appeared to be more complete nearer the particle boundaries where well formed equiaxed grains were evident. At the interiors of larger particles, the microstructure exhibited a more feathery looking appearance and often contained extensive microcracks, as shown in Fig. 36. Diffraction analysis performed on grains dislodged from the recrystallized phase confirmed its identity as α-cristobalite. Smaller etch resistant particles, residing at the SiO_2 particle boundaries, were found to be zircon ($ZrSiO_4$) with the mottled looking areas being porosity, as shown in Fig. 37. Again, as in the case of Fe_2TiO_5, the existence of microcracking does not appear to be a prerequisite for energy absorption on impact, as previously shown, and in this case the porous nature of the silica-zircon material is thought to be the controlling factor.

Since microcracking does not appear to play a significant role in the energy absorption noted for the various systems studied, it was decided to concentrate further efforts on porous coatings on Si_3N_4 that possess similar thermal thermal expansion coefficients, such as low density sintered Si_3N_4 and reaction bonded Si_3N_4.

3.6 Task III - Evaluation of Porous Si_3N_4 Layers on Dense Si_3N_4

It has become obvious that, for a Si_3N_4 or SiC sample with an energy absorbing surface layer to withstand the thermal cycling occurring in a gas turbine environment, the layer must have a similar thermal expansion coefficient to the substrate, and also that microcracking does not appear to be the mechanism governing the large energy absorption occurring during impact of Fe_2TiO_5 and silica-zircon layers on Si_3N_4 and/or SiC. Therefore, an eight month extension to the contract was added in order to investigate materials that have sufficient porosity so that crushing and energy absorption will occur upon impact and yet have low coefficients of thermal expansion similar to that of hot-pressed Si_3N_4. Silicon nitride (Norton NC-132) was chosen as the substrate material since it has been shown that commercially available SiC does not have the impact properties necessary to fully evaluate an energy absorbing surface layer, especially in Charpy impact. Low density reaction sintered Si_3N_4 was chosen as the primary energy absorbing surface layer.

3.6.1 Fabrication of Specimens

After a few initial efforts at bonding plates of reaction-sintered Si_3N_4 to hot-pressed Si_3N_4 using a refractory cement, it was decided to concentrate efforts on forming the reaction sintered Si_3N_4 layer in situ on the hot-pressed Si_3N_4 substrate by nitriding a layer of silicon metal powder.

The procedure used to form the porous reaction sintered Si_3N_4 layers was as follows. The Si powder was made into a thick slurry using toluene as the carrier liquid with 4 wt % polystyrene dissolved in it for additional green strength. In some cases, deionized water was used as the carrier liquid. Both Charpy and ballistic samples of NC-132 Si_3N_4 were then coated with 1.0 to 1.2 mm of the slurry on one face only and then allowed to dry overnight at a temperature of about 150°C. The samples were then loaded into Mo boats with loose fitting lids and placed in a horizontal tube furnace. The nominal firing cycle consisted of 16 hrs at 1100°C in flowing argon, 16 hrs at 1250°C in very slowly flowing nitrogen, and then 60 hrs at 1375°C in nitrogen. A few nitriding runs were done using a temperature of 1325°C for the final 60 hr step. After nitriding, all samples were slightly ground with a diamond wheel so that all energy absorbing R.S. Si_3N_4 surface layers were flat with a uniform thickness of 1.0 mm.

Initially, three different types of R.S. Si_3N_4 surface layers were investigated by using three different mesh size starting silicon powders: a rather coarse -100, +200 mesh Si to produce a R.S. Si_3N_4 layer with high porosity and large particle and pore size; a medium particle size - 200 mesh Si to produce a somewhat denser R.S. Si_3N_4 with smaller particle and pore size; and a fine

-325 mesh Si to produce a fairly dense R.S. Si_3N_4 surface layer. It was found that a nitriding cycle with a maximum temperature of 1325°C for 60 hrs was not sufficient to completely nitride any of the silicon layers with the -325 Si layers containing about 5 vol % unreacted Si, the -200 Si layers containing at least 10 vol % unreacted Si, and the -100, +200 Si layers containing over 25% unreacted Si. It was found that the 1375°C, 60 hr maximum nitriding step was sufficient to completely nitride the -325 and -200 Si layers, but still left some unreacted Si in the interior of the large -100, +200 Si grains. A typical interface between a nitrided -325 Si layer and NC-132 Si_3N_4 is shown in Fig. 38 while that between a nitrided -100, +200 Si layer and NC-132 Si_3N_4 is shown in Fig. 39. The darker grey areas in the R.S. Si_3N_4 layer consist of mounting material filling in the interconnected porosity. The porosity of the three types of R.S. Si_3N_4 layers was found to be approximately 45% for -100, +200 Si layers, 35% for -200 Si layers, and 30% for -325 Si layers.

3.6.2 Charpy Impact Testing

Instrumented Charpy impact tests were done at RT and 1370°C on samples of NC-132 Si_3N_4 with R.S. Si_3N_4 surface layers fabricated from -325 Si, -200 Si, and -100, +200 Si, nitrided at a maximum temperature of 1375°C. Charpy impact tests were also done on samples of R.S. Si_3N_4 fabricated from -325 Si and -200 Si that were nitrided at 1325°C maximum. The results of the latter tests were very similar to the results from 1375°C nitrided samples, which are presented in Table XVIII. Five samples of each type were impacted at the two temperatures.

The Charpy impact energies recorded for the nitrided -325 Si and -200 Si surface layers on NC-132 Si_3N_4 at RT are slightly higher than control values (0.40 joules) with the 1370°C Charpy impact energy for the -325 Si layer also being higher than comparable controls (0.40 joules) while that recorded for the nitrided -200 Si layers at 1370°C is somewhat lower than NC-132 Si_3N_4 controls. A typical RT instrumented Charpy impact trace for a -200 Si nitrided sample is shown in Fig. 40 and it is evident that very little crushing of the R.S. Si_3N_4 layer is occurring.

In contrast to the nitrided -325 Si and -200 Si layers on NC-132 Si_3N_4, the higher porosity nitrided -100, +200 Si layers on NC-132 Si_3N_4 exhibited quite respectable Charpy impact energies at RT and 1370°C (Table XVIII). While not reaching the program goal of 1.35 joules (1 ft-lbs) the impact energies of this system are 2 1/2 times Si_3N_4 controls at RT and slightly over twice that recorded for Si_3N_4 controls at 1370°C. A typical RT instrumented Charpy impact trace for this system is shown in Fig. 41 and it is evident from the load curve that crushing of the R.S. Si_3N_4 layer is occurring. The elevated temperature instrumented impact curves are very similar to Fig. 41. All of the samples

retained a good portion of their layers upon impact, indicating a fairly good layer to substrate bond. It was also noted that at the point of impact a definite dent in the porous R.S. Si_3N_4 layer was evident.

3.6.3 Ballistic Impact Testing

Ballistic impact tests were done on NC-132 samples with 1 mm thick nitrided -100, +200 Si and -200 Si surface layers at RT and 1370°C and on nitrided -325 Si surface layers at RT and 1250°C. All samples were nitrided at a maximum temperature of 1375°C. All tests were done using 4.4 mm chrome-steel projectiles.

The results of RT and 1370°C ballistic impact tests on -100, +200 Si reaction-sintered Si_3N_4 layers on NC-132 Si_3N_4 samples are given in Table XIX. It can be seen that six times the amount of energy can be absorbed at RT with no failure for the samples with R.S. Si_3N_4 layers compared to Si_3N_4 controls (11.4 joules compared to 1.9 joules). At the lower impact velocity of 191 m/sec part of the R.S. Si_3N_4 layer remained adhered to the sample after impact. The impact energy of 13.6 joules required to fail the Si_3N_4 substrate is substantially greater than the 9.1 joules of impact energy that was necessary to fail the samples with silica-zircon layers on NC-132 Si_3N_4. The impact energy necessary to fracture the Si_3N_4 substrate at 1370°C is also 13.6 joules, which at 1370°C is five times that necessary to fail Si_3N_4 control samples (2.8 joules). At the two lower velocities the layer remained adhered to the substrate after impact, being damaged only at the point of impact. The sample impacted at 230 m/sec is shown in Fig. 42. This type of impact behavior is very desirable, since the sample still retains most of its energy absorbing surface layer and could thus be expected to withstand multiple impacts as long as they did not occur at identical positions. Even the sample impacted at 282 m/sec retained a significant portion of its R.S. Si_3N_4 layer, although the Si_3N_4 substrate fractured at this velocity (Fig. 43).

The results of RT and 1370°C ballistic impact tests on NC-132 Si_3N_4 with nitrided -200 mesh Si powder surface layers are given in Table XX. Comparing these results to those obtained for the more porous -100, +200 nitrided Si layer, it can be seen that, unlike the Charpy impact results, the ballistic impact energy needed to fracture the Si_3N_4 substrate at RT and 1370°C is essentially the same for both types of R.S. Si_3N_4 surface layers. The sample impacted at RT at 191 m/sec is shown in Fig. 44. In this case, even though the R.S. Si_3N_4 layer exhibits good bonding to the substrate, the force of the ballistic impact has blown over half of the R.S. Si_3N_4 layer away.

The fabrication of nitrided -325 mesh Si layers on ballistic impact samples of NC-132 Si_3N_4 was found to be extremely difficult using toluene plus dissolved polystyrene as the carrier fluid for the silicon powder slurry. During the drying process, the shrinkage of the 1 mm thick layer was sufficient to debond the layer from the NC-132 Si_3N_4 substrate. After nitriding, R.S. Si_3N_4 layers that debonded during drying were found to have extremely poor adherence to the NC-132 Si_3N_4 substrate. Reducing the amount of dissolved polystyrene from 4 wt % to 1 wt % appeared to alleviate the problem somewhat, but not completely. Some of the samples still tended to debond during drying.

The results of RT and 1250°C ballistic impact tests on nitrided -325 Si layers on NC-132 Si_3N_4 that were somewhat weakly bonded are given in Table XXI. From Table XXI, it can be seen that the ballistic impact resistance of the denser -325 Si nitrided layers on Si_3N_4 is greater than Si_3N_4 controls, especially at RT (6.2 joules compared to 1.9 joules), but is much less than that recorded previously for both -100, +200 Si and -200 Si nitrided layers on NC-132 Si_3N_4. Figure 45 shows a sample of -325 Si nitrided surface layer impacted at 1250°C, 169 m/sec, that clearly indicates crushing of the R.S. Si_3N_4 surface layer on impact. However, at higher velocities the nitrided -325 Si layer did not appear to slow down the ballistic projectile enough so that by the time it reached the substrate the kinetic energy was still great enough to fracture the NC-132 Si_3N_4. It appears, that to be effective in absorbing energy during a ballistic impact event, an energy absorbing surface layer must be crushable but must also be somewhat resistant to penetration. From the work done on -100, +200 Si, -200 Si, and -325 Si nitrided surface layers on NC-132 Si Si_3N_4, a combination of porosity and fairly large pore and particle size appear to satisfy these conditions.

3.6.4 Artificially Introduced Porosity

In order to determine if the large pore size and not the large grain size present in the nitrided -100, +200 Si layers was responsible for the observed increase in both Charpy and ballistic impact resistance of these layers on NC-132 Si_3N_4 over that for NC-132 Si_3N_4 controls, -325 mesh Si powder was mixed with 10 vol %, 20 vol %, and 40 vol % polystyrene microspheres in a deionized water solution. The microspheres ranged in size between 44μ and 105μ. The -325 Si plus polystyrene sphere mixture was slurry coated on NC-132 Si_3N_4 substrates, both Charpy and ballistic impact specimens, and was then nitrided at temperatures to 1375°C. The polystyrene was decomposed during heat up in argon to the initial hold temperature of 1100°C.

The results of the Charpy impact tests on NC-132 Si_3N_4 with nitrided -325 Si mixed with either 10, 20, or 40 vol % polystyrene microspheres are given in Table XXII. The samples with -325 Si + 40% polystyrene microspheres R.S. Si_3N_4 layers were extremely porous and very weakly bonded to the NC-132 Si_3N_4 substrate. Figure 46 shows a cross-section of one of these layers with the light gray areas being Si_3N_4 and the darker gray areas being infiltrated resin used for polishing purposes. It is apparent that the porosity of these layers is well over 50%. Although some increase in impact energy occurred using these coatings, better results were obtained with the 20 vol % polystyrene mixture. The three samples tested at RT with -325 Si + 20 vol % polystyrene R.S. Si_3N_4 layers gave an average impact energy of 0.86 joules (7.6 in.-lbs) compared to the control values for NC-132 Si_3N_4 of 0.40 joules (3.5 in.lbs). Figures 47a and 47b show the RT Charpy instrumented impact traces for a Si_3N_4 control and for a sample with -325 Si + 20% polystyrene spheres, respectively. The shape of the load curve in Fig. 47b indicates that crushing of the R.S. Si_3N_4 layer and energy absorption during impact is occurring. Figure 48 shows a cross-section of a -325 Si + 20% polystyrene nitrided layer with the positions once occupied by the polystyrene spheres now being voids, i.e. filled in with resin in the polished sample. The porosity is quite high (~45%) and is a combination of large and small pores. The interfacial bonding is quite weak for the 20 and 40 vol % polystyrene samples but fairly good for the 10 vol % polystyrene R.S. Si_3N_4 layers, which were tested both at RT and 1370°C. Although the interfacial bonding was quite good for the latter samples, the Charpy impact energy at RT is increased by only 35% over that recorded for Si_3N_4 controls, with almost no increase at 1370°C.

Ballistic impact tests using 4.4 mm diameter hardened chrome-steel spheres were performed at RT and 1250°C on NC-132 Si_3N_4 plates with 1 mm thick R.S. Si_3N_4 layers containing 20 vol % and 10 vol % polystyrene spheres prior to nitriding, which results in porosities of approximately 45% and 40%, respectively. The results of these tests are shown in Table XXIII. It can be seen that both types of R.S. Si_3N_4 layers on NC-132 Si_3N_4 could withstand a ballistic impact at RT of 6.2 joules (4.6 ft-lbs) with no damage to the NC-132 Si_3N_4 substrate, but any impact energy over that resulted in substrate fracture. The 1250°C impact energy of 4.9 joules with no damage to the NC-132 Si_3N_4 substrate is somewhat lower than that recorded at RT but still higher than that for Si_3N_4 controls at 1250°C (3.3 joules).

It is interesting that while the -325 Si + 20 vol % polystyrene nitrided layers gave good results for RT Charpy impact, they were not particularly impressive in ballistic impact. It appears that the large spherical pores in this material lead to crushing and energy absorption during the low velocity Charpy impact event but the material is just too porous to build up sufficient resistance to the high velocity steel ball as it penetrates the R.S. Si_3N_4

layer during the ballistic test. Even though the porosity simulates that of a -100, +200 mesh Si layer, the particle size is much smaller. It is possible that the large particle size of the -100, +200 mesh nitrided Si layer is necessary for optimum energy absorption during a high velocity impact. It is obvious that porosity and pore size are not the sole controlling factors.

During the investigation of artificially introduced porosity in the R.S. Si_3N_4 layers, it was found that the use of water to make the silicon powder slurry, which is necessary so that the polystyrene spheres do not dissolve in the normally used toluene, resulted in ballistic impact properties for nitrided -200 Si and -100, +200 Si layers that were different from previous results. The use of water instead of toluene to form the silicon powder slurry was found not to affect the ballistic impact properties of nitrided -325 Si layers, although the interfacial bonding was usually better for the water slurry layers. Both types of slurries resulted in RT ballistic impact energies of 6.2 joules for the nitrided -325 Si layers on NC-132 Si_3N_4. However, whereas the nitrided -100, +200 Si and -200 Si layers on NC-132 Si_3N_4 gave ballistic impact energies at RT of 8.4 to 9.1 joules using toluene slurries, water slurry layers of the same mesh Si powders resulted in RT impact energies of only 4.9 to 6.2 joules without the NC-132 Si_3N_4 substrate fracturing.

Since the nitriding conditions were identical for both types of slurry layers and, from X-ray diffraction data taken on nitrided -100, +200 Si layers using the two different slurry medias, both types exhibited identical compositions (~55% β-Si_3N_4, 40% α-Si_3N_4, and 5% unreacted Si), the difference in impact behavior is surprising. However, the morphology of the layers appears to be different, at least for nitrided -100, +200 Si layers, as can be seen by comparing Fig. 49 (-100, +200 Si, water slurry) to Fig. 39 (-100, +200 Si, toluene slurry). The water slurry layer appears to have a more closely packed, skeletal structure than the toluene slurry layer with the interiors of the larger grains appearing to be hollow. Figure 50a shows a scanning electron micrograph of a fracture surface of a nitrided -100, +200 Si layer made with a water slurry, while Fig. 50b shows a fracture surface of a nitrided -100, +200 Si layer fabricated with a toluene slurry. The water slurry sample appears to consist of a denser skeletal R.S. Si_3N_4 structure with less dense areas in between while the toluene slurry sample appears to consist of islands of dense material interconnected by areas of porosity that is filled with a network of whiskers, most likely α-Si_3N_4. Figures 51a and 51b show the same surfaces in closer detail. It is possible that the water slurry R.S. Si_3N_4 layers experienced an over temperature during nitriding that allowed the unreacted Si to melt, which could account for the skeletal structure with hollow appearing grains. The packing density of the silicon particles could also have been different for the two slurries since it was noticed that the water slurries dried slower than the toluene slurries. The whole area of the effect of slurry media on the resistance to ballistic impact of the resulting R.S. Si_3N_4 layer needs to be investigated in more detail.

3.6.5 Mixed Particle Size R.S. Si_3N_4 Layers

A brief investigation was performed to evaluate the Charpy and ballistic impact properties of R.S. Si_3N_4 layers that were fabricated from mixtures of -325 Si and -100, +200 Si. This type of R.S. Si_3N_4 surface layer could be expected to contain large particle size material, similar to the nitrided -100, +200 Si layers, but have varying amounts of the large pores filled with the fine particle size nitrided -325 mesh Si. Initial compositions studied, using a water slurry, consisted of 90 vol % -100, +200 Si, 10 vol % -325 Si and 70 vol % -100, +200 Si, 30 vol % -325 Si.

The results of RT and 1250°C ballistic impact tests on nitrided mixtures of -100, +200 Si and -325 Si on NC-132 Si_3N_4 are given in Table XXIV. The ballistic impact resistance for both compositions was in the 3.7 to 4.9 joule range at RT and 1250°C, far less than that obtained previously for nitrided -100, +200 Si layers. When it was discovered that using water based slurries produced lower ballistic impact results than the previously used toluene slurries, a further series of samples of composition 80% -100, +200 Si, 20% -325 Si was fabricated using the toluene slurry method. The results of RT and 1370°C Charpy and ballistic impact tests on these samples are given in Tables XXV and XXVI, respectively. As found previously for R.S. Si_3N_4 surface layers fabricated from -100, +200 Si, the Charpy impact strength at RT is increased significantly over NC-132 Si_3N_4 controls while the 1370°C Charpy impact strength is only slightly increased. Bonding at the R.S. Si_3N_4/NC-132 Si_3N_4 interface was found to be quite strong.

The ballistic impact resistance at RT of 9.1 joules and at 1370°C of 13.6 joules for the 80% -100, +200 Si, 20% -325 Si composition R.S. Si_3N_4 layer on NC-132 Si_3N_4 (Table XXVI) is as high, or higher, than obtained previously for the -100, +200 Si nitrided surface layers. It appears, at least in ballistic impact, that filling the large voids between the nitrided -100, +200 Si grains with small grains of nitrided -325 Si does not adversely affect the ability of the layer to absorb energy upon impact and that the large grain size of the nitrided -100, +200 Si layers, or possibly the fairly large amount of unreacted silicon present, is the controlling factor for energy absorption.

3.6.6 R.S. Si_3N_4 - NC-132 Si_3N_4 Interfacial Strength Degradation

In order to evaluate the effect of the R.S. Si_3N_4 energy absorbing surface layers on the strength of the NC-132 Si_3N_4 when the interface between the R.S. Si_3N_4 and the NC-132 Si_3N_4 is subjected to tensile (bending) stresses, a series of Charpy impact tests were performed with the samples impacted on the side opposite the R.S. Si_3N_4 layer. Some of the samples were subjected to various oxidizing treatments in order to evaluate their effect on the interfacial bond strength. The results of the instrumented Charpy impact tests are given in Table XXVII.

From Table XXVII, it can be seen that all -100, +200 Si and -200 Si nitrided layers on unoxidized Si_3N_4 substrates degraded the R.S. Si_3N_4 - H.P. Si_3N_4 interface such that very low impact energies and maximum loads to failure resulted. A slow bend test on a -100, +200 mesh layered sample verified this degradation with a RT MOR value of 406 MPa (58.9 ksi) as compared to control values for NC-132 Si_3N_4 averaging 930 MPa (135 ksi). Preoxidized -200 mesh samples showed some loss in impact properties but preoxidized -325 mesh samples did not.

In Table XXVII the relative strength of the interfacial bond is characterized as either good, fair, or poor. A good bond was one where, upon impact, the R.S. Si_3N_4 layer remained completely adhered to the NC-132 Si_3N_4 substrate. A fair bond was one that resulted in part of the R.S. Si_3N_4 layer breaking away from the substrate and a poor bond was characterized as complete debonding between the R.S. Si_3N_4 layer and the NC-132 Si_3N_4 substrate. It can be seen that a poor interfacial bond always resulted in a relatively undegraded impact energy while well bonded samples always exhibited a large loss in impact energy.

A number of observations can be made from the tests done to date. It is apparent that the preoxidizing treatment of the NC-132 Si_3N_4 results in a subsequently weak bond between the NC-132 and either the -325 or -200 Si layers, and as a result of the weak bonding there is very little degradation of the NC-132 Si_3N_4 during the nitriding step. The post-oxidizing treatment of 1300°C in air for 1 hr after nitridation appears to increase the bonding between the NC-132 Si_3N_4 and the R.S. Si_3N_4 layer but also appears to lead to some degradation of the NC-132 Si_3N_4. A combination of the two oxidizing treatments appears to increase the interfacial bonding over that obtained for the preoxidizing treatment alone but offers no advantage over no oxidizing treatment at all. Finally, it is apparent that the samples with -325 Si layers are not degraded in strength as much as similarly treated samples with -200 Si layers, but with a sacrifice in interfacial bonding. Generally, it can be said that the better the interfacial bond, the more the interfacial degradation.

Figures 52 and 53 show the fracture surface and fracture origin, respectively, of sample 132-318 which has a -325 Si layer on NC-132 and has been post-oxidized for 1 hr at 1300°C. A relatively flat fracture surface is evident, indicative of a low impact strength, with the fracture origin appearing to be located at or near the layer-substrate interface but not occurring at an obvious flaw. No direct evidence of internal oxide formation is apparent from either fracture surface examination or polished cross-sections. However, X-ray analysis of crushed -325 Si nitrided layers that have been subjected to the 1 hr, 1300°C oxidation indicate a small amount of SiO_2 formation.

Figures 54 and 55 show the fracture surface and fracture origin, respectively, of sample 132-325 which has a nitrided -200 Si layer on NC-132 and which exhibited very strong interfacial bonding but very low impact energy when impacted on the side opposite the R.S. Si_3N_4 layer. The very flat fracture surface is again indicative of a low impact strength, with the fracture origin being similar to that of sample 132-318, (Figs. 52,53) i.e. at or near the interface but not associated with an obvious flaw.

The cause of the interfacial degradation of well bonded samples of R.S. Si_3N_4 on NC-132 Si_3N_4 can only be speculated upon at this time. It is possible that it is due entirely to the large pores in the R.S. Si_3N_4 layer near the interface acting as stress concentrating flaws. If so, minimizing pore size at the R.S. Si_3N_4/H.P. Si_3N_4 interface by using a graded density R.S. Si_3N_4 layer should help alleviate this problem. The large pores will still act as stress concentrating flaws but the cracks caused by them should undergo branching and deflection on passing through the underlying denser R.S. Si_3N_4 material. Using very fine Si powder in a thin layer at the interface with a gradation to quite coarse Si powder for the bulk of the R.S. Si_3N_4 layer should combine good interfacial bonding, good ballistic impact resistance, and possibly minimal interfacial strength degradation. Palm (Ref. 9) found, during an investigation of porous energy absorbing surface layers of SiC formed in situ on dense SiC, that the bend strength was not degraded for samples that had SiC surface layers with pore sizes that appear to be approximately 0.025 mm (1 mil). These pore sizes are about 4 to 5 times less than present in a nitrided -100; +200 Si layer. Using a -500 mesh Si powder at the R.S. Si_3N_4/NC-132 Si_3N_4 interface would yield approximately a 0.025 mm pore size.

It is also possible that reactions at the R.S. Si_3N_4/NC-132 Si_3N_4 interface during the nitriding process may be causing pitting of the NC-132 Si_3N_4 surface, similar to that occurring during NC-132 Si_3N_4 oxidation at temperatures over 1200°C. Impurities such as Mg, Ca (etc.) present in the NC-132 Si_3N_4 could be concentrating at the interface and reacting with Si, forming stress concentrating flaws or inclusions. In any case, a more thorough investigation of the R.S. Si_3N_4/NC-132 Si_3N_4 interface is required to clarify the situation.

3.6.7 Thermal Cycling of R.S. Si_3N_4 layers on NC-132 Si_3N_4

As reported in a previous section of this report, the major problem with titanate and silica-zircon energy absorbing surface layers on NC-132 Si_3N_4 was that they could not withstand thermal cycling due to the large difference in thermal expansion between these layers and hot-pressed Si_3N_4. Since the thermal expansion coefficient of reaction sintered Si_3N_4 and hot-pressed Si_3N_4 are

reported to be identical (Ref. 14) it was anticipated that thermal cycling of R.S. Si_3N_4 energy absorbing surface layers on NC-132 Si_3N_4 should not lead to interfacial debonding or cracking due to stresses developed during cycling. Accordingly, both Charpy and ballistic impact tests were performed on NC-132 Si_3N_4 control samples and samples with various R.S. Si_3N_4 surface layers that had been subjected to 50 cycles between approximately 200°C and 1370°C in air. The thermal cycling apparatus consisted of a platform that automatically cycled in and out of a resistantly heated air furnace, taking 15 min to heat from ~200°C to 1370°C, holding at 1370°C for 5 min, and then cooling from 1370°C to ~200°C in 10 min. Even with fans blowing ambient air on the samples when they emerged from the furnace, it was found impossible to cool them to much less than 200°C and keep the cycle time less than 45 min, due to the large heat retention of the ceramic pedestal that the samples rested upon.

The results of RT, 1250°C, and 1370°C Charpy impact tests on NC-132 Si_3N_4 control samples, that have been subjected to 50 cycles between 200°C and 1370°C, are given in Table XXVIII. By comparing these results to those for as-ground NC-132 Si_3N_4 (Table III) it can be seen that the thermal cycling did cause a small decrease in the impact strength of the material at all three temperatures. Apparently, the time the samples spent at temperatures over 1300°C (~4 hrs) was sufficient to cause some pitting of the NC-132 Si_3N_4 surface due to the oxidation problem of this material, as discussed previously.

The results of Charpy impact tests on cycled R.S. Si_3N_4 surface layers on NC-132 Si_3N_4 are given in Table XXIX. In general, thermal cycling tended to degrade both the RT and 1370°C Charpy impact resistance of all of the layers listed in Table XXIX over similar samples that had not been cycled. In addition, thermal cycling of the nitrided -325 Si layers, and to a lesser extent the -200 Si layers, tended to weaken the interfacial bonding between the R.S. Si_3N_4 and the hot-pressed Si_3N_4 to such an extent that of ten -325 Si samples thermally cycled, only two remained well bonded enough to subsequently test in Charpy impact.

After subjecting cycled layers of nitrided -325 Si and -100, +200 Si to X-ray analysis, it became very apparent why the -325 Si layers could not withstand the thermal cycling without debonding at the interface. The X-ray pattern for the cycled -100, +200 Si layer showed a fairly small peak at a d spacing of 4.09Å, indicating a small amount of silica in the form of cristobalite had formed during cycling. The X-ray pattern for the thermally cycled -325 Si layer showed an enormous peak at the same d spacing, indicating a very large amount of silica formation. Even though the porosity of the nitrided -325 Si layers is less than for the -100, +200 Si layers, the large amount of surface area present allows the formation of enough silica that the effective thermal

thermal expansion coefficient of the R.S. Si_3N_4 layer is determined largely by the silica present. Since silica (in the form of cristobalite) has a very high thermal expansion coefficient, the interface between the oxidized R.S. Si_3N_4 and the NC-132 Si_3N_4 cannot withstand the stresses that develop during thermal cycling and thus interfacial debonding results.

The ballistic impact testing of NC-132 Si_3N_4 controls, after they had been subjected to 50 cycles from 200°C-1370°C, showed very little difference in results from noncycled samples, as shown in Table XXX. Since the failure mode for NC-132 Si_3N_4 in ballistic impact is normally Hertzian cracking at the point of impact, the surface pitting due to high temperature oxidation has much less of an influence than it does for Charpy impact. The results for ballistic impact tests on cycled R.S. Si_3N_4 surface layers on NC-132 Si_3N_4, both -200 Si and -100, +200 Si, are given in Tables XXXI and XXXII. By comparing these results with that for noncycled samples (Tables XIX and XX), it can be seen that cycling reduces the ballistic impact resistance of nitrided -200 Si layers slightly, but has little or no effect on nitrided -100, +200 Si layers at RT and greatly increases the impact resistance of the latter layers at 1370°C. In fact, as shown in Table XXXI, five cycled -100, +200 Si layers on NC-132 Si_3N_4 were ballistically impacted at 1370°C up to an impact energy of 17.2 joules without failure of the NC-132 Si_3N_4 substrate. A 10.0 joule impact has been found to fail a similar noncycled sample at 1370°C. Figures 56 and 57 show the cycled -100, +200 Si layers impacted at RT and 191 m/sec (6.2 joules) and 1370°C and 315 m/sec (17.2 joules), respectively. The R.S. Si_3N_4 surface layers of both samples were destroyed only at the point of impact. It appears that the presence of small amounts of silica in the -100, +200 Si R.S. Si_3N_4 layer increases its resistance to ballistic type impact at elevated temperatures, possibly due to viscous flow and plastic deformation of the silica.

The nitrided -200 Si layers on NC-132 Si_3N_4 that have been subjected to thermal cycling tend to have much weaker interfacial bond strengrhs than the cycled -100, +200 Si layers and thus on ballistic impact these layers are completely blown off the substrate, as shown in Fig. 58. It is apparent that the amount of internal oxidation that occurs in the finer grain size R.S. Si_3N_4 surface layers using either -325 Si or -200 Si is sufficient to produce weakened interfacial bonding during thermal cycling. No thermal cycled -325 Si layers were bonded well enough even to test in ballistic impact.

From the results of thermal cycling tests done to date on R.S. Si_3N_4 energy absorbing surface layers on NC-132 Si_3N_4, it can be concluded that a small amount of internal silica formation, such as occurs with -100, +200 Si layers, can be tolerated and can actually increase the elevated temperature ballistic impact

resistance; however, excessive silica formation produces stresses that cause interfacial debonding and lower impact resistance. For a practical R.S. Si_3N_4 energy absorbing surface layer that must be able to operate in a gas turbine environment, it may be necessary to have an outer layer of dense, impermeable C.V.D. Si_3N_4 covering the R.S. Si_3N_4 surface to add oxidation and possibly erosion resistance.

IV. CONCLUSIONS

The major conclusions that can be reached from work done on this program to improve the toughness (impact resistance) of hot-pressed Si_3N_4 and SiC are as follows:

1. The ballistic and, in particular, the Charpy impact resistance of Norton NC-203 SiC is substantially less than that of Norton NC-132 Si_3N_4 in the temperature range of RT to 1370°C.

2. The impact resistance and bend strength of NC-132 Si_3N_4 is decreased substantially after exposure to air at temperatures greater than 1200°C due to the reaction of impurities such as Mg at the oxidized surface causing the formation of stress-concentrating pits.

3. Improving the impact resistance of either Si_3N_4 or SiC to any meaningful extent by attempting to establish compressive surface layers is not a viable method of impact improvement.

4. Energy absorbing surface layers, such as Fe_2TiO_5 and a silica-zircon mixture, have been found to increase the Charpy and ballistic impact resistance of NC-132 Si_3N_4 and, to a lesser extent, NC-203 SiC by factors of from five to seven at temperatures from RT to 1370°C. The energy absorbing mechanism of the extension of preexisting microcracks upon impact, which was thought at first to be responsible for the observed increase in impact resistance, has been found not to play a major role. Rather, the crushing of the silica-zircon material due to its porosity and the plastic deformation of the Fe_2TiO_5 material at elevated temperatures are now thought to be the controlling factors for energy absorption upon impact.

5. The two energy absorbing surface layers of Fe_2TiO_5 and silica-zircon on NC-132 Si_3N_4 have been found not to withstand thermal cycling in air between 200°C and 1370°C. During cycling, the layers debond from the NC-132 Si_3N_4 substrate due to stresses developed at the interface by the large difference in thermal expansion coefficient between the layers and the Si_3N_4 substrate.

6. Reaction sintered Si_3N_4 surface layers of varying porosity, grain size, and pore size have been fabricated in situ on NC-132 Si_3N_4 by nitriding slurry deposited silicon powder layers. From Charpy and ballistic impact tests at RT and 1370°C on 1 mm thick R.S. Si_3N_4 surface layers on NC-132 Si_3N_4, it was found that the Charpy impact resistance can be increased by up to a factor of 2 1/2 and the ballistic impact resistance increased by up to a factor of six over NC-132 Si_3N_4 control values.

7. Reaction sintered Si_3N_4 surface layers on NC-132 Si_3N_4 fabricated from large grain size -100, +200 mesh Si powder result in a much greater improvement in impact resistance than surface layers fabricated from smaller grain size -200 mesh and -325 mesh Si powder.

8. To realize optimum energy absorption during a ballistic impact event, a combination of porosity and fairly large grain size appear to be necessary to allow crushing of the R.S. Si_3N_4 layer but, at the same time, be somewhat resistant to penetration by the projectile.

9. The presence of a well bonded R.S. Si_3N_4 layer on NC-132 Si_3N_4 can degrade the bend strength of NC-132 Si_3N_4 in contact with the R.S. Si_3N_4 by up to 50%. Since, in general, the large particle and pore size nitrided -100, +200 Si layers degraded the strength more than the smaller particle and pore size -325 Si layers, the possibility exists that the strength degradation is due to the large pores in the R.S. Si_3N_4 layer near the interface acting as stress concentrating flaws.

10. Thermal cycling of R.S. Si_3N_4 layers on NC-132 Si_3N_4 in air for 50 cycles between 200°C and 1370°C resulted in no decrease in impact resistance for nitrided -100, +200 Si layers. However, the excessive silica formation due to internal oxidation of the finer grain size (thus larger surface area) nitrided -325 Si layers caused debonding of these layers from the NC-132 Si_3N_4 substrate during cycling, due to thermal expansion differences between the silica filled R.S. Si_3N_4 layer and the NC-132 Si_3N_4 substrate.

11. For a practical R.S. Si_3N_4 energy absorbing surface layer that must operate in a gas turbine environment, it may be necessary to have an outer layer of dense, impermeable CVD Si_3N_4 covering the R.S. Si_3N_4 surface to add oxidation and possibly erosion resistance.

12. From the results of various research programs carried out during the past five years that have been concerned with improving the impact resistance of either Si_3N_4 or SiC through the use of compressive surface layers (Refs. 4-6) or energy absorbing surface layers (Refs. 1,7-9), the system of R.S. Si_3N_4 surface layers on dense Si_3N_4, investigated during this contract, appears to be the only practical system investigated thus far for potential use as an energy absorbing surface layer on dense Si_3N_4 used as a high temperature structural ceramic. The approach used by Palm (Ref. 9) appears to be practical for the SiC system. A similar approach for Si_3N_4 using sinterable Si_3N_4 with additives for the structural member and Si_3N_4 without additives or with minimal additives to form a porous surface layer may warrant investigation.

13. Although the system of R.S. Si_3N_4 surface layers on dense Si_3N_4 has exhibited excellent ballistic impact properties, further work is necessary in order to fully evaluate the potential of this system, particularly in the areas of tolerance to thermal cycling and thermal aging, acceptable interfacial strength properties, and the use of a CVD Si_3N_4 coating over the R.S. Si_3N_4 layer for oxidation and erosion resistance.

V. REFERENCES

1. Rhodes, W. H. and R. M. Cannon, Jr.: "High Temperature Compounds for Turbine Vanes", AVCO Systems Division Report, NASA CR-134531, Contract NAS3-16757 (Jan. 1974) and NASA CR-120966, Contract NAS3-14333 (Sep. 1972).

2. Brennan, J. J.: "Development of Fiber Reinforced Ceramic Matrix Composites", UARL Report N911647-3, Contract N62269-73-C-2068 (Jan. 1974).

3. Brennan, J. J.: "Development of Fiber Reinforced Ceramic Matrix Composites", UARL Report R911848-4, Contract N62269-74-C-0268 (Feb. 1975).

4. Platts, D. R., H. P. Kirchner and R. M. Gruver: "Strengthening Oxidation Resistant Materials for Gas Turbine Applications", Ceramic Finishing Co. Report, NASA CR-121002, Contract NAS3-15561 (Sep. 1972).

5. Gruver, R. M., D. R. Platts and H. P. Kirchner: "Strengthening Silicon Carbide by Quenching", Bull. Amer. Ceram. Soc. 53 (7) 524-527 (July 1974).

6. Kirchner, H. P.: "Strengthening of Oxidation Resistant Materials for Gas Turbine Applications", Ceramic Finishing Co. Report, NASA CR-134661, Contract NAS3-16788 (June 1974).

7. Kirchner, H. P. and J. Seretsky: "Improving Impact Resistance by Energy Absorbing Surface Layers", Ceramic Finishing Co. Report, NASA CR-134644, Contract NAS3-17765 (Mar. 1974).

8. Palm, J. A.: "Improved Toughness of Silicon Carbide", General Electric Co., NASA CR-134921, Nov. 1975.

9. Palm, J. A.: "Improved Toughness of Silicon Carbide", NASA CR-134990, Final Report on Contract NAS3-17832 (Jan. 1976).

10. "Brittle Materials Design, High Temperature Gas Turbine", AMMRC CTR 75-28, Interim Report #8, Oct. 1975, p 133.

11. Kiehle, A. J., L. K. Heung, P. J. Gielisse, and T. J. Rockett: "Oxidation Behavior of Hot-Pressed Si_3N_4", J. Am. Cer. Soc., Vol. 58, No. 1-2, Jan.-Feb. 1975, p 17.

12. Green, D. J., P. S. Nicholson, and J. D. Embury, "Fracture Toughness of a Partially Stabilized ZrO_2 in the System $CaO-ZrO_2$", J. Am. Cer. Soc., Vol. 56, No. 12, Dec. 1973, pp 619-623.

13. Bradt, R. C.: Dept. of Materials Science, Penn State Univ., personal communication.

14. "Ceramics for Engine Components", Norton Co. Brochure.

Table I

Spectrochemical Analysis of Norton NC-132
Si_3N_4 and NC-203 SiC Impurity Content

NC-132 Si_3N_4	Element	Wt % Present
	*Al	0.20
	Cr	0.02
	Co	0.03
	Cu	0.002
	*Fe	0.18
	Pb	0.006
	*Mg	0.34
	Mn	0.03
	Ni	0.004
	Ti	0.01
	*W	4.3
	V	0.004
	Ca	0.05
	K	<0.01
	Na	0.05

NC-203 SiC	Element	Wt % Present
	*Al	3.0
	*B	0.2
	*Fe	0.5
	Mg	0.02
	Ni	0.05
	*Ti	0.1
	*W	5.0
	V	0.02

*Major impurities

Table II

Grain Size Measurements

Sample	Max. (μ)	Min. (μ)	Mean (μ)
NC-132 Si_3N_4	3.24	0.24	0.96
NC-203 SiC	8.5	1.5	3.6

Table III

RT, 1250°C, and 1370°C Instrumented Charpy Impact Results for Control Sample of Norton NC-132 Si_3N_4 and NC-203 SiC, 6.4 x 6.4 x 51 mm (1/4 x 1/4 x 2 in.)*

Material	Temperature	Impact Resistance		Maximum Load	
		joules	in.-lbs	kN	lbs
NC-132 Si_3N_4	RT	0.40	3.5	3.7	840
"	1250°C	0.45	4.0	3.2	715
"	1370°C	0.40	3.5	2.8	620
NC-203 SiC	RT	0.20	1.8	2.9	650
"	1250°C	0.20	1.8	1.7	390
"	1370°C	0.11	1.0	1.5	330

*Average of 10 tests at each temperature

Table IV

Instrumented Charpy Impact Tests on Carburized (1350°C, 24-48 hrs, ND-3000) Norton NC-132 Si_3N_4 (6.4 x 6.4 x 51 mm)

Test Temperature	Impact Resistance		Maximum Load	
	joules	in.-lbs	kN	lbs
RT*	0.38	3.3	3.0	670
1250°C**	0.38	3.4	2.6	570
1370°C**	0.36	3.2	2.2	500

*Average of 10 tests

**Average of 5 tests

Table V

RT Instrumented Charpy Impact Tests on Oxidized
NC-132 Si_3N_4 and Si_3N_4 + 15% Y_2O_3
(6.4 x 6.4 x 51 mm)

Material	Condition	Impact Resistance		Maximum Load	
		Joules	in.-lbs	kN	lbs
NC-132 Si_3N_4	As ground	0.40	3.5	3.7	840
NC-132 Si_3N_4	Oxidized 48 hrs 1350°C	0.14	1.2	2.0	440
Si_3N_4 + 15% Y_2O_3	As ground	0.35	3.1	3.2	710
Si_3N_4 + 15% Y_2O_3	Oxidized 48 hrs 1350°C	0.27	2.4	2.8	620

Table VI

Instrumented Charpy Impact Tests on Oxidized (1315°C, 50 hrs) Norton NC-203 SiC (6.4 x 6.4 x 51 mm)

Test Temperature	Impact Resistance		Maximum Load	
	joules	in.-lbs	kN	lbs
RT*	0.23	2.1	3.0	670
1250°C*	0.14	1.2	1.6	370
1370°C*	0.11	1.0	1.6	350

*Average of 5 tests

Table VII

Instrumented Charpy Impact Tests of Plasma Sprayed Mullite Layers on NC-203 SiC

Test Temperature	Layer Thickness	Impact Resistance		Maximum Load	
		joules	in.-lbs	kN	lbs
RT*	1.0 mm	0.22	2.0	2.3	500
RT**	1.75	0.16	1.4	2.2	490
1250°C*	1.0	0.19	1.7	1.6	350
1250°C**	1.75	0.25	2.2	1.5	340
1370°C*	1.0	0.17	1.5	1.4	310
1370°C**	1.75	0.13	1.2	1.3	290

*Average of 10 tests

**Average of 3 tests

Table VIII

Instrumented Charpy Impact Tests of Partially Stabilized ZrO_2 Layers on NC-132 Si_3N_4

Test Temperature	Layer Thickness	Impact Resistance		Maximum Load	
		joules	in.-lbs	kN	lbs
RT*	1.0 mm	0.75	6.6	4.3	960
1250°C*	1.0	0.63	5.6	3.5	780
1370°C*	1.0	0.50	4.4	2.8	640

*Average of 5 tests

Table IX

Instrumented Charpy Impact Tests of Titanate Layers on NC-132 Si_3N_4

Test Temperature	Layer	Layer Thickness	Impact Resistance		Maximum Load	
			joules	in.-lbs	kN	lbs
RT*	$MgTi_2O_5$	1.1 mm	0.66	5.8	4.0	890
1250°C**	"	1.0	0.69	6.1	3.4	760
1370°C**	"	1.0	0.61	5.4	2.9	660
RT*	Fe_2TiO_5	1.2 mm	0.69	6.1	4.0	870
1250°C**	"	1.2	2.56	22.7	3.1	700
1370°C**	"	1.2	2.14	18.9	3.1	700

*Average of 10 tests

**Average of 5 tests

Table X

Instrumented Charpy Impact Tests of Silica-Zircon Layers on NC-132 Si_3N_4

Test Temperature	Layer Thickness	Impact Resistance		Maximum Load	
		joules	in.-lbs	kN	lbs
RT*	1.2 mm	1.48	13.1	3.7	820
1250°C**	1.0	1.14	10.1	3.3	750
1370°C**	1.0	0.66	5.8	3.0	680

*Average of 10 tests

**Average of 5 tests

Table XI

RT Instrumented Charpy Impact Tests of Silica-Zircon Layers on NC-132 Si_3N_4 Subjected to Various Heat Treatments

Layer Type	Heat Treatment	Layer Thickness	Impact Resistance		Maximum Load	
			joules	in.-lbs	kN	lbs
UTRC*	1090°C, 2 hrs	1.0 mm	2.21	19.6	4.0	900
Sherwood*	>1100°C	1.2	1.48	13.1	3.6	820
Sherwood*	1200°C, 1 hr	1.0	2.19	19.4	3.8	850

*Average of 5 tests

Table XII

MOR Tests (4-pt bend) on NC-132 Controls (5.08 x 2.54 x 44.5 mm) and with Fe_2TiO_5 and Silica-Zircon Layers (1 mm)

Test Temperature	Layer	Modulus of Rupture	
		MPa	ksi
RT*	None	662	96
1250°C**	"	401	58
1370°C**	"	219	32
RT*	Fe_2TiO_5	747	108
1250°C**	"	403	58
1370°C**	"	231	34
RT*	Silica-Zircon	702	102
1250°C**	"	438	64
1370°C**	"	228	33

*Average of 10 tests
**Average of 3 tests

Table XIII

RT Ballistic Impact Properties of NC-132 Si_3N_4 and NC-203 SiC Controls (6.4 mm thickness) Using 0.37 gm (4.5 mm) Soft Steel Projectile*

Material	Impact Velocity		Impact Energy	
	m/sec	ft/sec	joules	ft-lbs
Si_3N_4	185	605	6.2	4.6
SiC	163	535	4.9	3.6

*Average of 10 tests

Table XIV

Ballistic Impact Properties of NC-132 Si_3N_4 and NC-203 SiC Controls (6.4 mm thickness) Using 0.34 gm (4.4 mm) Chrome-Steel Projectile*

Material	Temperature	Impact Velocity		Impact Energy	
		m/sec	ft/sec	joules	ft-lbs
Si_3N_4	RT	105	345	1.9	1.4
"	1250°C	137	450	3.3	2.4
"	1370°C	128	420	2.8	2.1
SiC	RT	99	325	1.6	1.2
"	1250°C	99	325	1.6	1.2
"	1370°C	Samples cracked on heating			

*Average of 5 tests

Table XV

Ballistic Impact Properties of NC-132 Si_3N_4 with 1 mm Thick Fe_2TiO_5 Cemented Layer

Temperature	Impact Velocity		Impact Energy		Comments
	m/sec	ft/sec	joules	ft-lbs	
RT	230	755	9.1	6.7	At lower velocities - layer destroyed, no damage to substrate. At higher velocities - Si_3N_4 fractured, Hertzian or tensile failure
1250°C	272	890	12.5	9.2	"
1370°C	302	990	15.4	11.4	"

Table XVI

Ballistic Impact Properties of NC-132 Si_3N_4 with 1 mm Thick SiO_2-Zircon Cemented Layer

Temperature	Impact Velocity		Impact Energy		Comments
	m/sec	ft/sec	joules	ft-lbs	
RT	230	755	9.1	6.7	At lower velocities - layer destroyed, no damage to substrate. At higher velocities - Si_3N_4 fractured, Hertzian failure.
1250°C	315	1045	17.2	12.7	"
1370°C	336	1100	19.0	14.0	"

Table XVII

1250°C Ballistic Impact Properties of NC-203
SiC with 1 mm Thick Cemented Layers

Layer	Impact Velocity		Impact Energy		Comments
	m/sec	ft/sec	joules	ft-lbs	
Fe_2TiO_5	212	695	7.6	5.6	Layer destroyed, no damage to SiC
"	221	725	8.3	6.1	SiC fractured
SiO_2-Zircon	195	640	6.5	4.8	Layer destroyed, no damage to SiC
"	202	670	7.1	5.2	SiC fractured

Table XVIII

Charpy Impact Properties of NC-132 Si_3N_4 with 1 mm Thick R.S. Si_3N_4 Layer*

Type of Layer	Temp. °C	Impact Energy		Maximum Load	
		joules	in-lbs	kN	lbs
-100,+200 mesh Si	RT	0.94	8.3	3.4	770
"	1370	0.81	7.1	2.7	620
-200 mesh Si	RT	0.47	4.2	3.7	840
"	1370	0.29	2.6	2.4	540
-325 mesh Si	RT	0.47	4.2	3.5	790
"	1370	0.43	3.8	2.8	630

*All values are averages of 5 tests

Table XIX

RT and 1370°C Ballistic Impact Properties of NC-132 Si_3N_4 with 1 mm Thick R.S. Si_3N_4 Layer (-100,+200 Mesh Si)

Temp. °C	Impact Velocity		Impact Energy		Comments
	m/sec	ft/sec	joules	ft-lbs	
RT	191	630	6.2	4.6	Third of layer retained, no damage to substrate.
RT	230	755	9.1	6.7	Layer destroyed, no damage to substrate.
RT	260	850	11.4	8.4	"
RT	282	925	13.6	10.0	Si_3N_4 substrate fractured, tensile failure.
1370	191	630	6.2	4.6	Layer destroyed only at point of impact, no damage to substrate.
1370	230	755	9.1	6.7	____ "
1370	260	850	11.4	8.4	Half of layer retained, no damage to substrate.
1370	282	925	13.6	10.0	Si_3N_4 substrate fractured, Hertzian failure.
NC-132 Controls					
RT	105	345	1.9	1.4	
1370	128	420	2.8	2.1	

Table XX

RT and 1370°C Ballistic Impact Properties of NC-132 Si_3N_4 with 1 mm Thick R.S. Si_3N_4 Layer (-200 mesh Si)

Temp. °C	Impact Velocity		Impact Energy		Comments
	M/sec	ft/sec	joules	ft-lbs	
RT	191	630	6.2	4.6	Half of layer retained, no damage to substrate.
RT	230	755	9.1	6.7	Layer destroyed, no damage to substrate.
RT	260	850	11.4	8.4	Si_3N_4 substrate fractured, tensile failure.
1370	260	850	11.4	8.4	Layer destroyed, no damage to substrate.
1370	300	980	15.4	11.4	Si_3N_4 substrate fractured, tensile failure.

Table XXI

Ballistic Impact Properties of NC-132 Si_3N_4 with
1 mm Thick R.S. Si_3N_4 Surface Layer (-325 Si)

Temp. °C	Impact Velocity		Impact Energy		Comments
	m/sec	ft/sec	joules	ft-lbs	
RT	191	630	6.2	4.6	Layer destroyed, no damage to substrate.
RT	191	630	6.2	4.6	Si_3N_4 substrate fractured, tensile failure.
RT	191	630	6.2	4.6	Si_3N_4 substrate fractured, tensile failure.
RT	230	750	9.1	6.7	Si_3N_4 substrate fractured, tensile failure.
1250	169	555	4.9	3.6	Layer destroyed, no damage to substrate.
1250	191	630	6.2	4.6	Si_3N_4 substrate fractured, tensile failure

Table XXII

Charpy Impact Properties of NC-132 Si_3N_4 with R.S. Si_3N_4 Surface Layers (-325 mesh Si + polystyrene spheres)

Layer	Temp.	Impact Energy		Max. Load		Comments
		joules	in-lbs	kN	lbs	
-325 Si + 10% polysytrene spheres	*RT	0.54	4.8	3.4	760	Fair-good interfacial bonding
"	**1370°C	0.43	3.8	2.8	630	"
-325 Si + 20% polystyrene spheres	**RT	0.86	7.6	3.3	750	Poor interfacial bonding
-325 Si + 40% polystyrene spheres	**RT	0.59	5.3	2.9	650	"

*Average of five tests
**Average of three tests

Table XXIII

Ballistic Impact Properties of NC-132 Si_3N_4 with 1 mm Thick R.S. Si_3N_4 Surface Layers (-325 Si + polystyrene spheres)

Layer	Temp. °C	Impact Velocity m/sec	Impact Velocity ft/sec	Impact Energy joules	Impact Energy ft-lbs	Comments
-325 Si + 20 vol % polystyrene spheres	RT	191	630	6.2	4.6	Layer destroyed, no damage to substrate
"	RT	212	695	7.6	5.6	Si_3N_4 substrate fractured, tensile failure.
"	RT	230	755	9.1	6.7	"
"	1250	169	555	4.9	3.6	Layer destroyed, no damage to substrate
"	1250	191	630	6.2	4.6	Si_3N_4 substrate fractured, tensile failure
-325 Si + 10 vol % polystyrene spheres	RT	191	630	6.2	4.6	Layer destroyed, no damage to substrate
"	RT	212	695	7.6	5.6	Si_3N_4 substrate fractured, tensile failure
"	1250	169	555	4.9	3.6	Layer destroyed, no damage to substrate
"	1250	191	630	6.2	4.6	Si_3N_4 substrate fractured, tensile failure

Table XXIV

Ballistic Impact Properties of NC-132 Si_3N_4 with .1 mm Thick R.S. Si_3N_4 Surface Layers (-325 Si + -100,+200 Si mixtures)

Layer	Temp. °C	Impact Velocity m/sec	Impact Velocity ft/sec	Impact Energy joules	Impact Energy ft-lbs	Comments
70%-100,+200Si 30%-325Si	RT	152	500	3.7	2.7	Layer destroyed only at point of impact, no damage to substrate
"	RT	169	555	4.9	3.6	Si_3N_4 substrate fractured, Hertzian failure
"	RT	191	630	6.2	4.6	Si_3N_4 substrate fractured, tensile failure
"	1250	152	500	3.7	2.7	Layer destroyed only at point of impact, no damage to substrate
"	1250	169	555	4.9	3.6	Si_3N_4 substrate fractured, tensile failure
90%-100,+200Si 10%-325Si	RT	169	555	4.9	3.6	Layer destroyed only at point of impact, no damage to substrate
"	RT	191	630	6.2	4.6	Si_3N_4 substrate fractured, tensile failure
"	1250	169	555	4.9	3.6	Layer destroyed only at point of impact, no damage to substrate
"	1250	169	555	4.9	3.6	Si_3N_4 substrate fractured, tensile failure

Table XXV

Charpy Impact Properties of NC-132 Si_3N_4 with 1 mm Thick R.S. Si_3N_4 Surface Layers (80% -100,+200 Si, 20% -325 Si Mixtures) (toluene slurry)

Temperature	Impact Energy		Maximum Load		Comments
	joules	in-lbs	kN	lbs	
RT	0.88	7.8	*		Good interfacial bond
"	0.66	5.9	*		
"	0.92	8.2	*		
"	0.66	5.9	*		
"	0.65	5.8	*		
"	0.58	5.2	*		
RT averages	0.73	6.5			
1370°C	0.38	3.4	2.3	530	Good interfacial bond
	0.39	3.5	2.5	570	
	0.62	5.5	3.1	700	
	0.49	4.3	2.8	630	
1370°C averages	0.47	4.2	2.7	610	

*Instrumented impact traces not obtained due to equipment malfunction

Table XXVI

Ballistic Impact Properties of NC-132 Si_3N_4 with 1 mm Thick R.S. Si_3N_4 Surface Layers (80% -100,+200 Si, 20% -325 Si Mixtures) (toluene slurry)

Temp. °C	Impact Velocity		Impact Energy		Comments
	m/sec	ft/sec	joules	ft-lbs	
RT	230	755	9.1	6.7	Layer destroyed, no damage to substrate
RT	260	850	11.4	8.4	Si_3N_4 substrate fractured, tensile failure
RT	282	925	13.6	10.0	Si_3N_4 substrate fractured, Hertzian failure
1370	230	755	9.1	6.7	Layer destroyed, no damage to substrate
1370	282	925	13.6	10.0	"
1370	315	1045	17.2	12.7	Si_3N_4 substrate fractured, tensile failure

Table XXVII

RT Charpy Impact Properties of NC-132 Si_3N_4 with R.S. Si_3N_4 Layer on Tensile (Reverse) Side

Sample No.	RSSN Layer Particle Size	Impact Energy		Max. Load		Comments
		joules	in.-lbs	kN	lbs	
132-318*	-325 Si	0.16	1.4	2.2	500	Good interfacial bond
-319	"	0.23	2.0	2.5	560	Fair interfacial bond
-320	"	0.33	2.9	3.0	670	Fair interfacial bond
-321***	"	0.33	2.9	3.1	690	Fair interfacial bond
-322**	"	0.35	3.1	3.2	730	Poor interfacial bond
-323**	"	0.35	3.1	3.2	730	Poor interfacial bond
-324*	-200 Si	0.05	0.5	1.2	260	Good interfacial bond
-325	"	0.09	0.8	1.4	320	Good interfacial bond
-326	"	0.11	1.0	1.4	320	Good interfacial bond
-327***	"	0.11	1.0	1.5	340	Good interfacial bond
-328**	"	0.20	1.8	2.2	480	Poor interfacial bond
-329**	"	0.26	2.3	2.6	580	Poor interfacial bond
-298	-100,+200Si	0.14	1.2	1.8	410	Good interfacial bond
-299	"	0.19	1.7	2.2	480	Good interfacial bond

*Post oxidized 1300°C, 1 hr
**Preoxidized at 1000°C, 60 hrs
***Preoxidized at 1000°C, 60 hrs plus post-oxidized 1300°C, 1 hr

Table XXVIII

Instrumented Charpy Impact Properties
of NC-132 Si_3N_4 Controls
(50 thermal cycles, 200°C-1370°C)*

Temperature	Impact Energy		Maximum Load	
	joules	in-lbs	kN	lbs
RT	0.35	3.1	3.5	790
1250°C	0.32	2.8	2.9	650
1370°C	0.32	2.8	2.8	640

*average of five tests at each temperature

Table XXIX

Instrumented Charpy Impact Properties of NC-132 Si_3N_4
with 1 mm Thick R.S. Si_3N_4 Surface Layers
(50 thermal cycles, 200°C-1370°C)

Layer	Temp.	Impact Energy		Maximum Load		Comments
		joules	in-lbs	kN	lbs	
-100,+200Si*	RT	0.64	5.7	N.D.		Fair interfacial bond
"	1370°C	0.44	3.9	N.D.		Good interfacial bond
-200Si*	RT	0.44	3.9	3.1	700	Fair interfacial bond
"	1370°C	0.51	4.5	3.3	750	Fair interfacial bond
-325Si**	RT	0.31	2.8	3.2	710	Poor interfacial bond
80%-100,+200Si* 20%-325Si	RT	0.60	5.3	3.1	690	Good interfacial bond

*average of five tests at each temperature
**average of two tests

Table XXX

Ballistic Impact Properties of NC-132 Si_3N_4 Controls
(50 thermal cycles, 200°C-1370°C)*

Temperature	Impact Velocity m/sec	Impact Velocity ft/sec	Impact Energy joules	Impact Energy in-lbs	Comments
RT	113	370	2.2	1.6	Hertzian failure
1250°C	134	440	3.0	2.2	"
1370°C	134	440	3.0	2.2	"

*average of five tests at each temperature

Table XXXI

Ballistic Impact Properties of NC-132 Si_3N_4 with 1 mm Thick Nitrided -100,+200 Si Energy Absorbing Surface Layer (50 thermal cycles, 200°C-1370°C)

Sample No.	Temperature	Impact Velocity		Impact Energy		Comments
		m/sec	ft/sec	joules	ft-lbs	
132-BI- 91	RT	191	630	6.2	4.6	Layer destroyed only at point of impact, no damage to subs.
-174	"	212	695	7.6	5.6	"
-173	"	230	755	9.1	6.7	Si_3N_4 subs. fractured, Hertzian failure
- 90	"	230	755	9.1	6.7	Si_3N_4 subs. fractured, tensile failure
-175	"	260	850	11.4	8.4	"
-181	1370°C	230	755	9.1	6.7	Layer destroyed only at point of impact, no damage to subs.
-182	"	260	850	11.4	8.4	"
-183	"	282	925	13.6	10.0	"
-184	"	300	980	15.4	11.4	"
-185	"	315	1045	17.2	12.7	"

Table XXXII

Ballistic Impact Properties of NC-132 Si_3N_4 with .1 mm Thick Nitrided -200 Si Energy Absorbing Surface Layer
(50 thermal cycles, 200°C-1370°C)

Sample No.	Temp.	Impact Velocity		Impact Energy		Comments
		m/sec	ft/sec	joules	ft-lbs	
132-BI-193	RT	191	630	6.2	4.6	Layer destroyed, no damage to substrate
-194	"	230	755	9.1	6.7	"
-195	"	230	755	9.1	6.7	Si_3N_4 substrate fractured, tensile failure
-196	"	260	850	11.4	8.4	"
-197	1370°C	191	630	6.2	4.6	Layer destroyed, no damage to substrate
-198	"	230	755	9.1	6.7	"
-199	"	260	850	11.4	8.4	Si_3N_4 substrate fractured, Hertzian failure

ELECTRON MICROGRAPH OF SiC SAMPLE NC–203

76-02-61-1

FIG. 2

ELECTRON MICROGRAPH OF Si_3N_4 SAMPLE NC–132

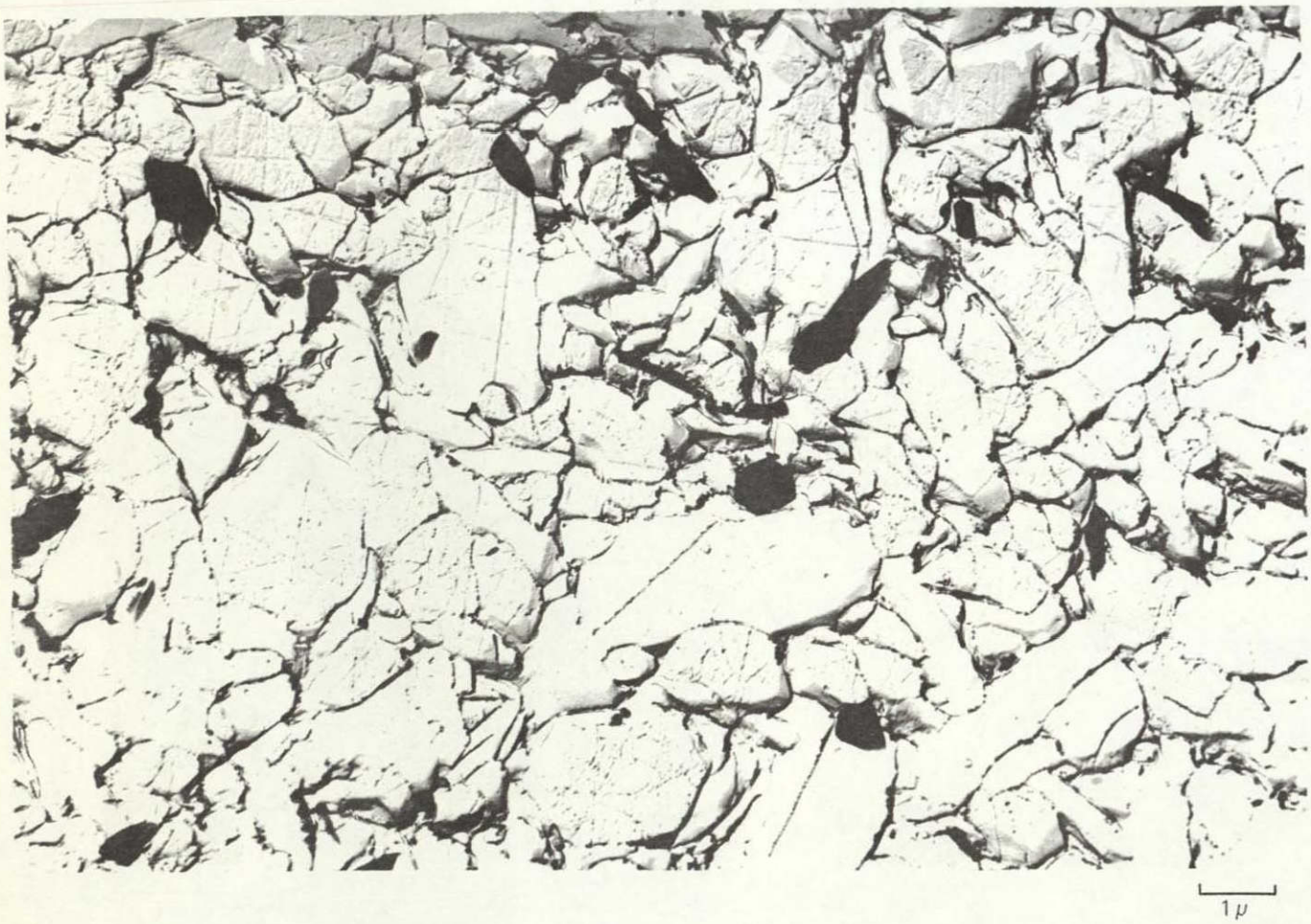

76–02–61–2

RT INSTRUMENTED CHARPY IMPACT TEST OF NC–132 Si_3N_4, AS GROUND

LOAD= 180 lbs/div

TIME= 0.1 ms/div

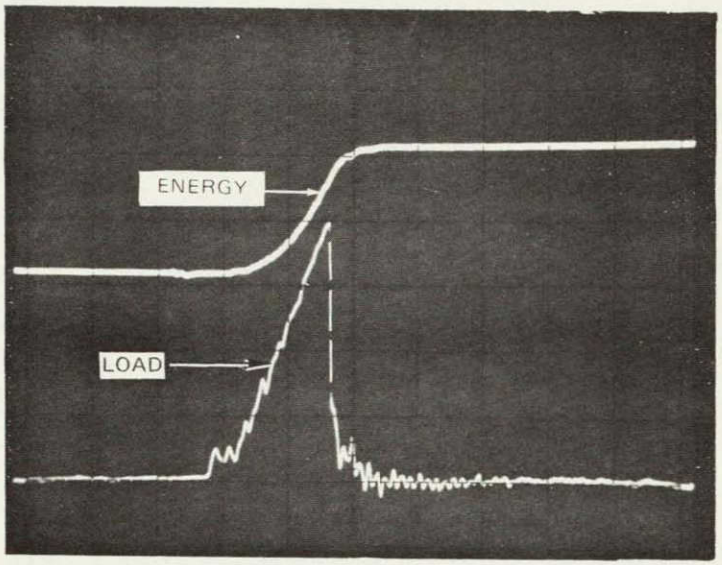

FRACTURE SURFACE OF Si_3N_4 IMPACT CONTROL (RT)

(ORIGIN AT FACE)

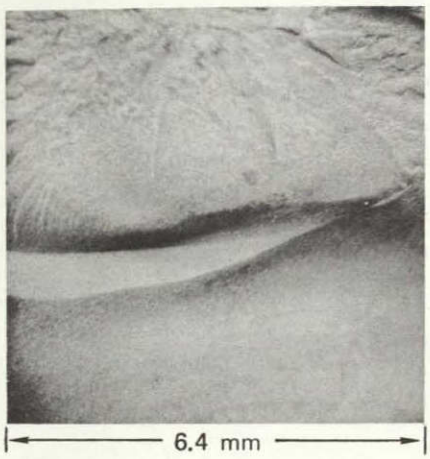

FRACTURE SURFACE OF Si_3N_4 IMPACT CONTROL (RT)

(ORIGIN AT EDGE)

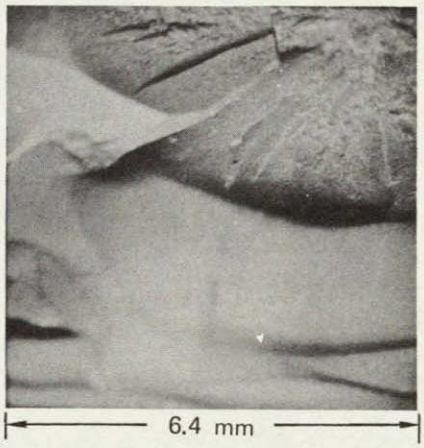

FRACTURE SURFACE OF OXIDIZED Si_3N_4 WITH GROUND TENSILE SIDE

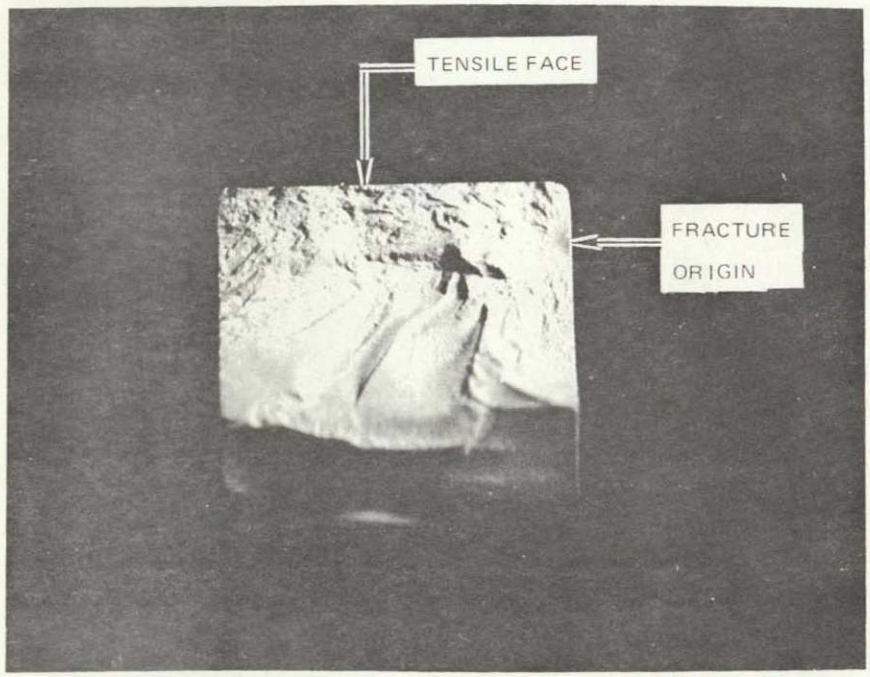

RT INSTRUMENTED CHARPY IMPACT TEST OF NC–132 Si_3N_4, OXIDIZED 24 HRS. AT 1370°C

LOAD= 180 lbs/div

TIME= 0.1 ms/div

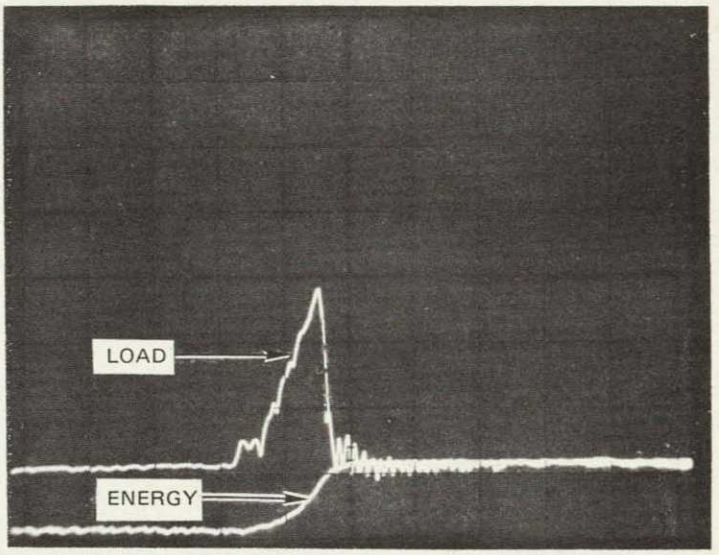

RT INSTRUMENTED CHARPY IMPACT TEST OF Si_3N_4 + 15% Y_2O_3 AS GROUND

LOAD= 180 lbs/div

TIME= 0.1 ms/div

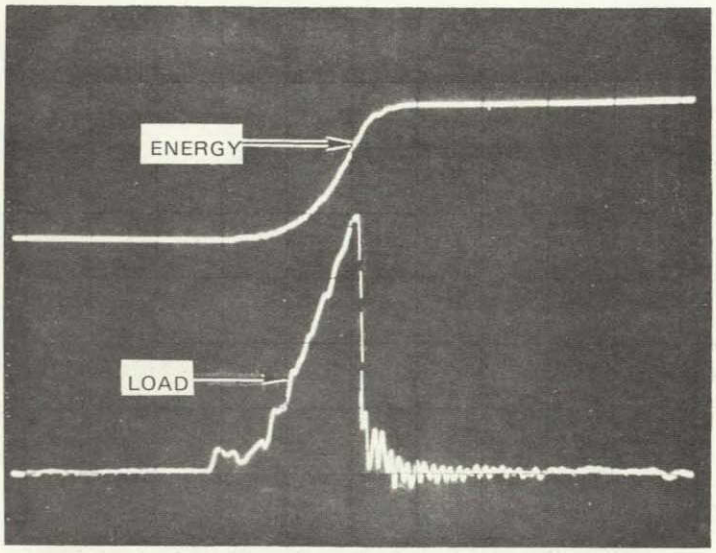

RT INSTRUMENTED CHARPY IMPACT TEST OF Si_3N_4 + 15% Y_2O_3, OXIDIZED 60 HRS AT 1350°C

LOAD= 180 lbs/div
TIME= 0.1 ms/div

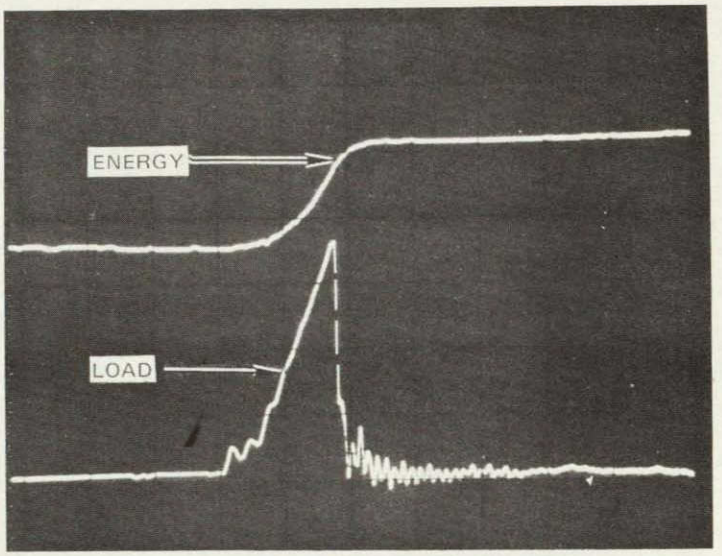

FIG. 10

OXIDIZED (60 HRS. AT 1350°C) SURFACE OF
NC–132 Si_3N_4 (400x)

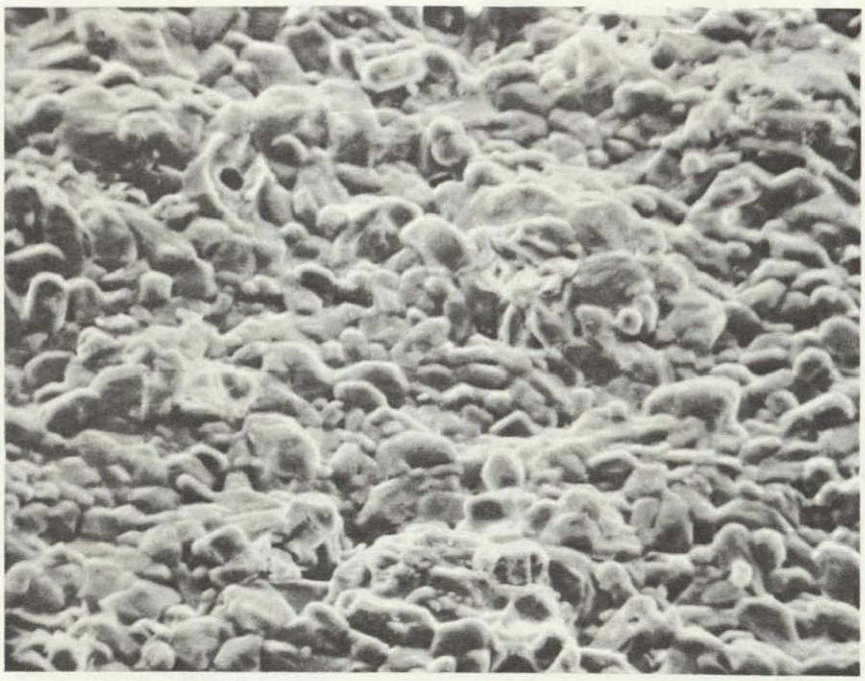

76–05–103–24

FRACTURE INITIATING FLAW ON SURFACE OF

OXIDIZED NC–132 Si_3N_4 (500x)

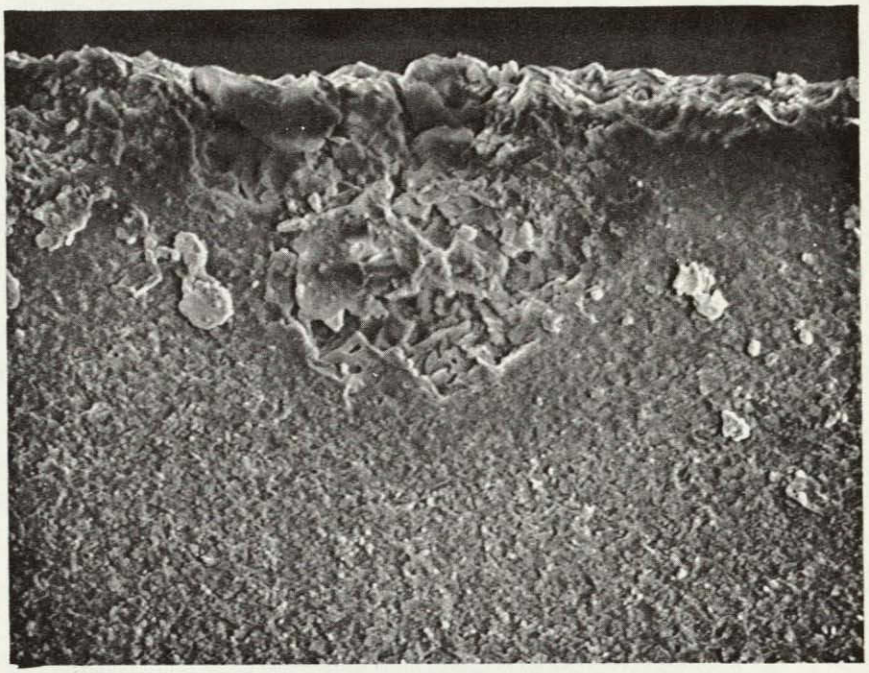

76–05–103–23

FIG. 12

OXIDIZED SURFACE (60 HRS. AT 1350°C) OF

UTRC Si_3N_4 + 15% Y_2O_3 (100x)

76-05-103-22

RT INSTRUMENTED CHARPY IMPACT TRACE FOR PLASMA SPRAYED MULLITE ON SiC

LOAD = 75LBS/DIV
TIME = 0.05 MS/DIV

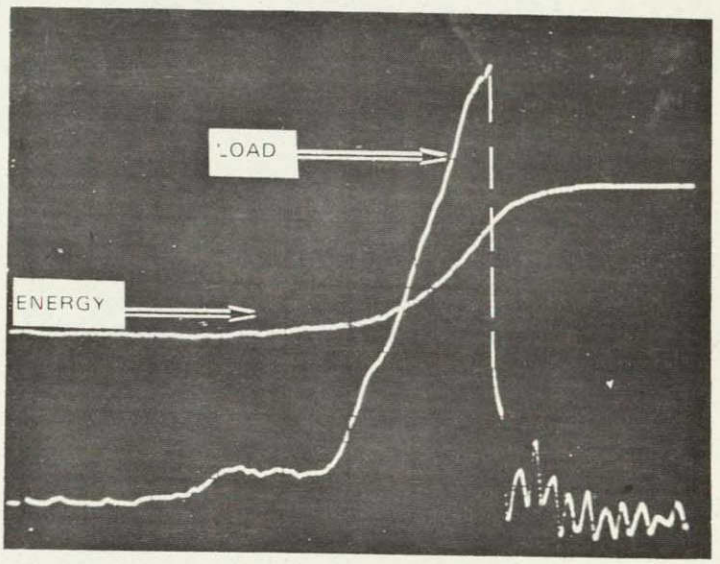

a.) 1250°C INSTRUMENTED CHARPY IMPACT TEST ON PARTIALLY STABILIZED ZrO_2 LAYER ON Si_3N_4

LOAD = 186 lbs/div

TIME = 0.1 ms/div

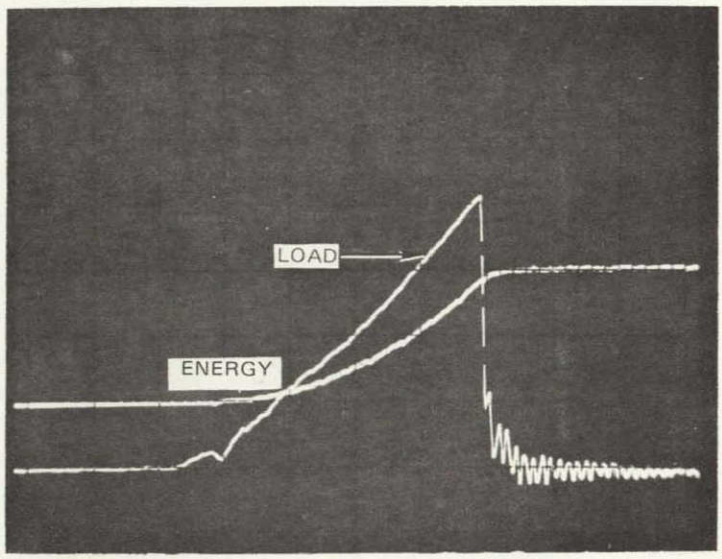

b.) RT INSTRUMENTED IMPACT TEST OF Si_3N_4 CONTROL

LOAD = 186 lbs/div

TIME=0.1 ms/div

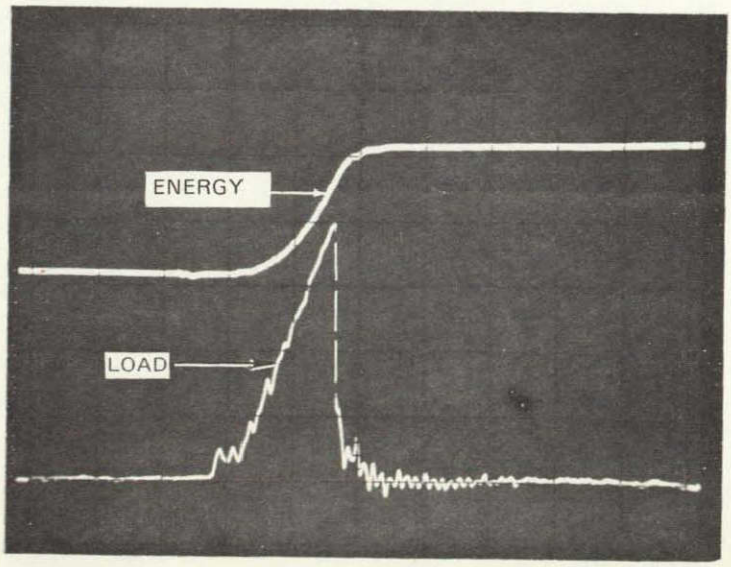

1350°C INSTRUMENTED CHARPY IMPACT TEST OF Fe_2TiO_5 LAYER ON Si_3N_4

LOAD= 190 lbs/div

TIME= 0.5 ms/div

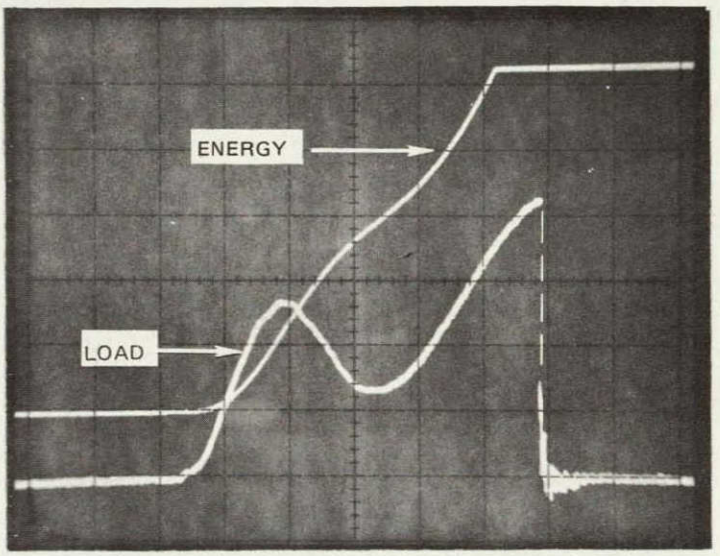

ONE HALF OF THE Fe_2TiO_5 LAYER CEMENTED ON Si_3N_4
AFTER UNDERGOING A 1370° CHARPY IMPACT

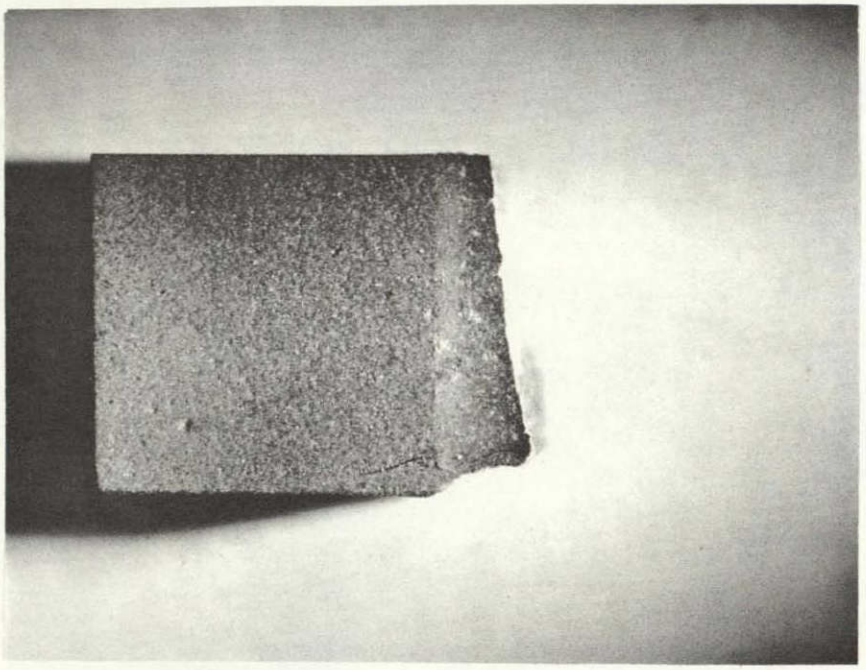

1370°C INSTRUMENTED CHARPY IMPACT TEST OF Fe_2TiO_5 LAYER ON SiC

LOAD= 190 lbs/div

TIME = 0.2 ms/div

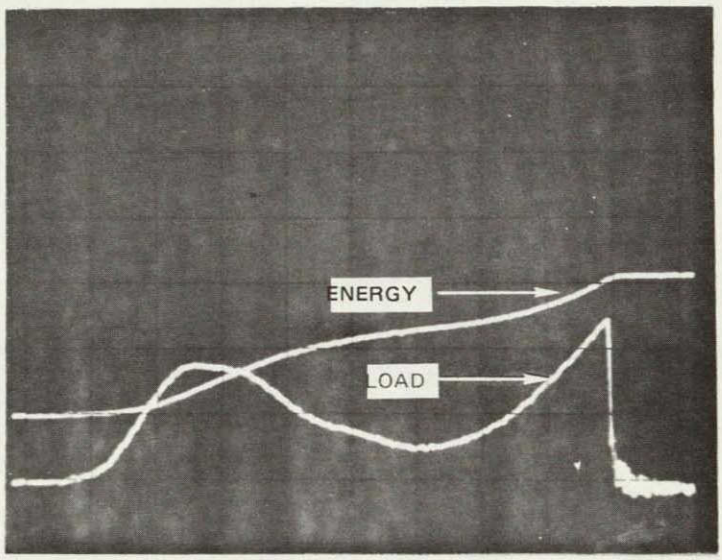

1370° INSTRUMENTED CHARPY IMPACT TEST OF Fe_2TiO_5 LAYER ON SiC

LOAD= 190 lbs/div
TIME= 0.1 ms/div

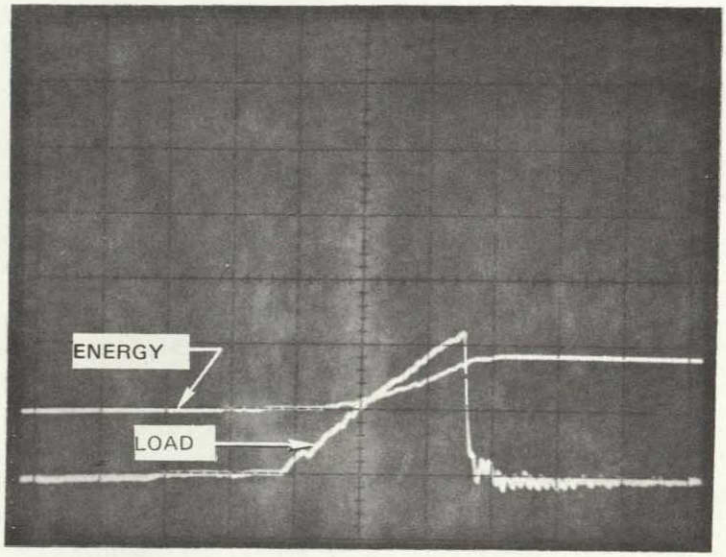

76-05-103-11

RT INSTRUMENTED IMPACT TEST OF SILICA–ZIRCON LAYER ON Si_3N_4

LOAD 178 LBS DIV
TIME 0.1 MS DIV

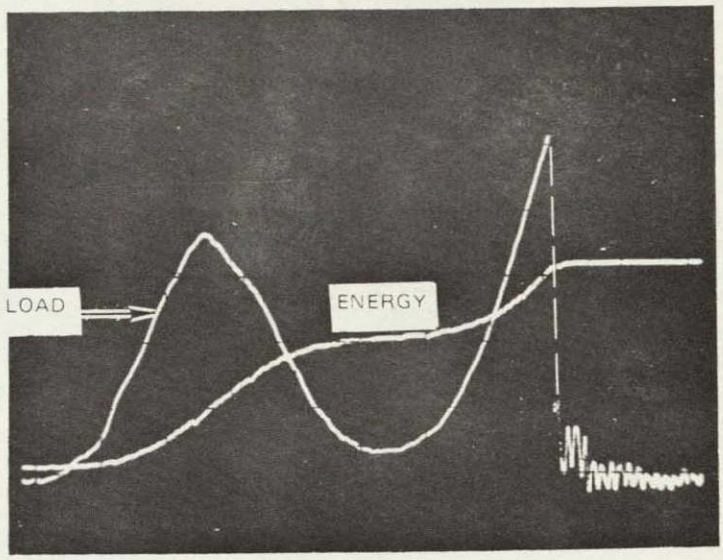

RT INSTRUMENTED IMPACT TEST OF SILICA–ZIRCON LAYER ON Si_3N_4

LOAD = 142 LBS/DIV
TIME = 0.1 MS/DIV

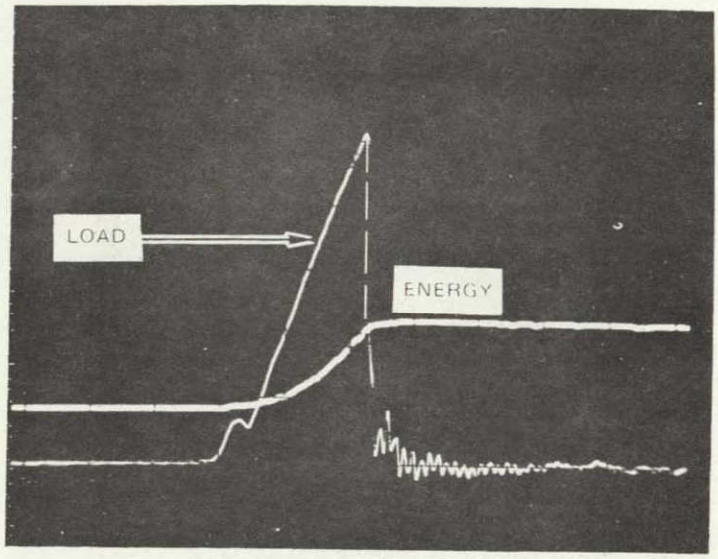

FIG. 21

TEMPERATURE VS EXPANSIVITY FOR SILICA–ZIRCON MATERIALS

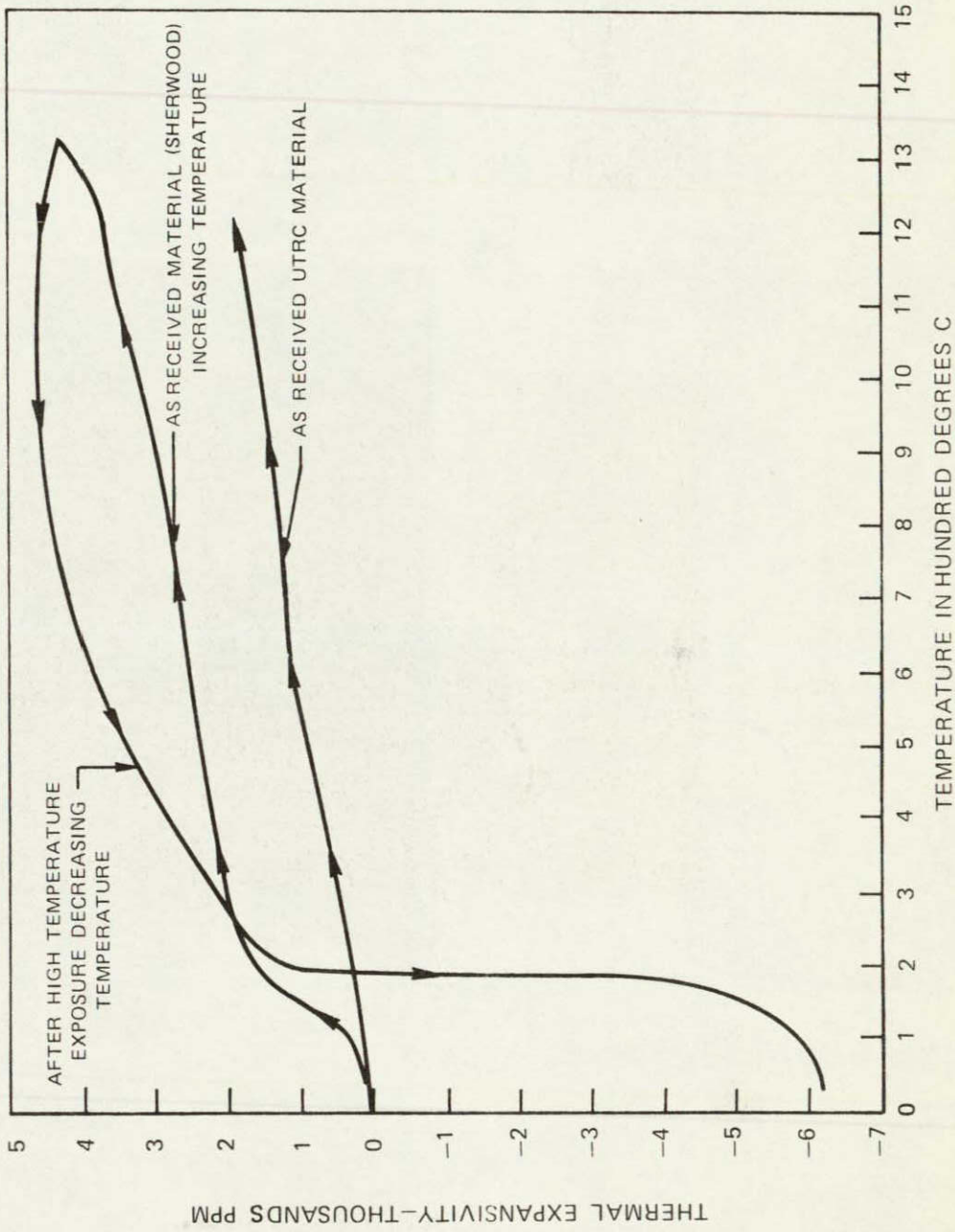

76–05–103–1

C-2

REVERSE SIDE OF SiC BALLISTIC SAMPLE IMPACTED AT 221 m/sec (8.1 JOULES), USING 4.5 mm SOFT STEEL PELLETS, ZYGLO DYE PENETRANT USED.

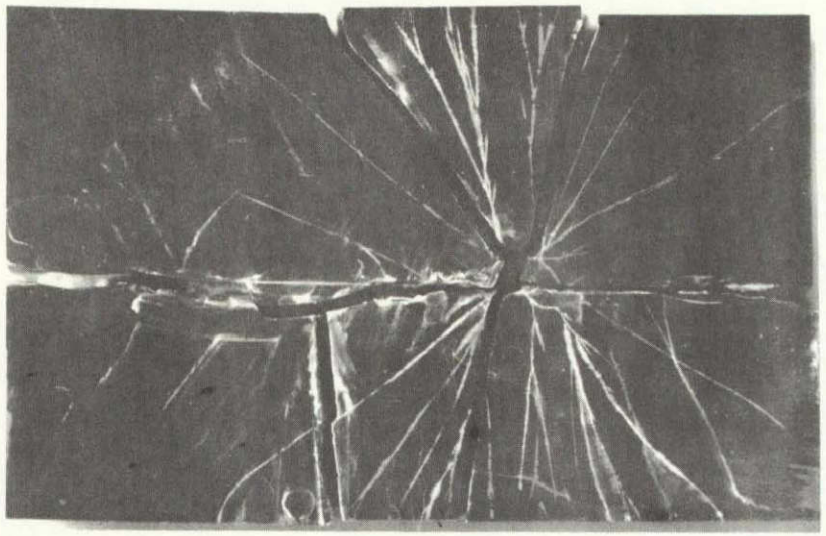

2 1/2X

FIG. 22

FIG. 23

RT BALLISTIC IMPACT SAMPLE OF Si_3N_4 USING 4.5 mm SOFT STEEL PELLETS.

(FRONT FACE)

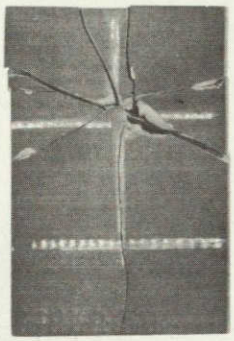

ACTUAL SIZE

SOFT STEEL PELLET AFTER 178 m/sec IMPACT WITH SiC

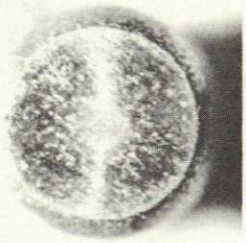

7X

1250°C BALLISTIC IMPACT OF Si_3N_4 WITH Fe_2TiO_5 LAYER
[SAMPLE 132–BI–48,202 M/SEC (7.1 JOULES)]

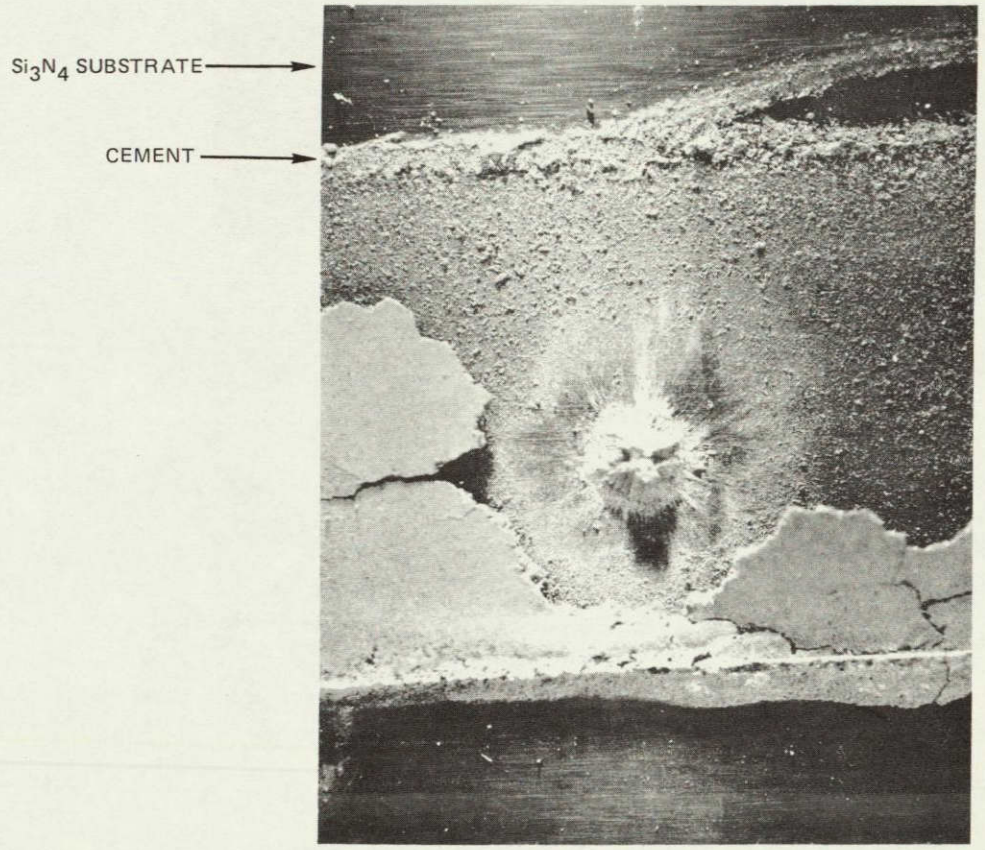

6X

76–11–130–3

1250°C BALLISTIC IMPACT OF Si_3N_4 WITH Fe_2TiO_5 LAYER
[(SAMPLE 132–BI–51, 260 M/SEC (11.4 JOULES)]

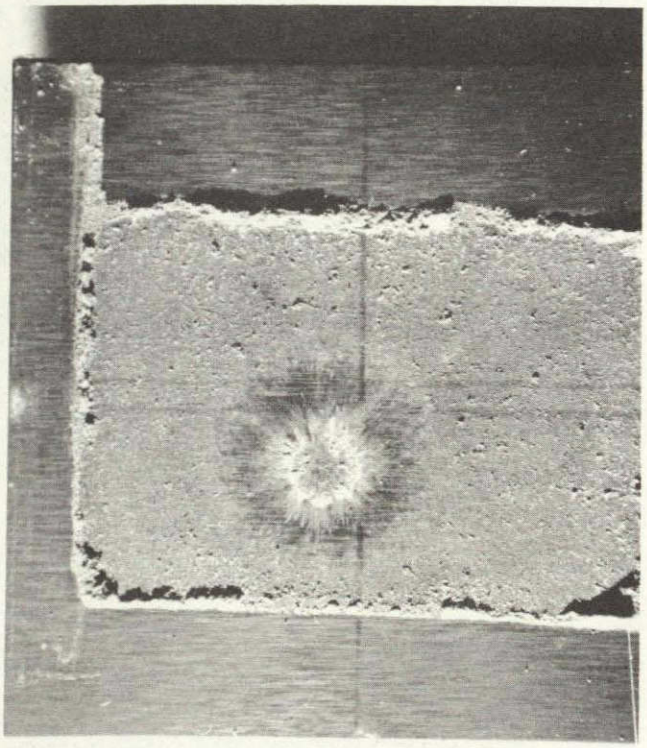

3 1/2X

76–11–130–1

1250°C BALLISTIC IMPACT OF Si_3N_4 WITH Fe_2TiO_5 LAYER
[SAMPLE 132–BI–52, 282 M/SEC (13.6 JOULES)]

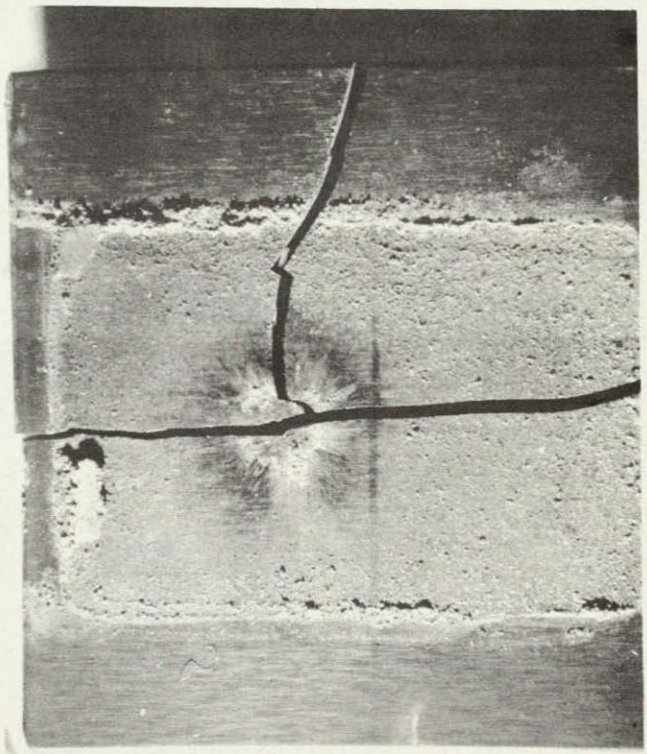

3 1/2X

76–11–130–5

R.T. BALLISTIC IMPACT OF SILICA–ZIRCON LAYER ON Si_3N_4 AT 230 M/SEC
(9.1 JOULES)

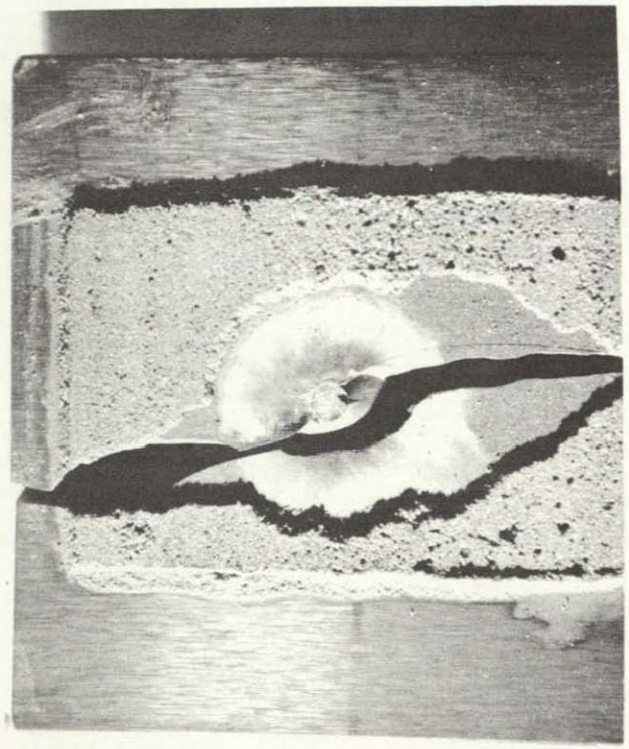

3 1/2X

76–11–130–4

1370° BALLISTIC IMPACT OF SILICA–ZIRCON COATED Si_3N_4 AT 315 m/sec
(17.2 JOULES)

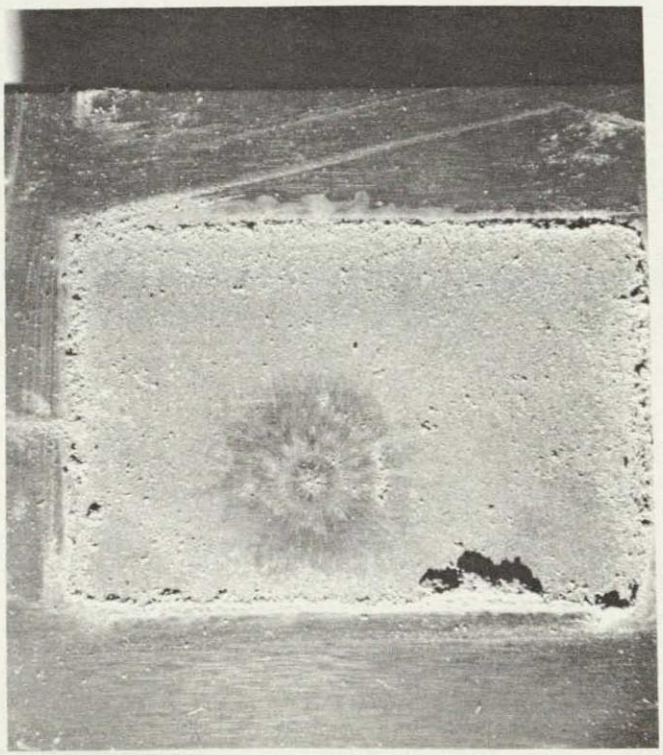

3 1/2X

SILICA –ZIRCON LAYER ON Si_3N_4 CHARPY IMPACT SAMPLE AFTER ONE CYCLE TO 1370°C.

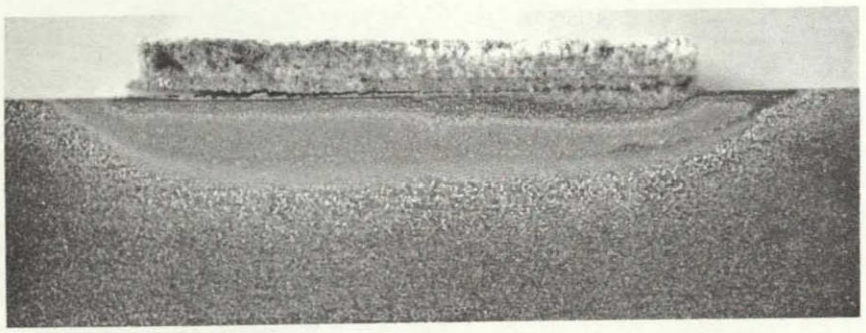

5X

Fe_2TiO_5 LAYER ON Si_3N_4 CHARPY IMPACT SAMPLE AFTER ONE CYCLE TO 1370°C.

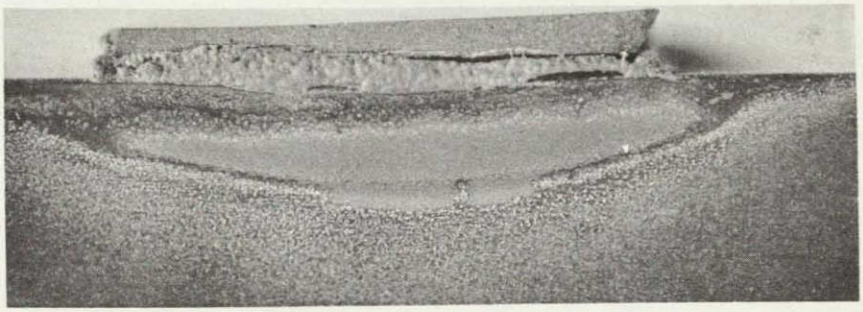

5X

SILICA–ZIRCON LAYER ON Si_3N_4 CHARPY IMPACT SAMPLE AFTER 50 HRS AT 1370°C.

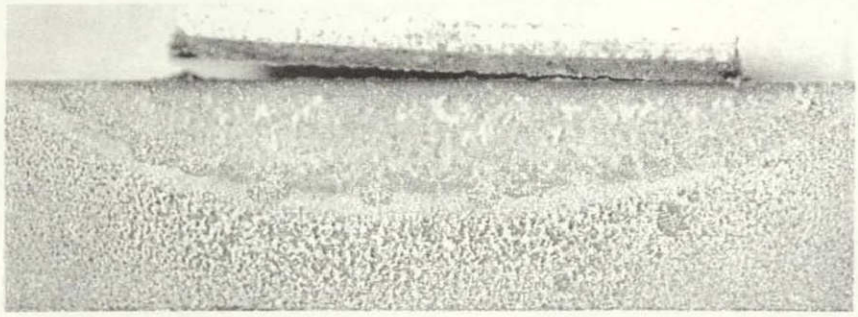

5X

TEM OF REPLICA FROM POLISHED + HF–ETCHED Fe_2TiO_5

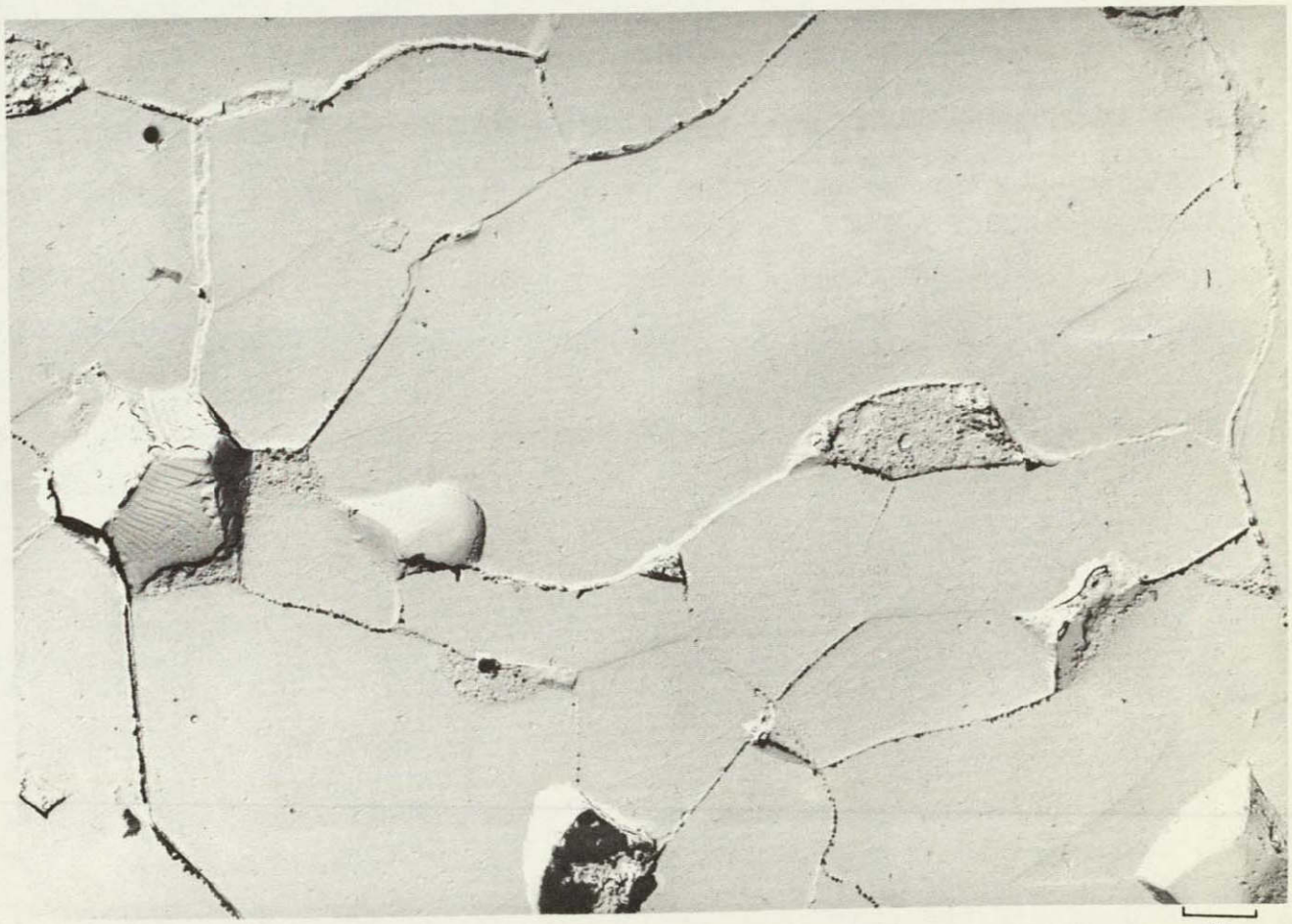

TEM OF REPLICA FROM POLISHED + HF–ETCHED SiO_2–ZIRCON

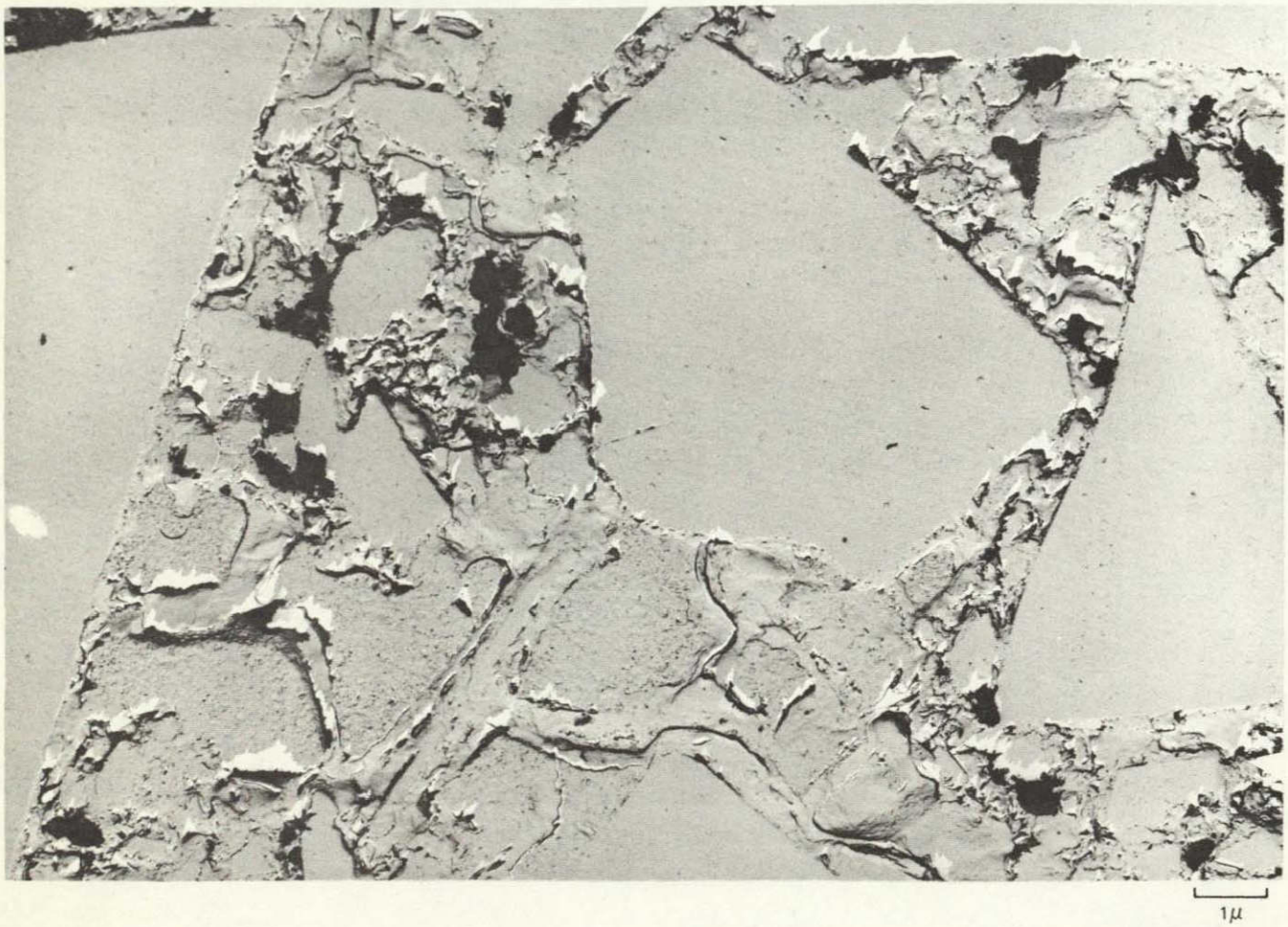

TEM OF REPLICA FROM $a Si_2O_3$ FORMED FROM AMORPHOUS SiO_2 AFTER 1200°C, 1 HR HEAT TREATMENT.

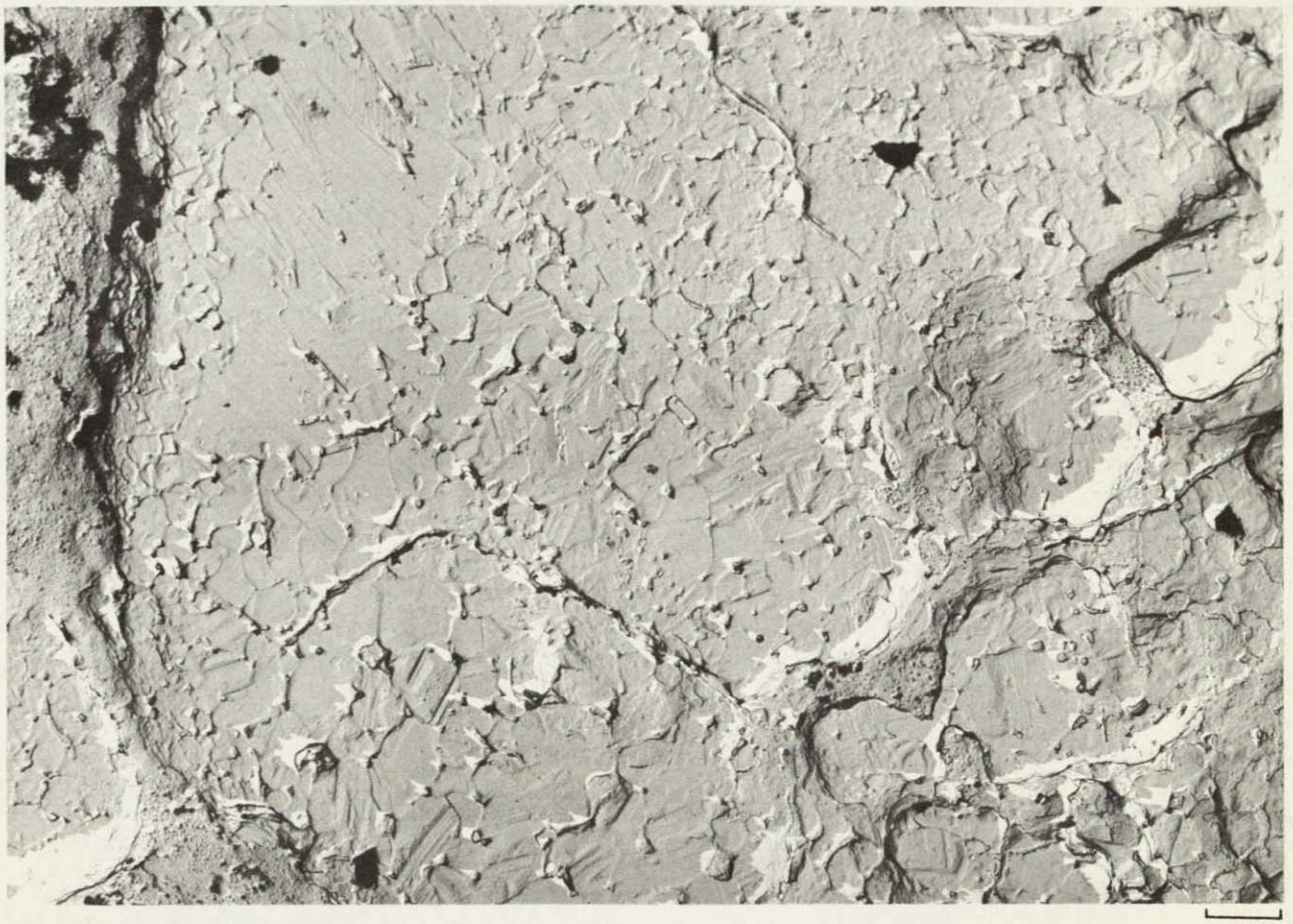

TEM OF REPLICA FROM INTERIOR OF LARGE $a SiO_2$ PARTICLE SHOWING MICROCRACKING WITHIN MARTENSITIC– LIKE STRUCTURE

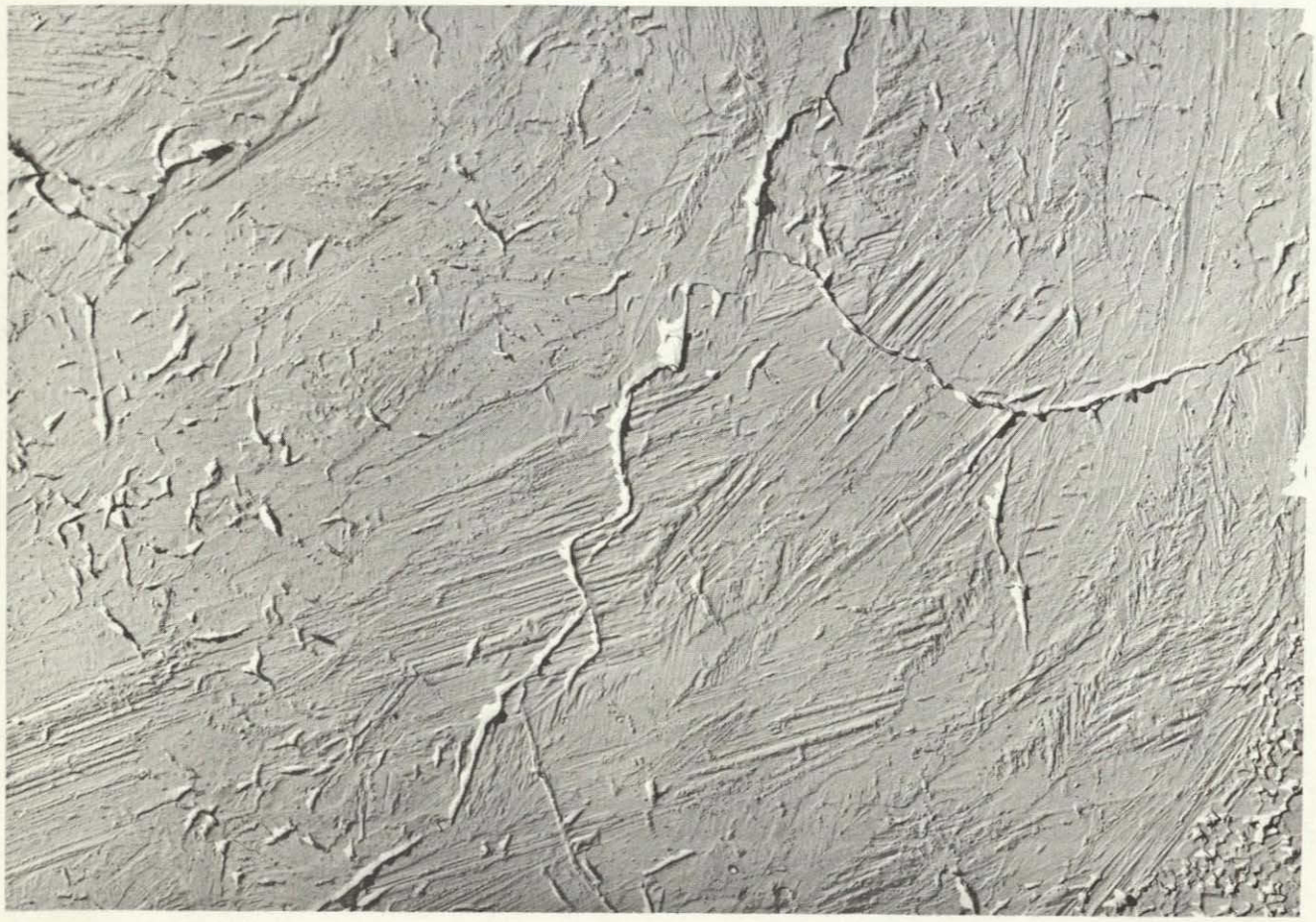

1μ

TEM OF REPLICA FROM $a SiO_2$ (S) ZIRCON (Z) AND POROSITY (P) AT PARTICLE BOUNDARIES

1μ

INTERFACE BETWEEN–325 Si LAYER AND NC–132 Si_3N_4, NITRIDED AT 1375°C
(POROSITY OF R.S. Si_3N_4 LAYER ~ 30%)

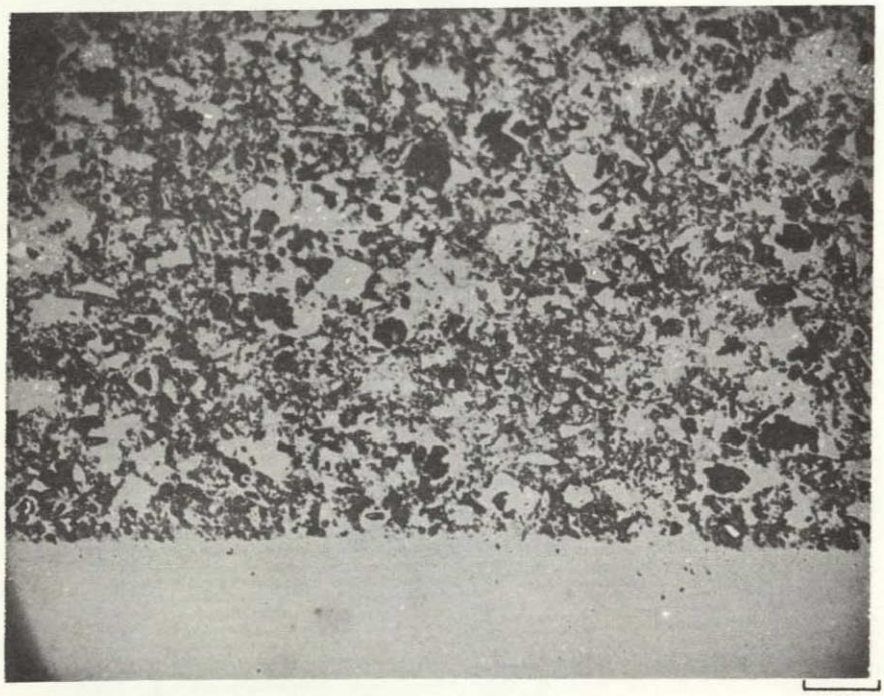

INTERFACE BETWEEN −100, + 200 Si LAYER AND NC−132 Si_3N_4, NITRIDED AT 1375°C.

(POROSITY OF R.S. Si_3N_4 LAYER ~45%)

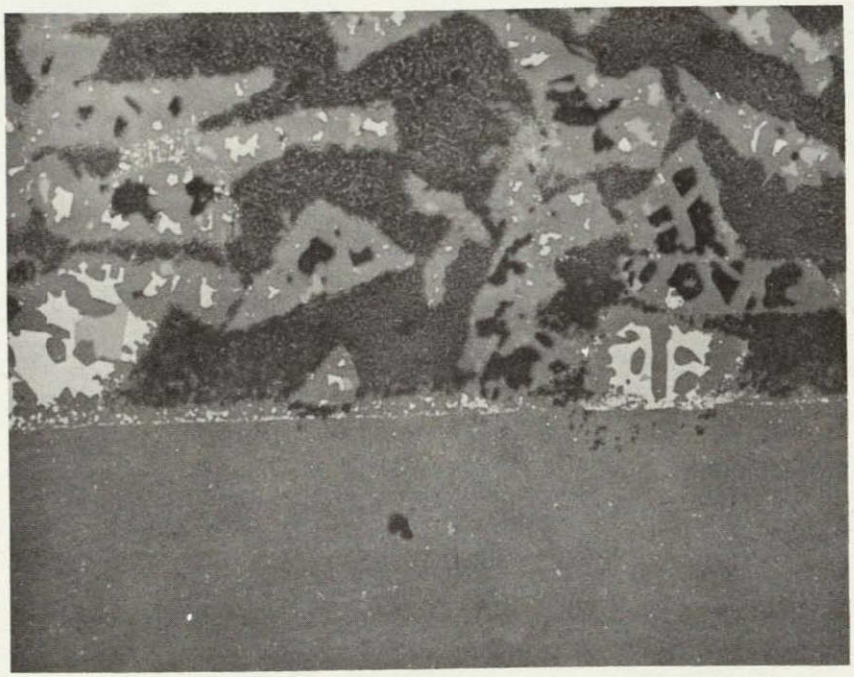

50μ

RT INSTRUMENTED CHARPY IMPACT TEST OF –200 Si NITRIDED SURFACE LAYER ON NC 132 Si_3N_4

LOAD = 190 lbs/div.

TIME = 0.1 ms/div.

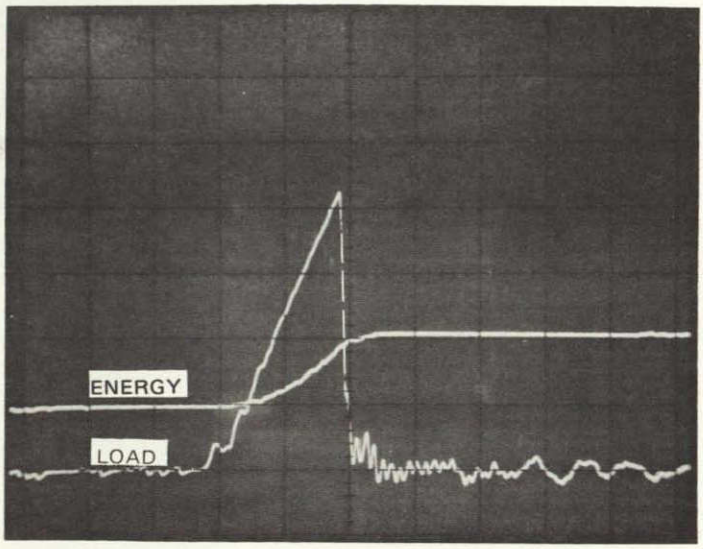

RT INSTRUMENTED CHARPY IMPACT TEST OF −100,+200 Si NITRIDED SURFACE LAYER ON NC−132 Si_3N_4

LOAD = 190 lbs/div
TIME = 0.1 ms/div

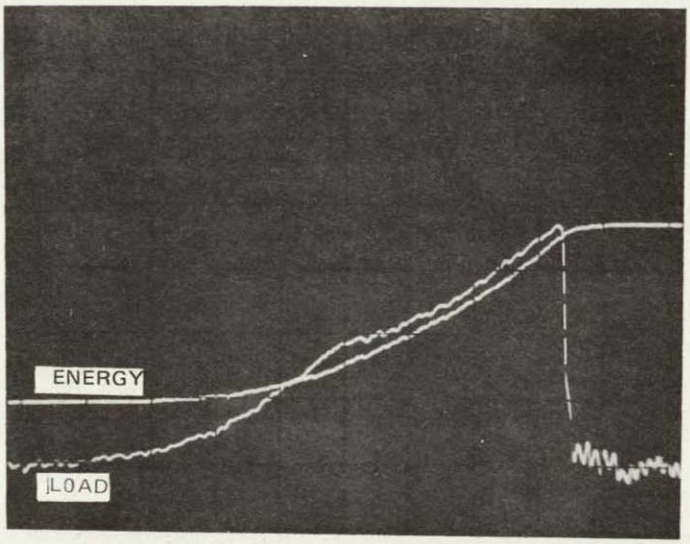

1370°C BALLISTIC IMPACT TEST OF –100, + 200 Si NITRIDED SURFACE LAYER ON NC 132 Si_3N_4 AT 230 m/sec (9.1 JOULES)

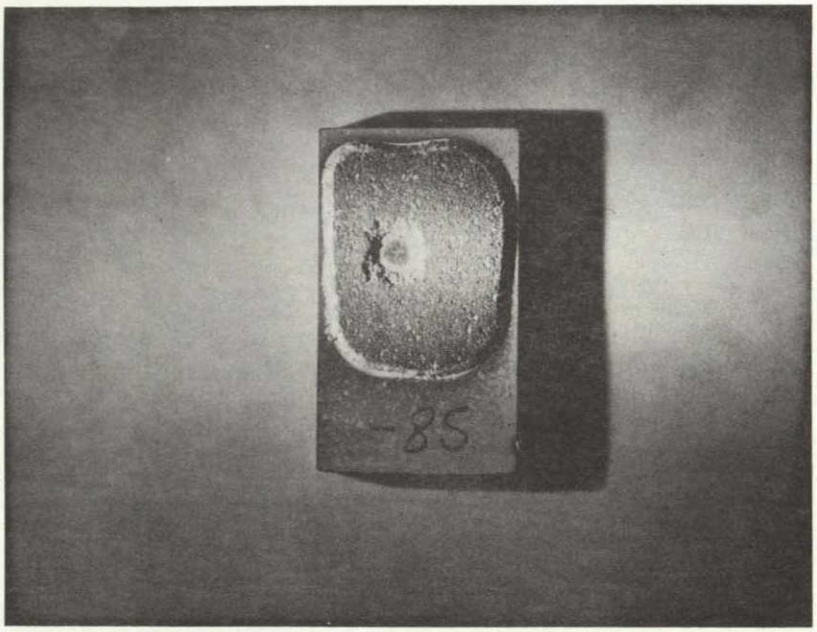

ACTUAL SIZE

1370° BALLISTIC IMPACT OF −100, + 200 Si NITRIDED SURFACE LAYER ON NC−132 Si_3N_4 AT 282 m/sec (13.6 JOULES)

(SAMPLE 132−BI−88)

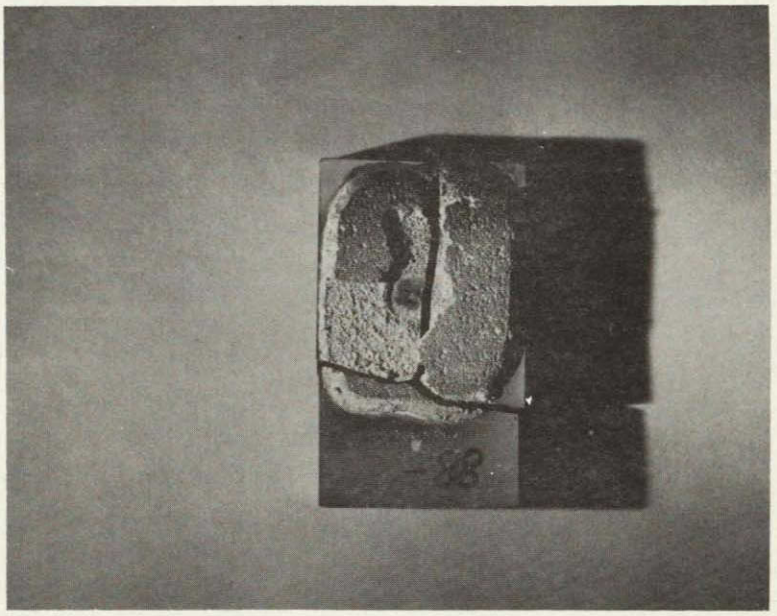

ACTUAL SIZE

RT BALLISTIC IMPACT OF –200 Si NITRIDED SURFACE LAYER ON NC–132
Si_3N_4 AT 191 M/SEC (6.2 JOULES)

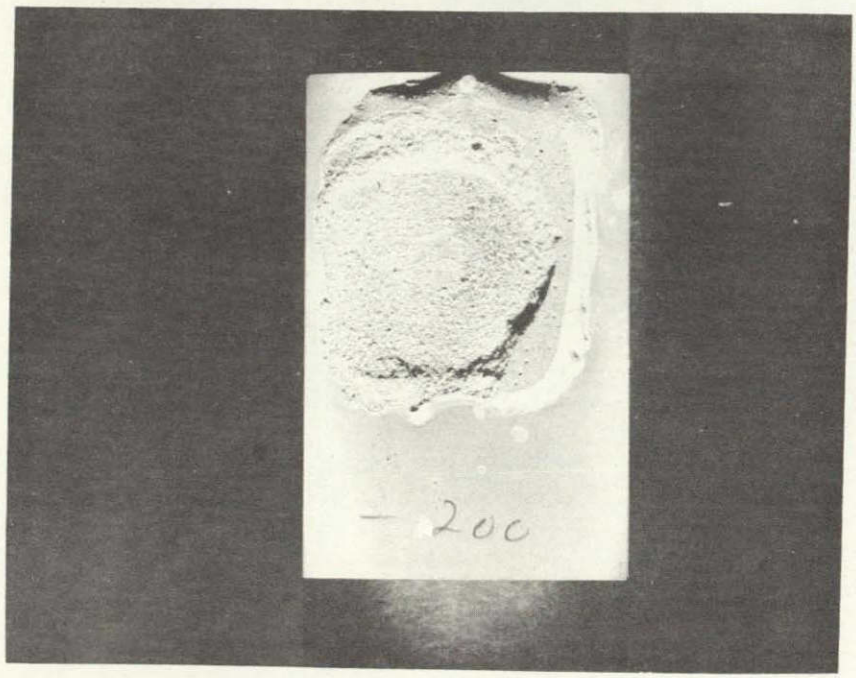

1.75X

77–10–134–1

1250°C BALLISTIC IMPACT OF −325 Si NITRIDED SURFACE LAYER ON NC−132 Si_3N_4 AT 169 m/sec (4.9 JOULES)

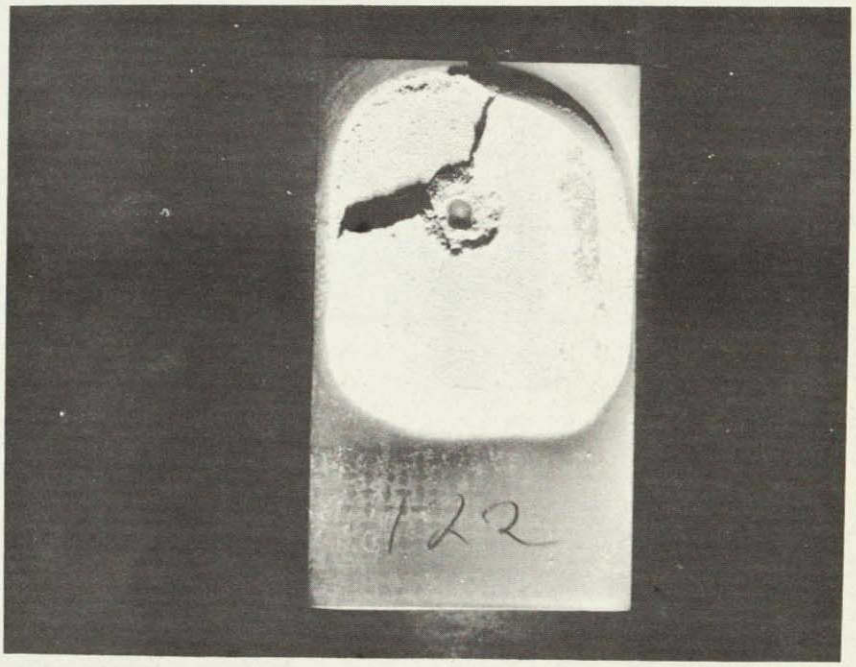

1.75X

77−10−134−3

CROSS–SECTION OF–325 Si + 40 VOL % POLYSTYRENE SPHERES SURFACE LAYER. (200x)
POROSITY > 50%

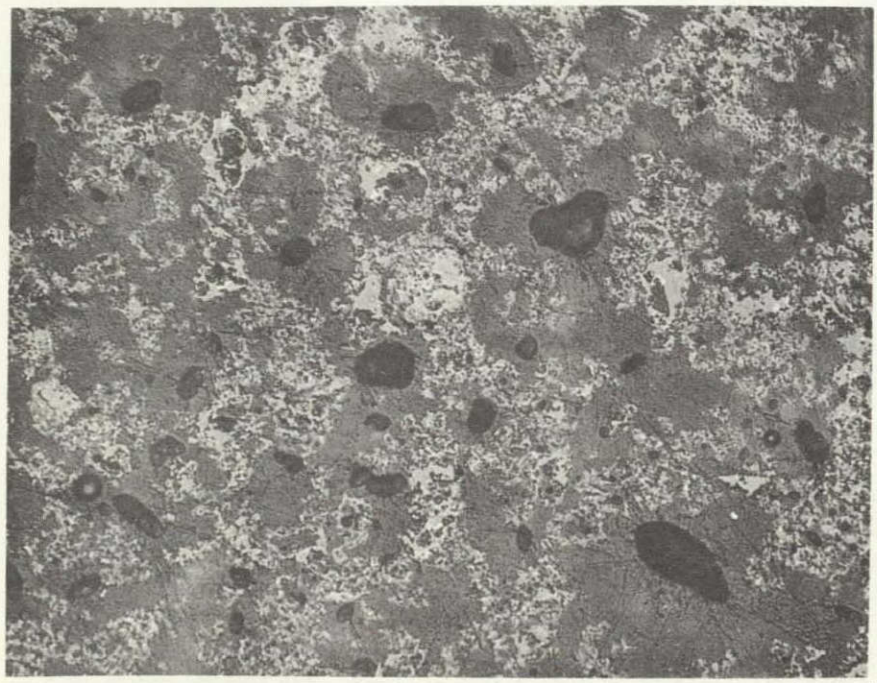

77–06–85–1

RT INSTRUMENTED CHARPY IMPACT TESTS

a. NC–132 Si_3N_4 CONTROL

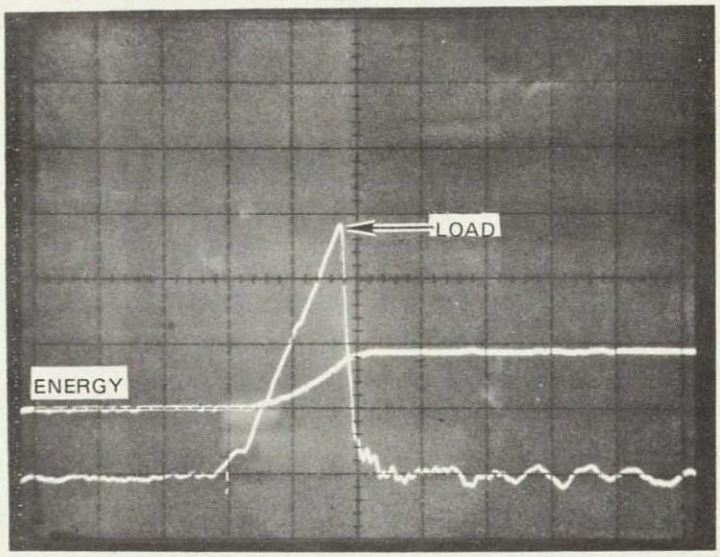

b. R.S. Si_3N_4 SURFACE LAYER (–325 Si + 20 $^{v}/_{o}$ POLYSTYRENE SPHERES) ON NC–132 Si_3N_4

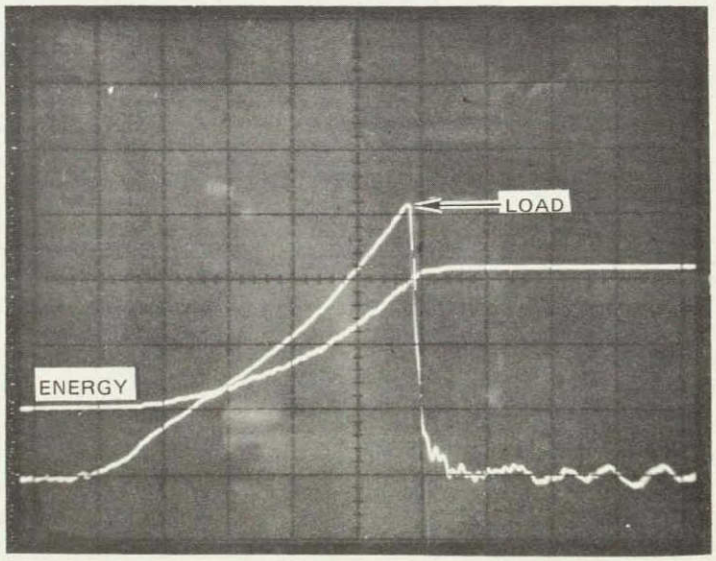

CROSS–SECTION OF – 325 Si + 20 VOL % POLYSTYRENE SPHERES REACTION SINTERED Si_3N_4 LAYER, NITRIDED AT 1375°C.

POROSITY ~ 45%

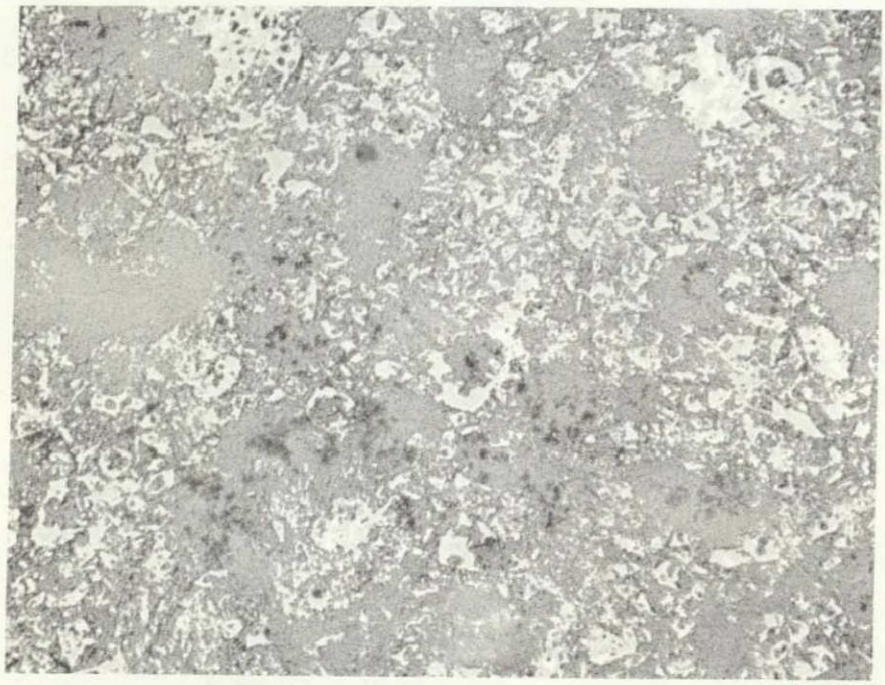

77–06–95–3

INTERFACE BETWEEN–100, + 200 Si LAYER (WATER SLURRY) AND NC–132 Si_3N_4,
NITRIDED AT 1375°C
(POROSITY OF R.S. Si_3N_4 LAYER ~ 50%)

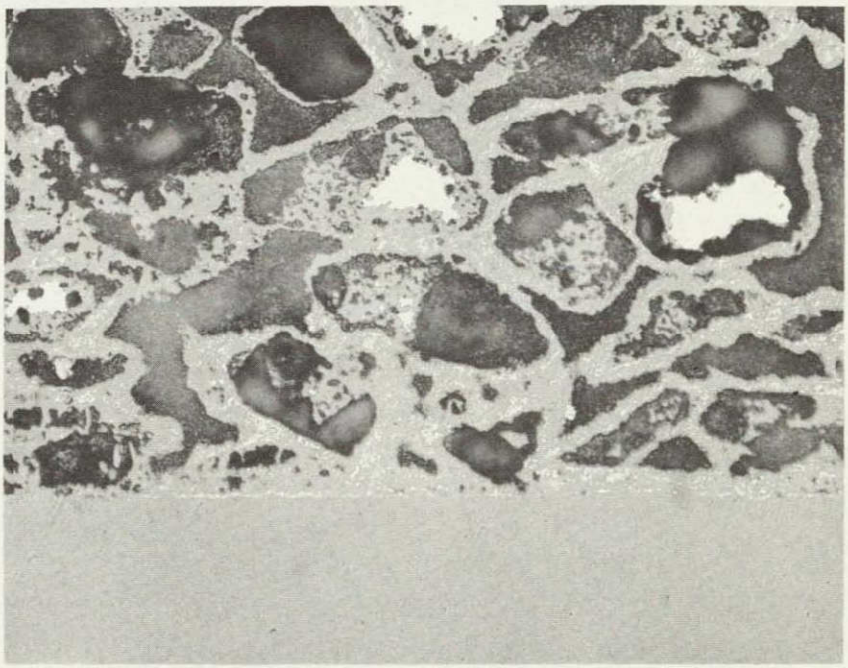

FIG. 50

SEM OF FRACTURE SURFACE OF NITRIDED – 100, +200 Si LAYERS

(a) WATER SLURRY

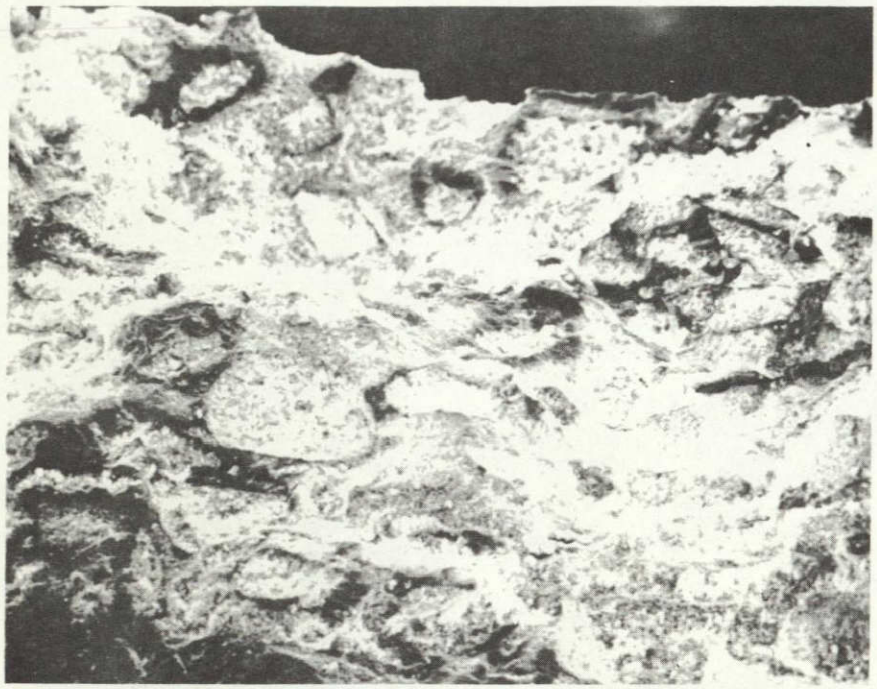

100μ

(b) TOLUENE SLURRY

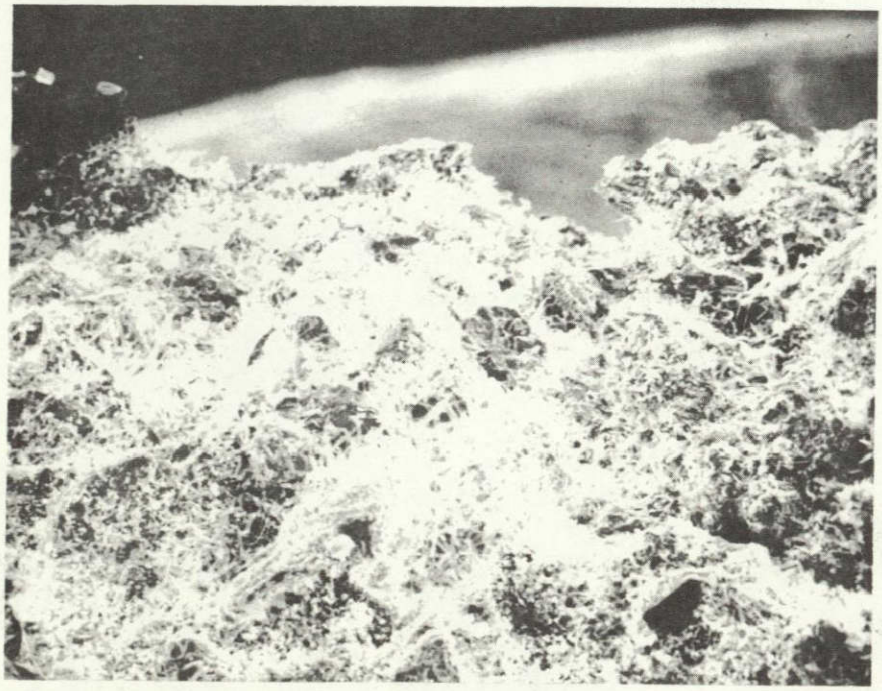

100μ

77–10–202–2

SEM OF FRACTURE SURFACE OF NITRIDED – 100, +200 Si LAYERS (250X)

(a) WATER SLURRY

40μ

(b) TOLUENE SLURRY

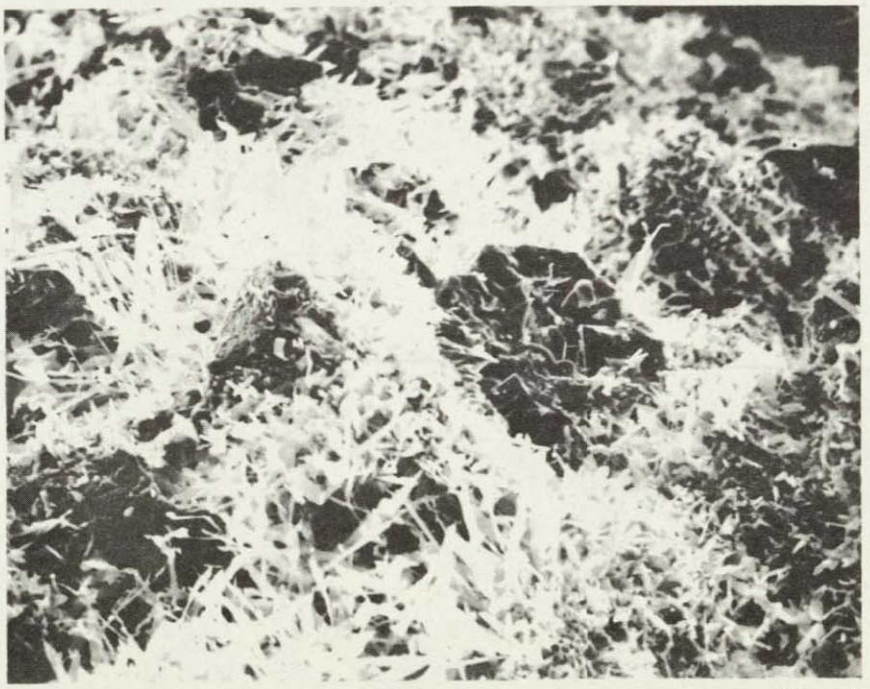

40μ

77-10-202-1

FRACTURE SURFACE OF NC132 WITH R.S. Si_3N_4 LAYER (–325 Si)
(SAMPLE 132–318) POST OXIDIZED 1300C, 1 HR

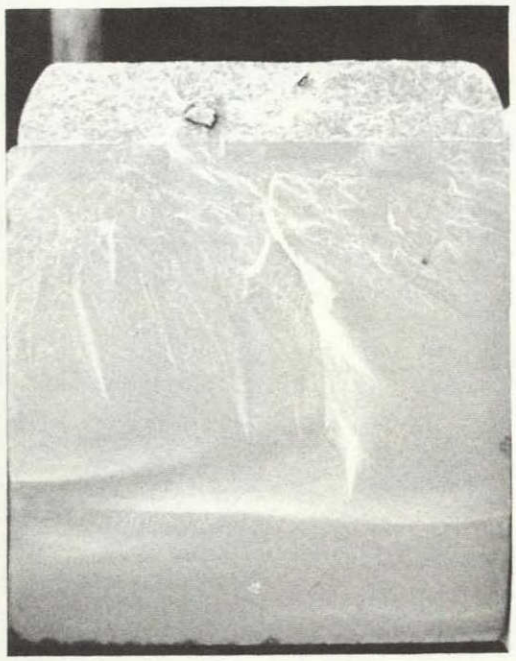

FRACTURE ORIGIN OF NC132 WITH R.S. Si_3N_4 LAYER (–325 Si)
(SAMPLE 132–318) POST OXIDIZED 1300C, 1 HR

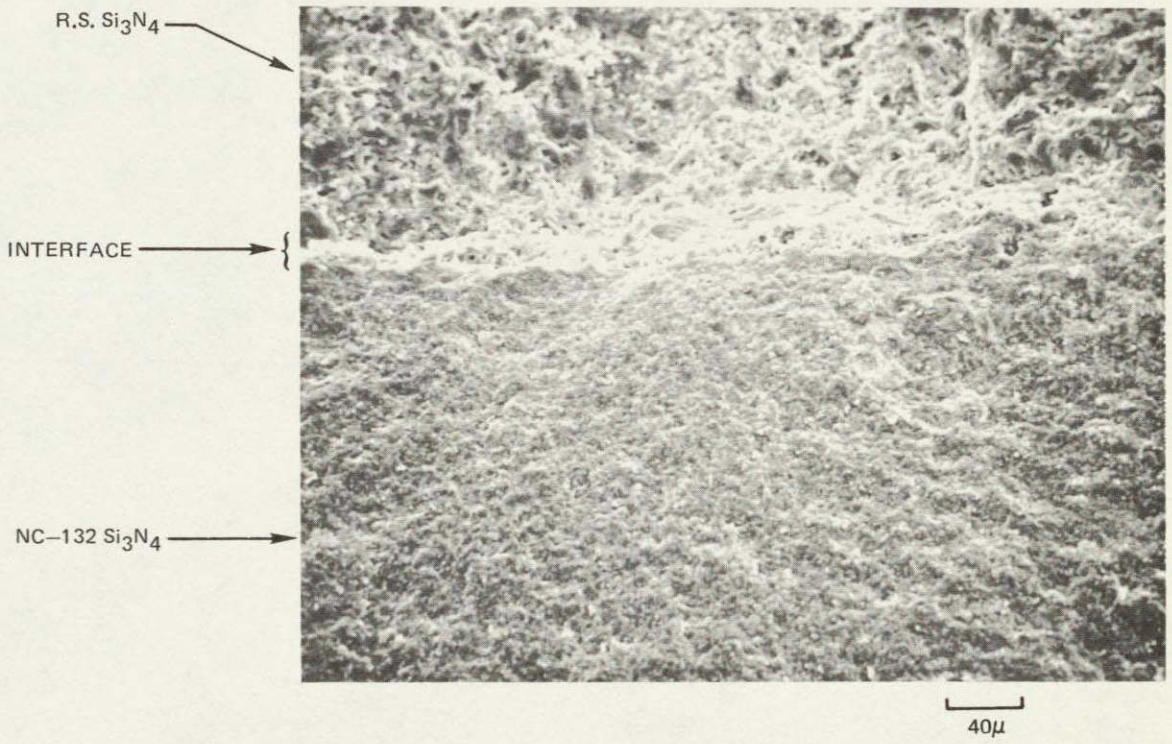

FRACTURE SURFACE OF NC–132 WITH R.S. Si_3N_4 LAYER (–200 Si)
(SAMPLE 132–325) (IMPACTED ON SIDE OPPOSITE R.S. Si_3N_4 LAYER)

1000μ

FRACTURE ORIGIN OF NC-132 WITH R. S. Si_3N_4 LAYER (–200 Si)
(SAMPLE 132–325)(IMPACTED ON SIDE OPPOSITE R. S. Si_3N_4 LAYER)

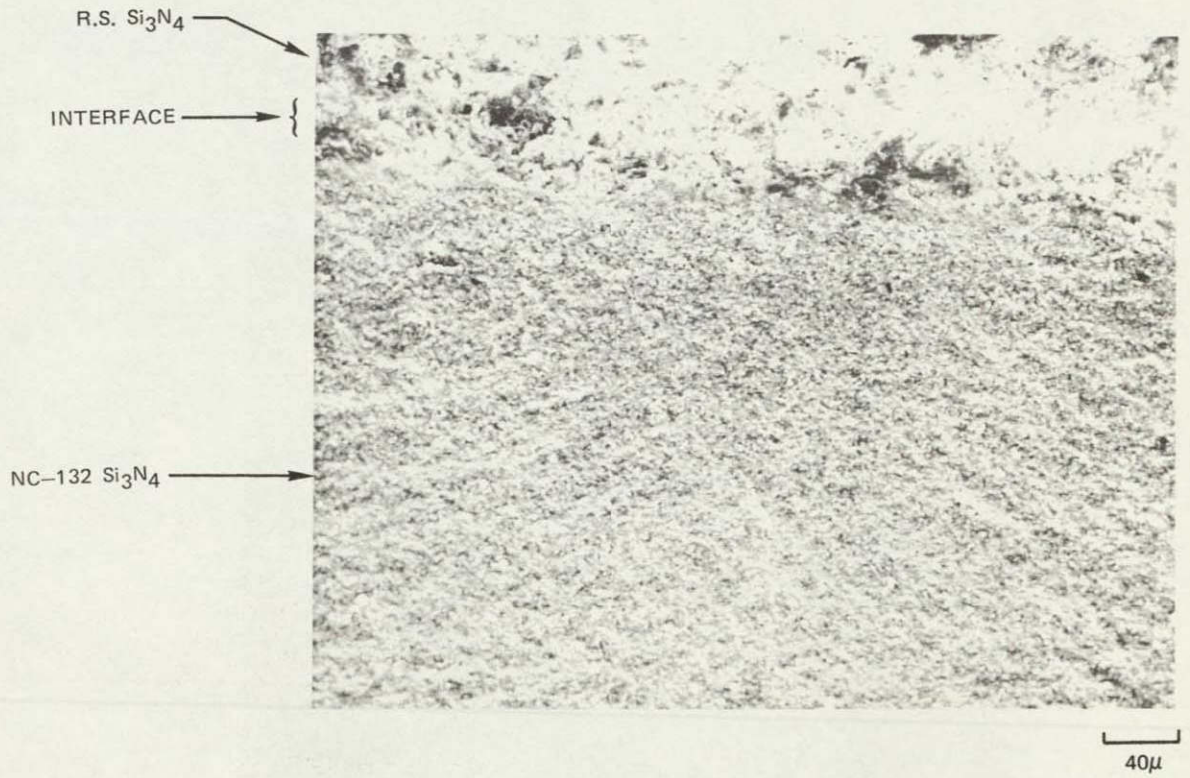

RT BALLISTIC IMPACT OF THERMALLY CYCLED (50 CYCLES, 200°C ⟶ 1370°C)
−100, +200 Si NITRIDED SURFACE LAYER ON NC−132 Si_3N_4 AT 191 m/sec

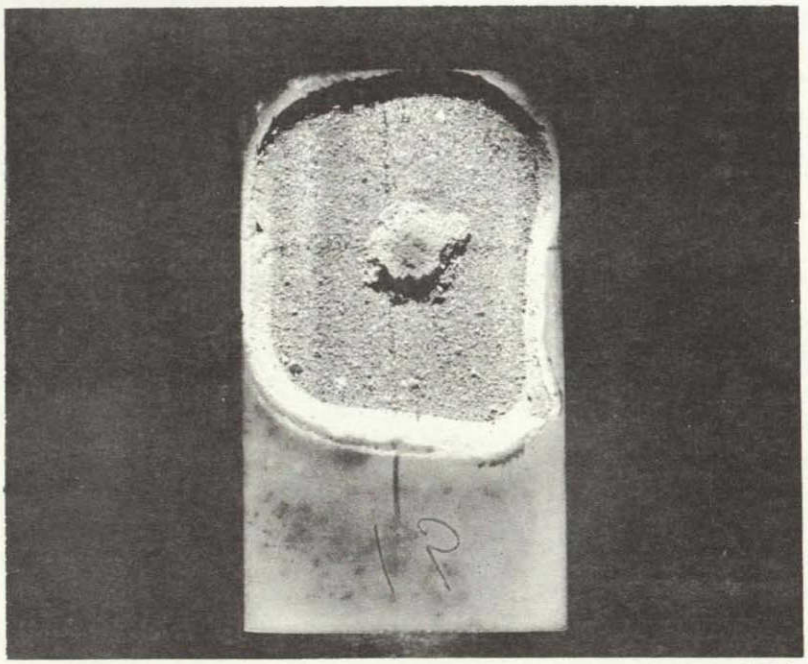

1.75X

77−10−157−1

1370°C BALLISTIC IMPACT OF THERMALLY CYCLED (50 CYCLES, 200°C ⟶ 1370°C)
−100,+200 Si NITRIDED SURFACE LAYER ON NC−132 Si_3N_4 AT 315 m/sec (17.2 JOULES)

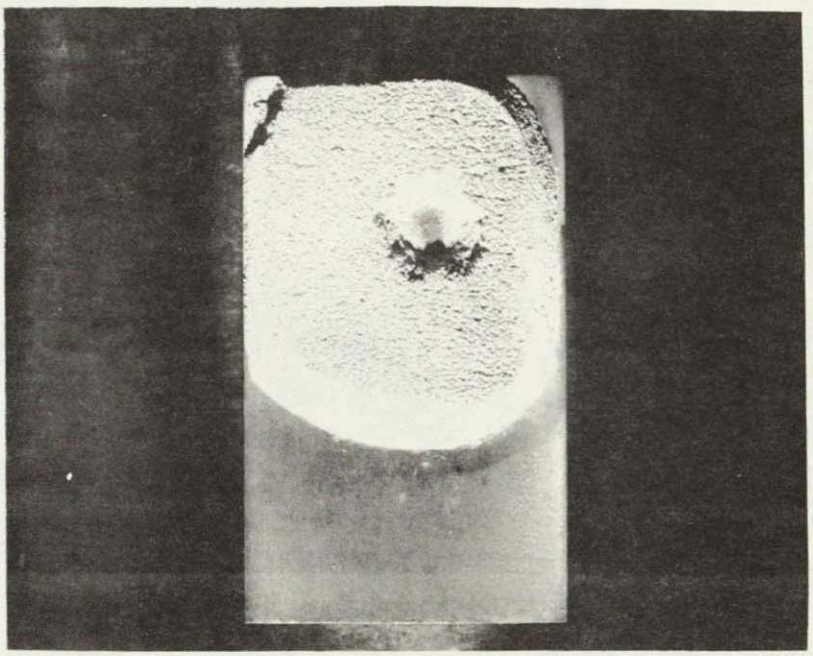

1.75X

1370°C BALLISTIC IMPACT OF THERMALLY CYCLED (50 CYCLES, 200°C ⟶ 1370°C) –200 Si NITRIDED SURFACE LAYER ON NC–132 Si_3N_4 AT 191 m/sec (6.2 JOULES)

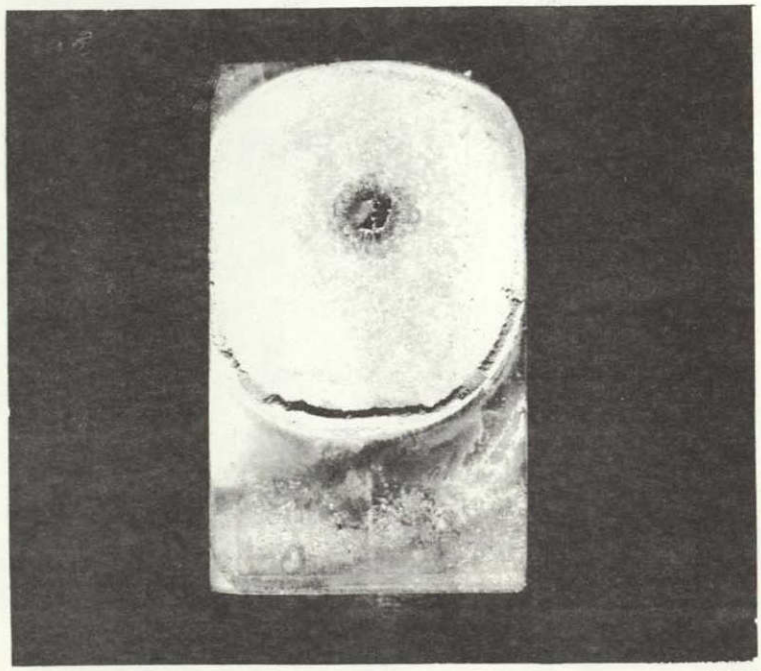

1.75X

77–10–157–2

APPENDIX A

United Technologies Corporation Hot Impact Testing Facility

A highly modified Physmet* CIM-24A impact testing machine developed under Corporate funding was used to obtain all the Charpy impact data reported in this program. The Physmet machine has the advantages for our purposes of high sensitivity with direct dial reading of energy to 0.007 joules (.005 ft-lbs) and a tup with no outriggers or mass below the point of sample contact. The base of this machine was replaced at UTRC by a steel block 25.4 x 55.9 x 10.2 cm high (10 x 16 x 4 in.) which was bolted to a cement block 83.8 x 55.9 x 77.5 cm high. A cavity machined in the steel block 7.6 x 15.2 x 9.5 cm deep (3 x 6 x 3.75 in.) permits the use of various anvils. An anvil of 17-4 PH steel was used for all room temperature testing. Shims were used to adjust the position of the anvil so that the tup struck every ceramic sample within $\pm$ .0078 mm ($\pm$ .002 in.) of the zero pendulum position.

The tup was instrumented at UTRC to measure force using 1000 Ω strain gages (M-M EA-06-250BK-10C) bonded with M-Bond AE15 adhesive**. The two active gages were placed near the front of the tup to minimize ringing effects and the bridge completion gages were positioned behind the tup. The active gages were covered with 0.40 mm thick Micarta using M Bond AE-10 adhesive to prevent damage to the gages.

The strain gage output from the tup was fed through a BAM-1*** strain gage amplifier and conditioner to one 2K channel of a Zonic**** data memory system. The same signal was also integrated and stored in a second 2K memory channel of the Zonic unit. The force trace and the energy trace (integration of force versus time) could then be displayed simultaneously on a Tektronix***** R5013N storage oscilloscope at any desired level of amplification or filtering and with the optimum time base and scope position.

*Physmet Corp., 156 Sixth St., Cambridge, MA
**Micro-Measurements Div., Vishay Intertechnology, Inc., Romulus, MI
***Vishay Instrument, Vishay Intertechnology, Inc., Malvern, PA
****Zonic Technical Laboratories, Cincinnati, OH
*****Spectronics, Inc., Richardson, TX

The data trigger for this system was provided by a GaAs light emitting diode and silicon NPN phototransistor unit (SPX-1160-3)* used in conjunction with small mirrors attached to the tup support structure. The solid state light source and sensor assembly was mounted on a micrometer slide for precise adjustment of the trigger impulse time. The two mirrors used also had many equally spaced strips of reflective and nonreflective surface running perpendicularly to the direction of travel. The spacing on one mirror was 0.0775 mm (.002 in.) and that on the other was 0.209 mm (.008 in.). The output from the phototransistor could also be amplified and displayed on the oscilloscope as a third trace which varied in voltage with the mirror spacing. This trace was used to directly measure the pendulum velocity.

The scale for the oscilloscope force traces was calibrated by breaking standard notched 6061-T6 aluminum samples** just prior to each test series. The Physmet dial energy values obtained in testing standard AMMRC samples*** showed good agreement with expected values and therefore the energies indicated on the Physmet dial were used for calibration of energy scales on the oscilloscope traces.

Although elevated temperature impact testing of metals is sometimes conducted by breaking a sample on a cold anvil after quickly removing the specimen from an auxiliary furnace, this procedure is not generally desirable for use with ceramic materials because of their relatively poor resistance to thermal shock and because their strengths are surface sensitive. This procedure would be particularly unsuitable for unambiguous studies of the effects of thin surface coatings on mechanical strength.

The Physmet machine was therefore modified as shown in Fig. A1 for hot impact testing to include a special furnace which permitted the test sample to be heated in place. Four bayonet type SiC resistance heaters whose axes were perpendicular to the longest dimension of the Charpy bar were used to heat the samples. These heaters were positioned symmetrically around the test span with two heaters above the sample and two below.

The furnace consisted of three parts, a lower section with two heating elements and two upper sections which contained one heater each. A top view of the lower furnace section is shown in Fig. A2. A water-cooled stainless steel block supports firebrick and fibrous zirconia insulation**** as well as

*Spectronics, Inc., Richardson, TX
**Effects Technology, Santa Barbara, CA
***Army Materials & Mechanics Research Center, Watertown, MA
****"Zircar", Union Carbide Corp.

two carefully machined alumina* anvil pieces. The alumina anvils are clamped in place with a Bellville washer assembly against stainless steel struts which extend upward from the water-cooled base. The upper two sections of the furnace are each mounted on individual air cylinders whose axes make an angle of approximately 55° with the horizontal. When activated for testing, these cylinders quickly separated the two upper furnace sections sufficiently to permit the instrumented tup to swing freely through the furnace. The two upper furnace sections were also moved upward at the same time by the air cylinders to permit the broken sample fragments to fly out of the furnace in the horizontal plane. Figure A3 presents another closer view of the furnace details with one of the upper furnace sections removed to show a sample in position and the other hot SiC heaters.

Temperatures inside the impact furnace were measured using a Pt-Pt + 10% Rh thermocouple bead positioned just below the lower tensile edge of the samples between the two lower SiC heaters at the midspan position. Preliminary experiments with thermocouples wired in place against the tensile surface of a sample at midspan indicated that for sample temperatures of 1250° and 1370°C the furnace thermocouple needed to be 36°C higher. The typical elapsed time between opening the furnace slightly and sample fracture was two (2) seconds. Typical sample surface temperature drops during this time period determined using five thermocouples wired against the tensile surface of a sample at midspan at 1250° and 1370°C were 13° and 39°C, respectively. Appropriate adjustments in furnace power using the furnace thermocouple were made to compensate for these temperature differences.

Instrumented impact data from brittle, high elastic modulus materials can easily be misinterpreted. Figure A4 shows, for example, RT data obtained using the UTRC impact facility with solid alumina rod samples at 3.47 m/sec (11.4 ft/sec). The double peak in the force curve could easily suggest that an energy absorbing coating was affecting the shapes of these traces. In fact, there is no coating present and these data could only be used with great caution. In the upper trace of Fig. A4, the initial force peak is due to an inertial effect and is not directly related to sample behavior. The second peak is the elastic strength limit of this sample. In the lower picture in Fig. A4, the band pass has been reduced to almost eliminate the inertial peak. Unfortunately, as can be seen by comparison, this has also reduced the rise time of the measurement system so that the peak force indicated for this sample is also reduced and the data are thus in error.

*Wesgo 995 Alumina, Western Gold & Platinum, Belmont, CA

Figure A5 illustrates that the appropriate technique to use for this brittle system is to reduce the impact speed. The inertial peak and the associated ringing oscillations are largely eliminated and do not confuse the data as before. Even with the low-blow technique or slower speed impact testing, too much electronic filtering can still result in inaccurate data. The lower picture in Fig. A5 and especially Fig. A6 show these effects for the same size specimens. Note that the reduced rise time (small band pass) did not permit the maximum force to be accurately measured and, also, the traces indicate that energy was absorbed subsequent to the peak force which in fact is not correct. Because of the possible complications associated with the inertial peak room temperature testing on this project was conducted at a low blow trigger position resulting in a tup velocity of 1.11 m/sec (3.66 ft/sec). At elevated temperatures this low blow trigger position could not be used because it would have required part of the tup support structure to be within the furnace. The counterweights shown in Fig. A1 were used to overcome this problem. The elevated temperature tests in this program were normally conducted at tup velocities of 0.933 m/sec (3.06 ft/sec).

UNITED TECHNOLOGIES CORP.
HOT IMPACT TESTING FACILITY

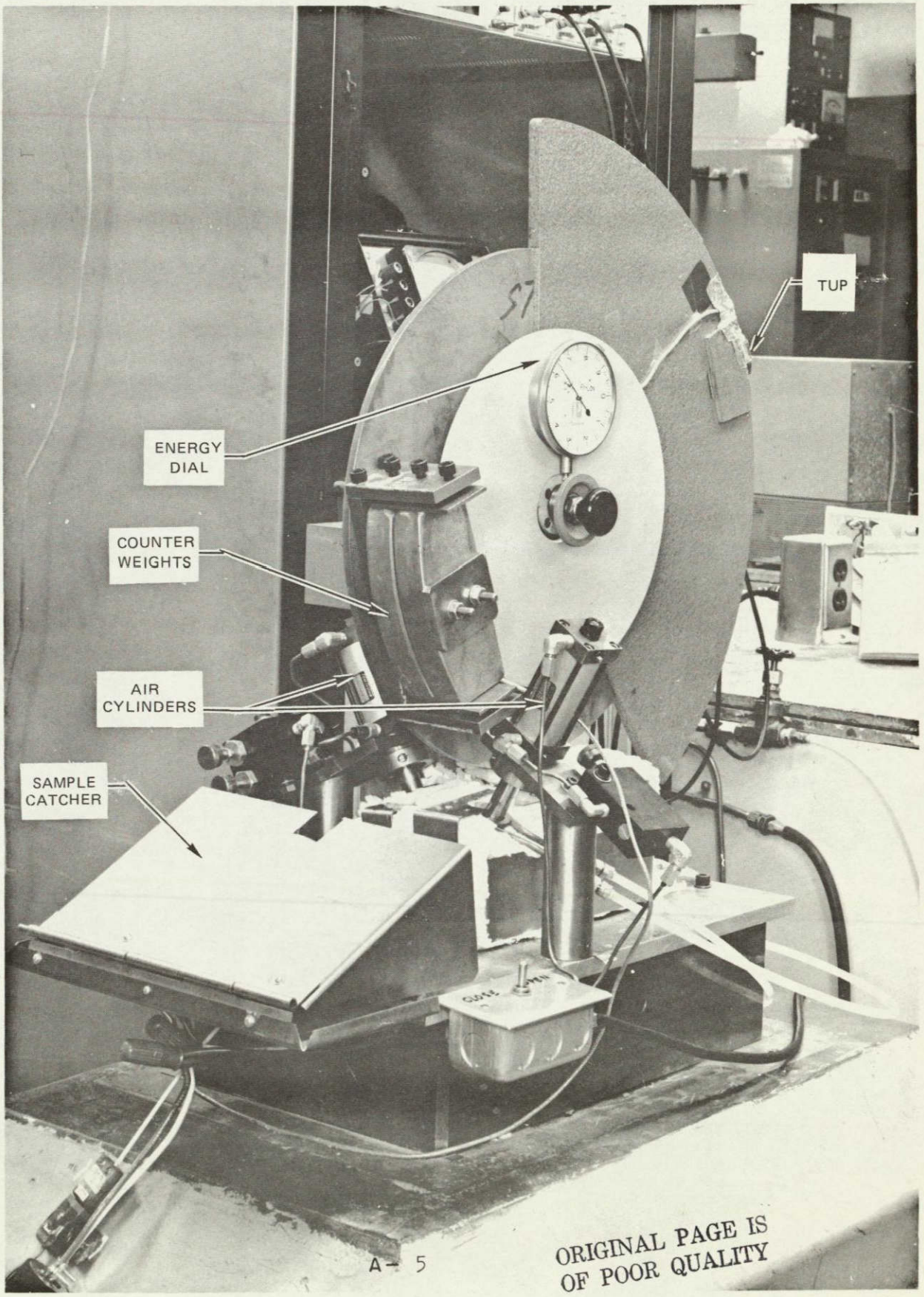

76-05-139-2

UNITED TECHNOLOGIES RESEARCH CENTER
HOT IMPACT TESTING FURNACE

PLAN VIEW – FURNACE SECTIONS REMOVED

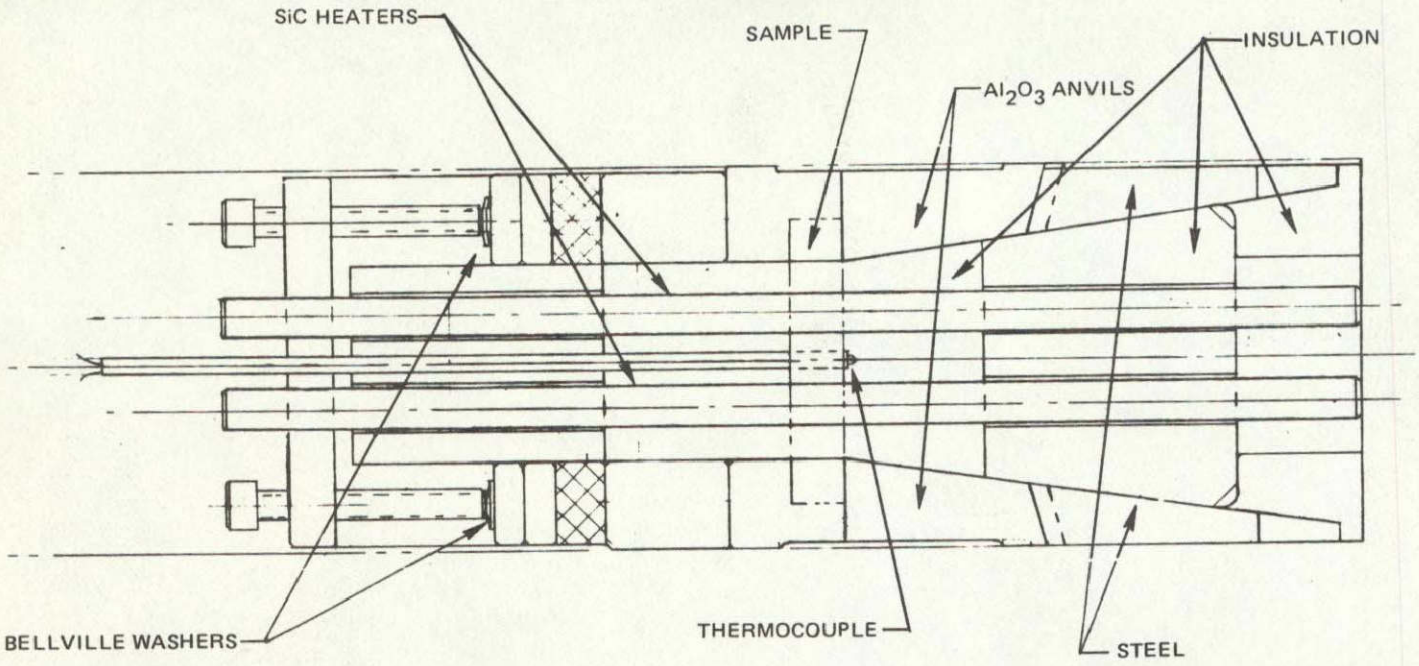

FIG.A2

FIG. A3

UTRC HOT IMPACT FACILITY WITH ONE OF THE UPPER FURNACE SECTIONS REMOVED

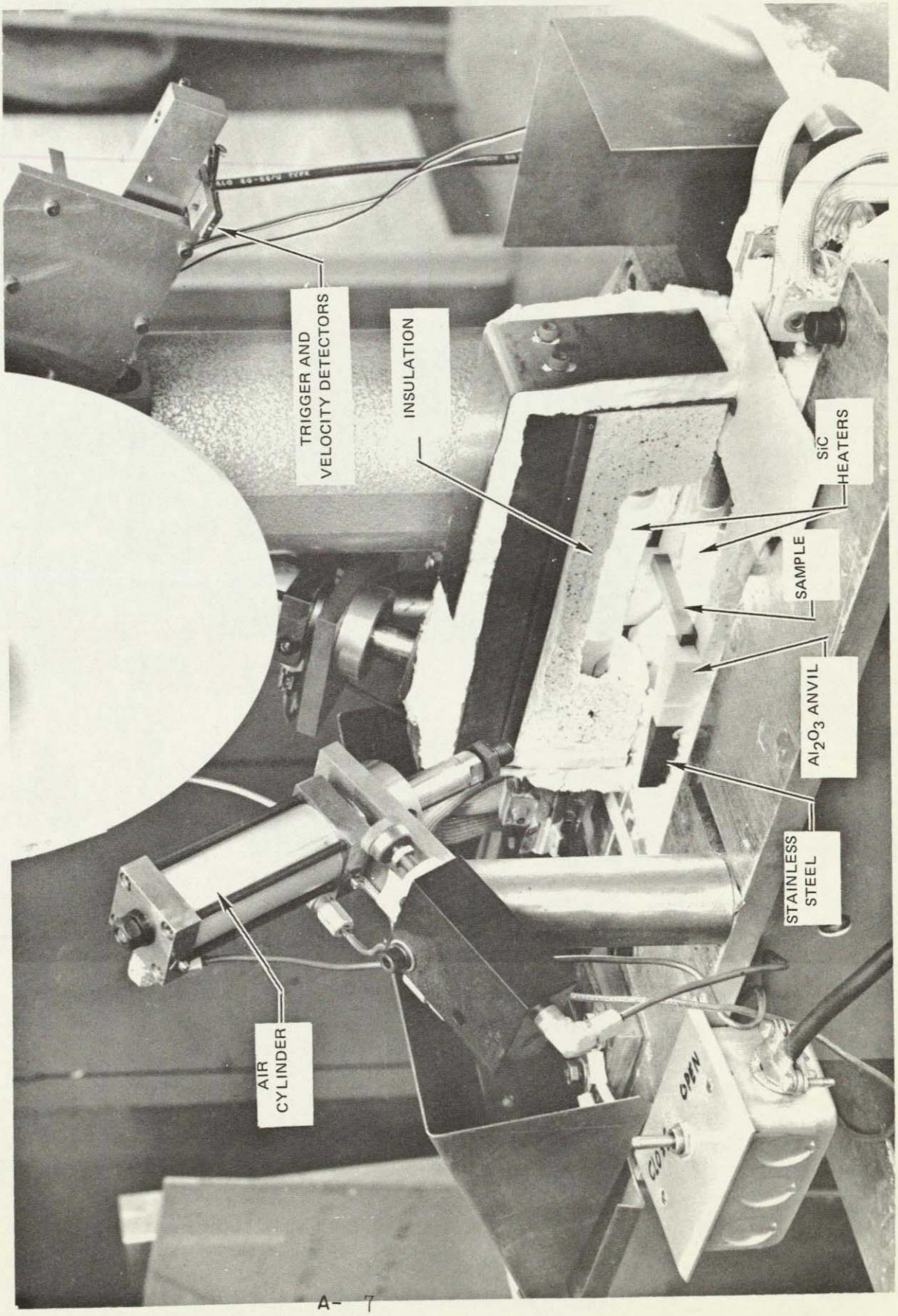

EFFECT OF FILTERING ON INSTRUMENTED IMPACT RESULTS

0.95 CM –DIA Al_2O_3 ROD AT 3.47 M/SEC (11.4 FT/SEC)

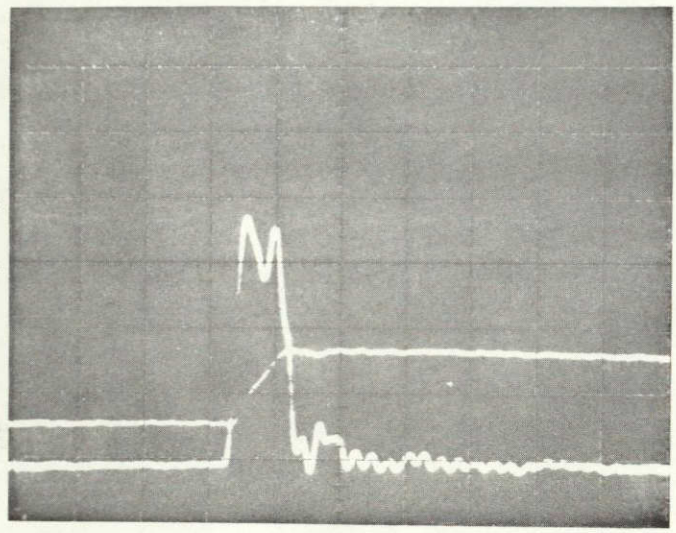

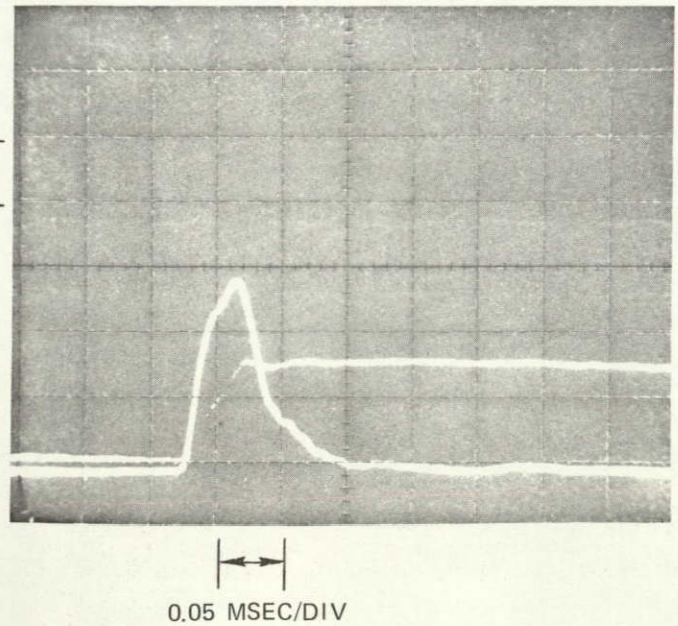

OVER FILTERED LOW–BLOW INSTRUMENTED IMPACT RESULTS
0.95 CM–DIA Al_2O_3 ROD AT 0.741 M/SEC (2.43 FT/SEC)

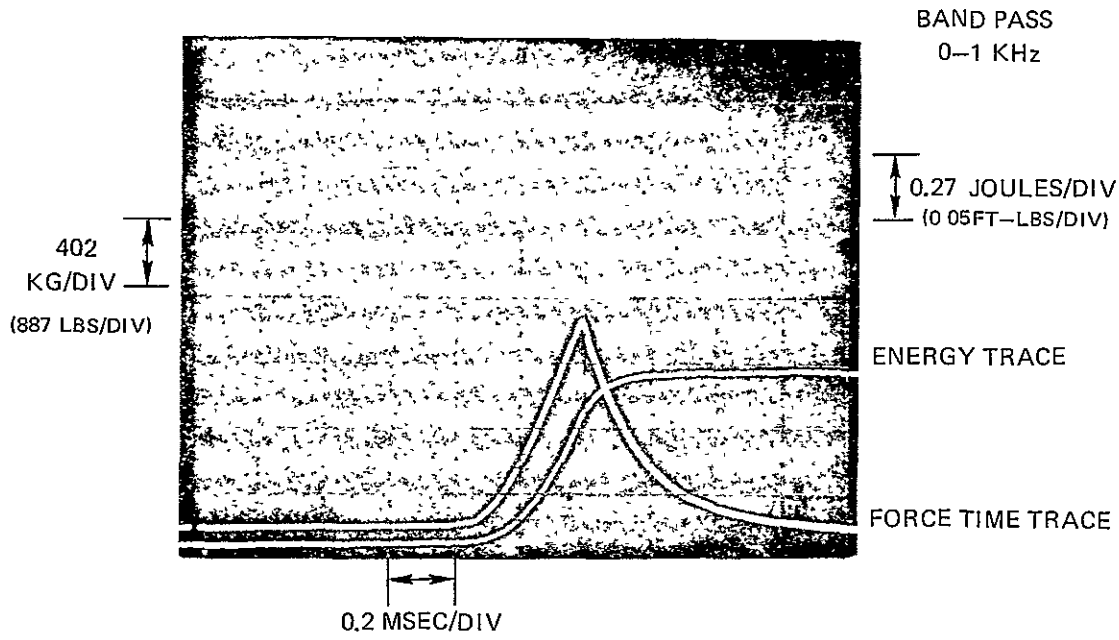

APPENDIX B

Accuracy of Impact Machine

Evaluation of the Charpy impact properties of ceramic materials is complicated by the fact that they have high elastic moduli combined with low impact energies. Because of this, the instrumented data can be confused or even lost in a large "inertial" peak which appears on the oscilloscope force versus time trace at the instant of sample contact with the moving tup. This undesirable peak can be largely removed by testing at lower speeds. Most of the data reported under this program has been obtained using a special "low blow" trigger position which reduced the impact speed from 11.4 ft/sec to 3.66 ft/sec.

When using the "low blow" trigger positions, the distances between the tup and the sample before pendulum release is of the order of one to three inches. This arrangement is clearly not feasible for testing with the sample enclosed in a furnace. In order to surround the sample with a furnace suitable for elevated temperature testing, it was necessary to use a trigger position which rotated the tup away from the sample until the impact surface of the tup was almost horizontal. In order to reduce the speed of impact under this circumstance, the pendulum system was counterweighted with a special frame containing two lead weights tightly clamped in a special case. This case was movable so that the pendulum zero could be easily adjusted to be just at specimen contact. The lead weights revolve around the pivot in a radius which is about one-half of that for the tup.

Use of the counterweight system at our #6 trigger position results in a speed at contact of 3.09 ft/sec. These speeds were measured using our mirror trigger and velocity measuring system previously described. The widths of the mirrored and unmirrored strips sensed by our photodiode system and displayed on the oscilloscope for these speed determinations were each 0.209 mm (0.008 in.).

Use of the counterweighted pendulum required a recalibration of the absorbed energies as read-out on the Manlab energy dial indicator. Because this indicator simply measures how high the pendulum swings after impact, the energy values on the dial are directly proportional to the mass or weight of the pendulum. This was measured with the counterweights in place using a balance and the pendulum in a horizontal position. The results of these measurements was to increase the sensitivity of the dial read-out by a factor of six. Thus, each unit on the dial energy scale represented only 16.5% of the energy measured without the counterweights in place.

Use of a counterweighted pendulum system raised the question of what, if any, were the effects resulting from the fact that the center of percussion was now not at the sample. Were there energies absorbed in the pendulum arm or at the pivot? The unusual construction of the Manlabs instrument would tend to offset effects of this type. In order to experimentally determine if there were any possible effects, a series of Plexiglas samples were prepared which had force and impact energies similar to those of our ceramic samples. Table B-1 presents data for peak forces and energies for Plexiglas samples with and without the counterweights in place using steel anvils. The counterweights were removed and installed twice during this series of tests. The results were that the average maximum force measured was 1.3% greater when the counterweights were used and the average energy was 3.1% less when the counterweights were used. Considering the data scatter and the magnitude of these differences we conclude that errors due to the use of the counterweighted pendulum were not significant in this program.

A second question concerned the effect of using Wesgo solid alumina anvils versus the hardened steel anvils. Some room temperature experimental results using Norton SiC comparing the steel and alumina anvils are presented in Table B-2. These results show similar values either way with the average measured energies 6.5% less when the steel anvils were used.

Table B-1

Effect of Pendulum Counterweights on Force and Energy
Plexiglas Samples - .368 x .368 x 2.0 in. (0.69 x 0.69 x 5.08 mm)

	No Counterweights 3.66 ft/sec (1.11 m/sec)				Counterweights 3.09 ft/sec (.94 m/sec)			
	Energy		Force		Energy		Force	
	ft-lbs	Joules	lbs	N	ft-lbs	Joules	lbs	N
	1.00	1.36	417	1855	0.93	1.26	378	1681
	1.06	1.44	417	1855	0.67	0.91	338	1503
	0.68	0.92	338	1503	1.14	1.55	398	1770
	0.86	1.17	358	1592	0.92	1.25	398	1770
	1.00	1.36	398	1770	0.83	1.13	358	1592
	1.04	1.41	398	1770	1.01	1.37	417	1855
	1.00	1.36	398	1770	0.77	1.04	358	1592
	1.02	1.38	398	1770	0.96	1.30	398	1770
	1.00	1.36	398	1770	0.95	1.29	398	1770
	1.01	1.37	398	1770	0.90	1.22	398	1770
Avg.	0.95	1.29	385	1712	0.92	1.25	390	1735
Std. Dev.	±0.11	0.15	±29	129	±0.10	0.14	±21	93

Table B-2

Comparison of Hardened Steel and Alumina Anvils
at Room Temperatures
No Counterweights - 3.66 ft/sec (1.11 m/sec)

Al_2O_3 Anvil			Steel Anvil		
Sample Number	Energy ft-lbs	Energy joules	Sample Number	Energy ft-lbs	Energy joules
NC-203-210	0.20	0.28	NC-203-220	0.18	0.24
-211	0.18	0.24	-221	0.16	0.22
-212	0.17	0.23	-222	0.18	0.24
-213	0.14	0.19	-203	0.11	0.15
-214	0.16	0.22			
Avg.	0.168	0.228	Avg.	0.157	0.213

N78-17216
Case File
Do Not Use for Printing
Use Better Archive Copy

DISTRIBUTION LIST FOR NASA CR-135306
NAS 3-19731

Mr. J. Acurio
MS 77-5
NASA Lewis Research Center
21000 Brookpark Road
Cleveland, OH 44135

Mr. A. Arias
MS 49-3
NASA Lewis Research Center
21000 Brookpark Road
Cleveland, OH 44135

Dr. R. L. Ashbrook
MS 49-3
NASA Lewis Research Center
21000 Brookpark Road
Cleveland, OH 44135

Mr. G. M. Ault
MS 3-5
NASA Lewis Research Center
21000 Brookpark Road
Cleveland, OH 44135

Mr. R. T. Barrett
MS 500-210
NASA Lewis Research Center
21000 Brookpark Road
Cleveland, OH 44135

Mr. D. G. Beremand
MS 500-215
NASA Lewis Research Center
21000 Brookpark Road
Cleveland, OH 44135

Mr. C. P. Blankenship
MS 105-1
NASA Lewis Research Center
21000 Brookpark Road
Cleveland, OH 44135

Mr. H. M. Cameron
MS 500-215
NASA Lewis Research Center
21000 Brookpark Road
Cleveland, OH 44135

Mr. H. W. Davison
MS 500-210
NASA Lewis Research Center
21000 Brookpark Road
Cleveland, OH 44135

Dr. S. Dutta
MS 49-3
NASA Lewis Research Center
21000 Brookpark Road
Cleveland, OH 44135

Mr. R. C. Evans
MS 49-2
NASA Lewis Research Center
21000 Brookpark Road
Cleveland, OH 44135

Mr.J. C. Freche
MS 49-1
NASA Lewis Research Center
21000 Brookpark Road
Cleveland, OH 44135

Mr. W. E. Goette
MS 500-210
NASA Lewis Research Center
21000 Brookpark Road
Cleveland, OH 44135

Mr. R. W. Hall
MS 49-1
NASA Lewis Research Center
21000 Brookpark Road
Cleveland, OH 44135

Mr. F. H. Harf
MS 49-3
NASA Lewis Research Center
21000 Brookpark Road
Cleveland, OH 44135

Mr. J. R. Johnston
MS 49-3
NASA Lewis Research Center
21000 Brookpark Road
Cleveland, OH 44135

M&S Division Files
MS 49-1
NASA Lewis Research Center
21000 Brookpark Road
Cleveland, OH 44135

Dr. H. B. Probst
MS 49-3
NASA Lewis Research Center
21000 Brookpark Road
Cleveland, OH 44135

Mr. J. W. Weeton
MS 106-1
NASA Lewis Research Center
21000 Brookpark Road
Cleveland, OH 44135

Library (2)
MS 60-3
NASA Lewis Research Center
21000 Brookpark Road
Cleveland, OH 44135

Technology Utilization
MS 7-3
NASA Lewis Research Center
21000 Brookpark Road
Cleveland, OH 44135

Mr. J. Gangler/RWM
NASA Headquarters
Washington, DC 20546

Dr. T. P. Herbell
MS 49-3
NASA Lewis Research Center
21000 Brookpark Road
Cleveland, OH 44135

Mr. R. A. Lindberg
MS 49-3
NASA Lewis Research Center
21000 Brookpark Road
Cleveland, OH 44135

Mr. S. M. Nosek
MS 500-210
NASA Lewis Research Center
21000 Brookpark Road
Cleveland, OH 44135

Mr. W. A. Sanders (20)
MS 49-3
NASA Lewis Research Center
21000 Brookpark Road
Cleveland, OH 44135

Contracts Section B
MS 500-313
NASA Lewis Research Center
21000 Brookpark Road
Cleveland, OH 44135

Report Control Office
MS 5-5
NASA Lewis Research Center
21000 Brookpark Road
Cleveland, OH 44135

Mr. G. C. Deutsch/RW
NASA Headquarters
Washington, DC 20546

Library
NASA
Goddard Space Flight Center
Breenbelt, MD 20771

Library
NASA
Langley Research Center
Hampton, VA 23365

Technical Library/JM6
NASA
Johnson Space Center
Houston, TX 77058

Library
NASA
Dryden Flight Research Center
P.O. Box 272
Edwards, CA 93523

Accessioning Dept (10)
NASA Scientific & Techn.
Information Facility
Box 8757
Baltimore, MD 21240

Dr. E. C. van Reuth
Materials Science Office
Adv. Res. Proj. Agency
1400 Wilson Blvd
Arlington, VA 22209

Dr. H. Graham
AFML/LLM
Wright Patterson AFB, OH 45433

Dr. R. Katz AMXMR-RC
Army Materials and
Mechanics Research Center
Watertown, MA 02172

Mr. C. F. Bersch Air-52031B
Naval Air Systems Command
Navy Department
Washington, DC 20361

Library
NASA
Marshall Space Flight Center
AL 35812

Library - Acquisitions
Jet Propulsion Lab.
4800 Oak Grove Drive
Pasadena, CA 91102

Library - Reports
MS 202-3
NASA Ames Research Center
Moffett Field, CA 94035

Defense Documentation Center
Camerson Station
5010 Duke Street
Alexandria, VA 22314

Mr. I. L. Krulac
Analysis Center
Griffis Air Force Base
NY 13441

Dr. R. Ruh
AFML/LLM
Wright Patterson AFB.
OH 45433

Mr. G. G. Engle
US Army Tank Automotive Command
AMSTA-GR
Warren, MI 48090

Mr. I. Machlin AIR-52031B
Naval Air Systems Command
Navy Department
Washington, DC 20361

Dr. A. M. Diness
Navy Department
ONR Code 471
800 N. Quincy Street
Arlington, VA 22217

Dr. C. W. Spencer
Materials Adv. Bd.
Nat. Acad. of Sciences
2101 Constitution Ave.
Washington, DC 20418

MCIC
Battelle Memorial Inst.
505 King Avenue
Columbus, OH 43201

Dr. M. Richman
Engineering Department
Brown University
Providence, RI 02912

Dr. Y. Harada
IIT Research Institute
10 West 35th Street
Chicago, IL 60616

Mr. R. J. Diefendorf
Rensselaer Polytechnical
Institute
Troy, NY 12181

Dr. T. Vasilos
AVCO Systems Division
201 Lowell Street
Wilmington, MA 01887

Mr. C. McMurtry
Carborundum Co.
P.O. Box 367
Niagara Falls, NY 14302

Mr. R. Schultz
ERDA
Transp. Div. Energy Cons.
Washington, DC 20545

Mr. L. G. McCoy
Battelle Memorial Inst.
505 King Avenue
Columbus, OH 43201

Dr. M. S. Seltzer
Battelle Memorial Inst.
505 King Avenue
Columbus, OH 43201

Dr. P.E.D. Morgan
Franklin Institute
20 and Race Streets
Philadelphia, PA 19103

Prof. R. C. Bradt
Dept. of Material Science
Pennsylvania State Univ.
University Park, PA 16802

Dr. J. Mueller
Ceramic Eng. Dept. FB10
University of Washington
Seattle, WA 98105

Library
Carborundum Corpration
Res. and Dev. Division
Niagara Falls, NY 14300

Mr. K. H. Sandmeyer
Carborundum Co.
P.O. Box 367
Niagara Falls, NY 14302

Mr. J. A. Rubin
Ceradyne Inc
8948 Fullbright Avenue
Chatsworth, CA 91311

Mr. J. B. Mann
418-19-30
Chrysler Corp - 9410
Box 1118
Detroit, MI 48231

Mr. R. E. Engdahl
Deposits & Composites Inc
318 Victory Drive
Herndon Industrial Park
Herndon, VA 22070

Mr. E. Fisher
Product Development Group
Ford Motor Company
Dearborn, MI 48120

Technical Representative
Garrett Corporation
333 West First Street
Dayton, OH 45402

Mr. F. W. Rutledge
Garrett Airesearch
Cast Company
2525 W 190th Street
Torrance, CA 90509

Dr. R. J. Charles
R. & D. Center
General Electric Company
P.O. Box 8
Schenectady, NY 12301

Mr. A. Gatti
Space Sciences Laboratory
General Electric Company
P.O. Box 8555
Philadelphia, PA 19101

Mr. J. M. Corwin
418-19-30
Chrysler Corp
Box 1118
Detroit, MI 48231

Mr. R. Kamo
Director of Research
Cummins Engine Company
Columbus, IN 47201

Mr. J. C. Withers
Deposits & Composites Inc
1821 Michael Faraday Drive
Reston, VA 22090

Mr. A. F. McLean
Product Development Group
Ford Motor Company
Dearborn, MI 48120

Dr. R. F. Kirby
Chief, Materials Eng.
Garrett Airesearch
402 S. 36th Street
Phoenix, AR 85034

Mr. N. B. Elsner
General Atomic Company
P.O. Box 81608
San Diego, CA 92138

Dr. S. Prochazka
R. & D. Center
General Electric Company
P.O. Box 8
Schenectady, NY 12301

Mr. L. R. McCreight
Space Sciences Laboratory
General Electric Company
P.O. Box 8555
Philadelphia, PA 19101

Mr. P. Heitman
Detroit Diesel Allison DV
P.O. Box 894
Indianapolis, IN 46206

Dr. A. Alper
Chem. & Metall. Div.
GTE Sylvania
Towanda, PA 18848

Mr. A. Stetson
Solar Division
International Harvester
2200 Pacific Highway
San Diego, CA 92112

Dr. J. D. Venables
Martin-Marietta Labs.
1450 South Rolling Road
Baltimore, MD 21227

Mr. R. K. Bart
Industrial Ceramics Div.
Norton Company
Worchester, MA 01606

Mr. M. L. Torti
Refractories Division
Norton Company
Worcester, MA 01606

Dr. F. F. Lange
Rockwell International
Rocketdyne Division
6633 Canoga Avenue
Canoga Park, CA 91304

Techn. Information Center
AEG
General Electric Company
Cincinnati, OH 45215

Library
Materials Science Lab. W5
Detroit Diesel Allison
General Motors
Indianapolis, IN 46206

Dr. R. Kleiner
Chem. & Metall. Div.
GTE Sylvania
Towanda, PA 18848

Mr. R. J. Longenecker
Kawecki Berylco Ind., Inc
P.O. Box 1462
Reading, PA 19603

Mr. R. A. Alliegro
Refractories Division
Norton Company
Worcester, MA 01606

Mr. H. R. Baumgartner
Industrial Ceramics Div.
Norton Company
Worcester, MA 01606

Mr. F. Stroke
PPG Industries
One Gateway Center
Pittsburgh, PA 15222

Mr. R. Beck
Teledyne-CAE
P.O. Box 6971
Toledo, OH 43612

Mr. J. N. McCarthy
Materials Technology
TRW Equipment Group
23555 Euclid Avenue
Cleveland, OH 44117

Dr. R. Kossowski
Westinghouse Research Lab
Beulah Road
Pittsburgh, PA 15235

Prof. K. H. Jack
Metallurgy Department
University of Newcastle
Newcastle upon Tyne
England

Dr. R. J. Lumby
Joseph Lucas Ltd
Shirley, Solihull, Warws.
England

Dr. R. J. Bratton
Westinghouse Research Lab
Beulah Road
Pittsburgh, PA 15235

Mr. D. Goldberg
Westinghouse Electric
Astronuclear Laboratory
P.O. Box 10864
Pittsburgh, PA 15236

Dr. P. Popper
Special Ceramics Division
Brit. Ceramic Res. Assoc.
Queens Road, Penkhull
Stoke-on-Trent, England